N° d'ordre :

الجمهورية الجزائرية الديمقراطية الشعبية

République Algérienne Démocratique et Populaire

وزارة التعليم العالي والبحث العلمي

Ministère de L'enseignement Supérieur et de La Recherche Scientifique

جامعة عين تموشنت بلحاج بوشعيب

Université d'Ain Témouchent-Belhadj Bouchaib

Faculté : Sciences et de la Technologie

Département : Electrotechnique

Laboratoire : Structures Intelligentes

THESE

Présentée pour l'obtention du diplôme de **DOCTORAT**

Domaine : Sciences et technologies

Filière : Electrotechnique

Spécialité : Réseaux Electriques

Présenté par : Imane ZENNANI

Thème

Réalisation d'un séparateur électrostatique de particules par l'utilisation d'un disque rotatif alimenté par des tensions polyphasées

Soutenue publiquement devant le jury composé de :

Mr.	Mohammed FLITTI	Prof.	(Université d'Ain Temouchent)	Président
Mr.	Samir ZELMAT	Prof.	(Université d'Ain Temouchent)	Directeur de thèse
Mr.	Amar TILMATINE	Prof.	(Université de Sidi Bel-Abbes)	Co-Directeur de thèse
Mr.	Kamel NASSOUR	Prof.	(Université de Sidi Bel-Abbes)	Examinateur
Mr.	Massinissa AISSOU	Prof.	(Université d'Ain Temouchent)	Examinateur

Année Universitaire 2025/2026

Order number:

الجمهورية الجزائرية الديمقراطية الشعبية
People's Democratic Republic of Algeria
وزارة التعليم العالي والبحث العلمي
Ministry of Higher Education and Scientific Research
جامعة عين تموشنت بلحاج بوشعيب
University of Ain Temouchent-Belhadj Bouchaib

Faculty: Sciences and Technology
Department: Electrotechnical
Laboratory: Smart Structures

THESIS

Presented for **the DOCTORATE degree**

Domain: Science and Technology

Field: Electrotechnics

Specialty: Electrical Networks

Submitted by: Imane ZENNANI

Title

Realization of a new electrostatic separator device using a rotating disk powered by a polyphase high voltage supply

Defended publicly before the jury members:

Mr.	Mohammed FLITTI	Prof.	(University of Ain Temouchent)	President
Mr..	Samir ZELMAT	Prof.	(University of Ain Temouchent)	Thesis Supervisor
Mr.	Amar TILMATINE	Prof.	(University of Sidi Bel-Abbes)	Thesis Co-Supervisor
Mr.	Kamel NASSOUR	Prof.	(University of Sidi Bel-Abbes)	Examiner
Mr.	Massinissa AISSOU	Prof.	(University of Ain Temouchent)	Examiner

Academic Year 2025/2026

DEDICATIONS

Dedications

I would like to dedicate this work,

To my dearest parents, whose boundless love, unwavering support, and endless prayers have lit my path and carried me through every challenge. You are the roots of my strength.

To my beloved brothers Houcine, Walid, Mohamed Ramzi, Nasr-Eddine, and Amine, your friendship, laughter, and faith in me have been a constant source of courage and joy.

To my precious fiancée, Ferhouh Belhadri, for your endless patience, your gentle words, and your belief in me even in my most uncertain moments. Your love has been my calm and my motivation.

To the cherished souls of my dear uncle Mohamed and my grandmother, whose memories live on in my heart and whose love continues to guide me from beyond this world.

And to my entire family, for every prayer, every kind word, and every embrace that gave me strength when I needed it most.

Zennani Imane, 2025

ACKNOWLEDGMENTS

Acknowledgments

First and foremost, I offer my deepest gratitude to Allah, the Most Merciful, for granting me the strength, wisdom, and patience to complete this work. Without His guidance, none of this would have been possible.

I would like to express my heartfelt thanks to my beloved parents, whose unconditional love, constant encouragement, and endless sacrifices have been the foundation of everything I have achieved.

My sincere appreciation goes to my advisor, Prof. S. Zelmat, for his invaluable guidance, patience, and support throughout this research. His insightful advice and continuous encouragement have been a source of inspiration for me. I am equally grateful to my co-advisor, Prof. A. Tilmatine, for his valuable assistance, constructive remarks, and precious time dedicated to guiding me through this work.

I would like to express my sincere gratitude to the entire team of the APELEC laboratory at the University of Sidi-Bel-Abbès for their warm welcome and technical support throughout the experimental part of this work. Their professional expertise, availability, and valuable advice greatly contributed to the successful completion of this study. We sincerely thank them for their valuable collaboration and assistance.

I also extend my thanks to the members of the examination committee for their time, insightful feedback, and thoughtful evaluation of my thesis. To my dear friends, thank you for your constant support, understanding, and the moments of joy we shared that lightened this journey.

To all who contributed, in one way or another, to the realization of this work, I am sincerely grateful.

ZENNANI Imane, 2025

ABSTRACTS

Realization of a new electrostatic separator device using a rotating disk powered by a polyphase high voltage supply

Abstract

Electrostatic separation techniques used actuator have emerged as an effective solution for the sorting of granular materials by exploiting differences in their electrical properties. These technics typically employ rotating or linear actuators combined with high-voltage electrodes to create non-uniform electric fields, enabling selective control over particle behaviour. The generated electro-adhesion force allows conductive particles to be attracted and retained on charged surfaces, while insulating particles can be removed through mechanical or pneumatic means.

The objective of this work is to develop a new electrostatic separation device using a rotating disk to separate millimetre-sized plastic and metal particles. It will be evaluated experimentally. The actuator is powered by a high-voltage polyphase supply, producing a non-uniform electric field that induces electro-adhesion forces on conductive particles, while plastic particles are extracted by a vacuum blower system placed above the disk.

Two different configurations of actuator disks were created and evaluated. The first type of actuator is a single-sided rotating disk-shaped, which is made from a single-layer printed circuit board (PCB) and has two helical concentric electrodes on its top surface. The second type of actuator is a double-sided rotating disk-shaped made from a double-layer PCB and has a helical electrode on its top side and a plan circular electrode on its bottom side. The study was conducted in two stages: the study of the electro-adhesion force than the examination of the separation performance of the metal/plastic combination. Each actuator was investigated separately using different high-voltage supplies.

Important operating parameters such as applied voltage level, frequency, signal wave-form, air suction flow rate, vibrator feeding rate, disk rotation speed, and ambient humidity were all thoroughly examined for their effects.

The high recovery and purity rates of the separation were validated by the results. Importantly, this device was insensitive to ambient humidity, in contrast to traditional electrostatic separation techniques, confirming its dependability for industrial applications in changeable settings.

Keywords: Electrostatic separation; rotating disk; metal/plastic particles; and electro- adhesion force.

انشاء فاصل جسيمات كهرو ستاتيكي باستخدام قرص دوار يعمل بجهد ثنائي الطور

ملخص:

برزت تقنيات الفصل الكهرو ستاتيكي المستخدمة في أنظمة المشغلات كحل فعال لفرز المواد الحبيبية من خلال استغلال الاختلاف بين خصائصها الكهربائية .تستخدم هذه الأنظمة عادة مشغلات دوارة أو خطية موصولة بأقطاب كهربائية عالية الجهد لإنشاء مجالات كهربائية غير منتظمة، مما يتيح التحكم الانتقائي في سلوك الجسيمات .تسمح قوة الجذب الكهربائي المتولدة بجذب الجسيمات المعدنية والاحتفاظ بها على الأسطح المشحونة، بينما يمكن إزالة الجسيمات البلاستكية باستعمال وسائل ميكانيكية أو هوائية.

الهدف من هذه الأطروحة هو تطوير جهاز فصل إلكترو ستاتيكي جديد باستخدام قرص دوار لفصل الجزيئات المعدنية عن البلاستيكية ذات الحجم الميليميتري، كما سيتم تقييمه تجريبيا . القرص الدوار يتم تغذيته بواسطة مولد كهربائي ثنائي الطور عالي الجهد، مما يسمح بانبعاث مجال كهربائي غير منتظم ينتج عنه قوى الجذب الكهربائية المؤثرة على الجسيمات الناقلة للكهرباء (المعدن) بحيث تبقيها ملتصقة على سطح القرص، بينما يتم سحب الجزيئات البلاستيكية بواسطة نظام شفط هوائي مثبت فوق القرص.

تم إنشاء قرصين مختلفين، الأول عبارة عن قرص دوار ذو وجه واحد مصنوع من لوحة دارة مطبوعة (PCB) أحادية الطبقة وله قطبان على شكل حلزوني متحدي المركز على سطحه العلوي. اما النوع الثاني فهو قرص ثنائي الوجه مصنوع من دارة مطبوعة (PCB)ثنائية الطبقة يضم قطبًا كهربائيًا حلزوني الشكل على الوجه العلوي وقطبًا مسطحا دائري الشكل على الوجه السفلي .أجريت الدراسة على مرحلتين :دراسة قوة الجذب الكهربائي للمعدن ثم فحص أداء الفصل الكهرو ستاتيكي لخليط حبيبات المعدن والبلاستيك .تمت دراسة كل قرص باستخدام عدة مصادر للجهد العالي.

تمت دراسة وتحليل عدة عوامل مؤثرة على الجهاز منها قيمة الجهد المطبق على القرص، التردد، شكل موجة التوتر، معدل تدفق شفط الهواء، معدل سكب الخليط على سطح القرص، سرعة دوران القرص، وكذا رطوبة المحيط.

النتائج النهائية أثبتت المردودية العالية للجهاز من ناحية نسبة المواد المسترجعة ودرجة نقاوتها كما أظهرت أن هذا الجهاز لا يتأثر سلبا بالرطوبة المحيطة على عكس تقنيات الفصل الكهرو ستاتيكي التقليدية، مما يؤكد جاهزيته للاستعمال في التطبيقات الصناعية في بيئات مختلفة.

الكلمات المفتاحية: الفصل الكهرو ستاتيكي؛ القرص الدوار؛ جزيئات المعدن/البلاستيك؛ وقوة الالتصاق الكهربائي.

Réalisation d'un séparateur électrostatique de particules par l'utilisation d'un disque rotatif alimenté par des tensions polyphasées

Résumé

Les techniques de séparation électrostatique utilisées les actionneurs sont apparues comme une solution efficace pour le tri des matériaux granulaires en exploitant la différence entre leurs propriétés électriques. Ces systèmes utilisent généralement des actionneurs rotatifs ou linéaires reliés à des électrodes à haute tension pour créer des champs électriques non uniformes, permettant un contrôle sélectif du comportement des particules. La force d'électro-adhérence générée permet d'attirer et de retenir les particules conductrices sur les surfaces chargées, tandis que les particules isolantes peuvent être éliminées par des moyens mécaniques ou pneumatiques.

L'objectif de ce travail est de développer un nouveau dispositif de séparation électrostatique utilisant un disque rotatif pour séparer des particules de plastique et de métal de taille millimétrique. Il sera évalué expérimentalement. L'actionneur est alimenté par une alimentation polyphasée à haute tension, produisant un champ électrique non uniforme qui induit une force d'électro-adhérence sur les particules conductrices, tandis que les particules de plastique sont extraites par un aspirateur placé au-dessus du disque.

Deux configurations différentes d'actionneur ont été créées et évaluées. Le premier type d'actionneur est un disque rotatif simple face, qui est fabriqué à partir d'une carte de circuit imprimé (PCB) monocouche et possède deux électrodes concentriques hélicoïdales sur sa surface supérieure. Le deuxième type d'actionneur est un disque rotatif double face, qui est réalisé à partir d'un circuit imprimé à double face et comporte une électrode hélicoïdale sur sa face supérieure et une électrode plan circulaire sur sa face inférieure. L'étude s'est déroulée en deux étapes : l'étude de la force d'électro-adhérence puis l'examen des performances de séparation du mélange métal/plastique. Chaque actionneur a été étudié séparément avec différentes sources haute tension.

Des facteurs importants tels que le niveau de tension appliqué, la fréquence, la forme d'onde du signal, le débit d'aspiration d'air, le débit du mélange sur la surface du disque, la vitesse de rotation du disque et l'humidité ambiante ont été examinés en profondeur pour leurs effets.

Des taux élevés de récupération et de pureté de la séparation ont été validés par les résultats. Il est important de noter que ce séparateur était insensible à l'humidité ambiante, contrairement aux techniques de séparation électrostatique traditionnelles, confirmant ainsi sa fiabilité pour les applications industrielles dans différents environnements.

Mots Clés : séparation électrostatique ; disque rotatif ; particules de métal/plastique ; et force d'électro-adhésion.

CONTENT

Contents

LIST OF FIGURES

List of Figures

GENERAL INTRODUCTION

General introduction

The term "e-waste," which stands for electrical and electronic waste, describes any discarded electrical or electronic item, such as electrical wire, computers, phones, televisions, refrigerators, and other home appliances. Millions of tons of e-waste are produced worldwide each year as a result of the quick advances in technology. One of the waste streams that is expanding the quickest in the globe is e-waste. Electronic device upgrades and shorter product lifespans are the main causes of this trend, which causes older products to be thrown out [1–3].

E-waste must be managed and recycled effectively in order to recover resources, protect the environment, and lower pollution. Inefficient separation techniques and human disassembly were part of the recycling of e-waste in the past, but these issues are being resolved by recent technical developments. More effective recycling techniques, including electrostatic separation, are being developed with the goal of recovering valuable materials with the least amount of environmental damage possible [4–6].

Electrostatic separation is one of the primary techniques used to separate essential components from e-waste. The principle of this technique is that materials have different electrical characteristics, such as conductivity and permittivity, which can be exploited to separate these materials. Metals and polymers in e-waste can be separated by an electric field since they usually have highly different electrostatic characteristics. The electrostatic separation process involves subjecting the e-waste mixture to a high-voltage electric field; the electric force acting on charged or polarized bodies is used to separate the granular materials. Electrostatic separators, which may be set to maximize efficiency, are frequently used for this separation procedure. A popular tool for electrostatic separation is the drum separator, which applies an electric field to the materials after the revolving drum creates an electric charge on them. This process has the advantage of being able to handle complex material mixtures and separate them with a high degree of purity, which is crucial for recovering precious components [7–10].

The efficiency of separation can be influenced by various factors, including particle size, material shape, and the conductivity of the particles involved. As a result, ongoing efforts are focused on enhancing the precision and effectiveness of electrostatic separation technologies [11-12].

To address the constraints of traditional separation processes, a new technique using electrostatic actuators has been developed from a print circuit board. this technique employs electrostatic actuators to dynamically change the electrostatic fields applied to particles, allowing for the controlled adhesion and detachment of particles from electrode surfaces. By adjusting the intensity and design of the electric field, the system can improve separation efficiency and throughput for a variety of material types, including metals, minerals, and other electrically

charged particles.

Electrostatic actuators use high-voltage electric fields to create adhesion forces between the actuator's surface and metal particles. This technology has been investigated for numerous applications, including the transportation, sorting, and assembly of metal components, as well as the reduction of airborne particulate matter in industrial environments. Coulomb forces drive the adhesion mechanism, which is dependent on the charge distribution on the actuator's surface and metal particles. Recent advances have focused on increasing the efficiency, controllability, and scalability of electrostatic actuators for manipulating metal particles. According to studies, the shape and material properties of the actuator and particles, as well as the applied voltage, play critical roles in optimizing adhesion performance [13–15].

The objective of this thesis is to create a new electrostatic separator using a rotating actuator, which was investigated through testing to analyse the electro-adhesion force applied to metal particles and the electrostatic separation of millimetre-sized metal/plastic mixtures. To meet this thesis objective, two different types of actuators will be used separately. The first is a Single Sided Rotating Disk Shape Actuator created from a single-sided printed circuit board (PCB), while the second is a Double-Sided Rotating Disk Shape Actuator made from a double-sided. The factors of high voltage level given to the actuator, signal form, frequency, disc rotation speed, air suction flow rate, and vibrator feeding rate were evaluated for each type of actuator.

To validate the results of this study, a paper was published in an international journal of Particulate Science and Technology. Then, we participated in two international communications (ICASE and ICAEE) and one national communication (CNHT). Finally, we obtained a national invention patent from INAPI.

- I. Zennani, S. Zelmat, A.Tilmatine, « (2023): Electrostatic separation process of metal/plastic granular mixtures using a horizontal rotating disk, Particulate Science and Technology, DOI: 10.1080/02726351.2023.2201920
- I. Zennani, S. Zelmat, A.Tilmatine, "Experimental analysis of a new separation tech- nique using an electrostatic device based on an electro-adhesion force applied on metal particles," International Conference on Applied Science and Engineering—ASE 2022.
- I. Zennani, S. Zelmat and A. Tilmatine, "A New Electrostatic Separator Device Using a Double Side Rotating Actuator," 2024 3rd International Conference on Advanced Electrical Engineering (ICAEE), Sidi-Bel-Abbes, Algeria, 2024, pp. 1-6, doi: 10.1109/ICAEE61760.2024.10783320.
- I. Zennani, S. Zelmat, A.Tilmatine, "Experimental Investigation of a New Electrostatic Separation Process of Metal/Plastic Particles using a Horizontal Rotating Disk", national conference, International Journal of Electronics and Electrical Engineering Systems (ISSN: 2602-7437) Volume 6, Issue 3 (September 2023)

This thesis is divided into four chapters:

- The first chapter discusses the state of the art. It will be provided an overview of particle

charging mechanisms, electric field properties, and the forces operating on particles. A general overview of travelling wave technology will be covered, as well as prior works and application areas. Additionally, electrostatic separators will be discussed. Finally, an overview of the electrostatic separation of metal/plastic mixtures using travelling wave conveyors will be presented.

- The second chapter provides a description of the experimental materials and methodology used to achieve the thesis objectives. It will be detailed the materials; actuators and the product used in this study. It will be explained the methodology for analysing the adhesion force and the separation process results.
- The third chapter will be focused on analysing the adhesion force and recovery/purity rates of the separation process that are obtained using a single-sided rotating disk-shaped actuator.
- In the final chapter, the adhesion force and recovery/purity rates of the separation process achieved with a double-sided rotating disk-shaped actuator will be evaluated.

The conclusion will be provided a summary of the thesis work's contributions and suggests future directions for theoretical and practical advancement.

Chapter I: The state of the art

Chapter I: The state of the art

I.1. Introduction

This chapter will cover a general overview of particle charging mechanisms, electrical field characteristics, and various forces acting on the particle. Then, the state of the art for traveling waves technology will be discussed, along with predecessor works and applications areas. Additionally, the electrostatic separators will be mentioned. Finally, a summary of the electrostatic separation of the metal/plastic mixture using traveling wave conveyors will be provided.

I.2. Particulate charging mechanisms.

In general, electron transfers explain all electrification processes. The particle loading modes that are initially neutral include:

- Natural ion attachment charges
- Triboelectrification
- Ionic space charge charging

I.2.1. Natural ion attachment charges

Positive and negative ions are continuously produced in the earth's atmosphere by the impact of cosmic radiation and radioactive substances emitted from the ground.
According to Hinds [16], air contains around 1000 ions/cm^3 with roughly an equal quantity of positive and negative ions. Fine particles, which are originally neutral, can acquire a charge by collision (due to their random thermal movement) with ions. Charged particles tend to shed their charges slowly by attracting ions of opposite sign. As a result, this process tends to a state equilibrium known as "Boltzmann equilibrium charge distribution". This Boltzmann equilibrium illustrates the charge distribution of small particles in the presence of bipolar ions.

I.2.2. Triboelectrification

Triboelectricity has two causes of electrification: friction and contact.

I.2.2.1. Friction charging

Certain rubbing bodies develop the characteristic of attracting light bodies. They're thought to be energized by friction. The electrification in certain materials can be distributed in all of its contact points; these are the conductors (the electrification only appears if the rubbed body is held by an insulating handle); in others, it only manifests itself on the part rubbed; in other words, the electricity remains localized where it developed; these are the insulators. In all

circumstances, electrification is a charge transfer phenomenon.

I.2.2.2. Contact charging.

When dielectric materials come into contact and then separate, static electricity is produced. For centuries, it was supposed that contact charging results from spatially uniform material characteristics (along the material's surface), and that within a given pair of materials, one charges uniformly positively and the other negatively [17].

I.2.3. Ionic space charge charging

According to P. Atten [18], particle movement is generated by a high ion density due to a corona discharge in the interelectrode region, which increases particle charge. The charging process depends on several factors, among which the most important are the ion charge density, the local electrical field, and the size of the particles. Multiple studies [16,19–21] have demonstrated that the charging process is primarily influenced by two mechanisms:

- Electric field charging.
- Diffusion charging

I.2.3.1. Electric field charging

This charging mechanism is connected to the functioning of the electrical field, as stated by its name. Localized electrical field distortion is caused by a particle in a gas; the field lines appear on its surface. The nature of the particle contributes to this localized field distortion; conductor particles exhibit the largest field distortion. The permittivity of a non-conducting particle affects the field perturbation. As a result, the electrical field intensity at the particle’s surface increases. In this case, the ions in the gas that move along the electrical field lines may come into contact with the surface of the particle. Each ion that reaches the particle modifies the local electrical field distribution. The ions continue to reach the surface of the particle as long as the electrical field produced by its charge is less than the maximum electrical field that exists there when it is not charged. The term "particulate has acquired the charge of saturation by field" refers to the condition when the charge acquired is sufficient and the field lines contour the particle.

I.2.3.2. Diffusion charging

When the applied electrical field is small (or even zero) and the particle size is just right (allowing for some free paths), the mechanism of charge via diffusion has been proposed to explain particle charging. Therefore, it is important to consider the phenomenon of ion diffusion in the charging process. In this mechanism, the likelihood of collision between particles and ions driven by random thermal agitation is taken into account. The distribution of ions around the particles is uniform in a region where there is no electrical field applied. In these conditions, a particle’s surface elements all have an equal chance of colliding with ions, and the particle may also be able to build up some electrical charge. The relevance of this diffusion-charge

mechanism is greater for extremely small particles with a diameter less than 0.5 m [19, 21]. The size of the particulates, the ion density, the average thermal ion agitation speed, the particulate's dielectric constant, the absolute gas temperature, and the amount of time the particulates have been in the field all affect how much charge is accumulated in a charge by diffusion.

I.2.3.3. Mixed charging

Practically, for particles with diameters between 0.5 and 1 m, both processes operate concurrently, which further complicates the situation. A particle's total charge is not only the sum of its total charge by field and total charge by diffusion, though. Numerous solutions have been suggested to deal with this incredibly complex issue because of the interaction between the two systems [22, 23].

I.3. Gaseous Discharges

Types With a wide range of gas pressures and currents that can reach up to 106A, electrical discharges might be conducted in a variety of gases. The discharge current may oscillate at high and low frequencies, with the steady state lasting for a shorter time.

I.3.1. Corona discharge

When there is a uniform electric field, a steady rise in voltage across a gap results in the breakdown of the gap in the form of a spark without preliminary discharge. However, when the field is non-uniform, a surge in voltage will instantaneously result in a localized discharge in the gas to appear at points with the concentrated electric field intensity (Figure I.1). Corona discharge characteristics are transitory, audible, and faintly luminous. In the high electric field zone close to edges and sharp points, a corona discharge occurs. Depending on the geometrical arrangements of the electrode and the polarity of the field, corona discharges can take on a variety of shapes. High electric field electrode polarity suggests two different corona types: negative corona (high electric field region is concentrated around the cathode) and positive corona (high electric field area is concentrated around the anode). Multiple avalanches in the negative corona cause the ionization, but none do so in the positive corona because the electric field at the cathode is essentially too weak. It seems that the ionization activities here are associated with the emergence of so-called positive streamers. Sharp non-uniformity exists in the electric field. The field must be substantially greater than the remainder of the gas around one or both electrodes. Close to edges, sharp points, or thin wires that transform into low-power plasma sources are where this phenomenon occurs [24].

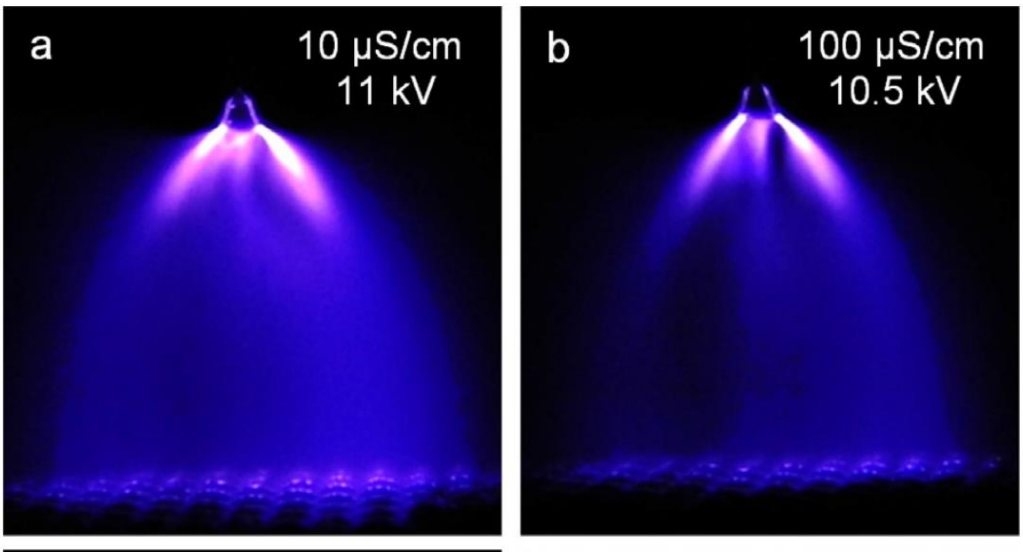

Figure I-1: Corona discharge [25].

I.3.2. Arc discharge

Electric arc is self-contained electrical discharges that carry large currents under small potential differences (Figure I.2).it characterizes by low cathode fall, high luminosity, and relatively high current density. In actuality, a rise in the current density corresponds to an increase in the area taken up by the discharge on the electrodes. When the discharge completely covers the surface, increasing the current density to a critical point may trigger the transition to an electrical arc [26], which is accompanied by an increase in the gas's temperature. In this case, the plasma produced is close to the thermodynamic equilibrium, and the energy injected into the gas is primarily dissipated via the Joule effect. Therefore, insufficient electron kinetic energy prevents the ionization and breakdown of environmental molecules. This is why, in the majority of corona discharge applications, the phenomenon of transition to an electrical arc must be avoided, either by applying repeated impulsion voltage with a duration of no more than a few hundreds of nanoseconds or by lowering the voltage to stop the discharge before it reaches the counter electrode [27].

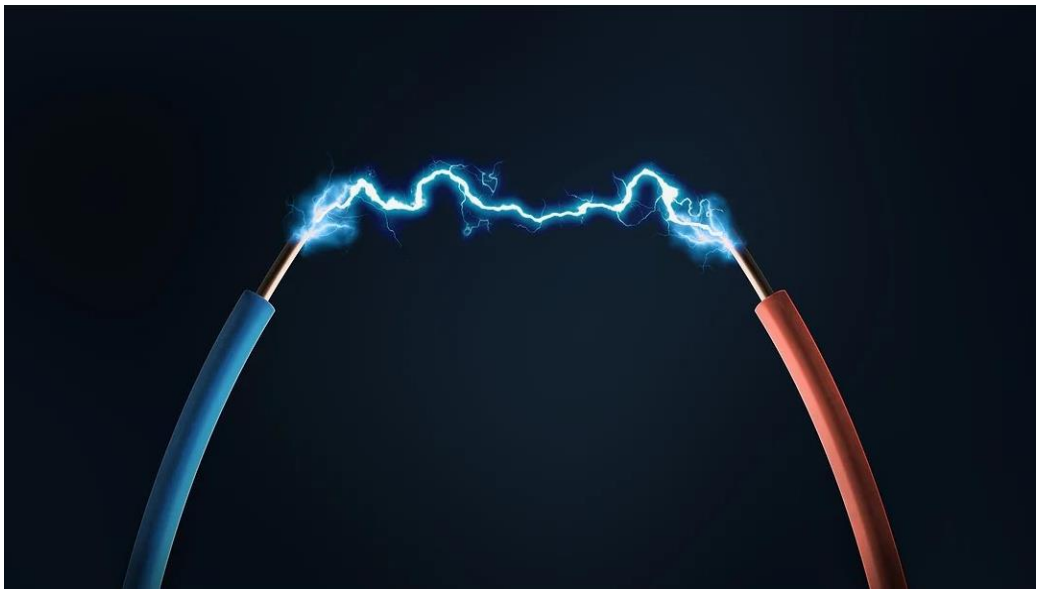

Figure I-2: Arc discharge.

I.3.3. Spark discharge

When the pressure is above atmospheric, a spark discharge happens at a voltage greater than the threshold breakdown level. The discharge phenomenon is a quick, transient event that resembles lightning on a massive scale. High-voltage streamers move swiftly in the direction of the electrode and create a conductor between them. Low current will result in decreased conductivity. High current causes the gas to thermally heat up, which lowers its density and further boosts its conductivity. Depending on the sort of pulse power circuit being utilized, the current will rise. Many orders of magnitude greater than the corona can be the current. this type of discharge is known as a spark discharge. The fundamental difference between a streamer and a spark is that a spark's plasma moves towards the thermal plasma, but a streamer's channel has gas that is almost always at ambient temperature. A spark is created by short discharges; however, the spark actually ends before the discharges resolve into arcs. The high field strength spots, or tips, are where the sparks are most likely to grow. Such tips are lost to sparking. If the sparks' energy is insufficient, the plasma resistivity will surround their tips and condition the gap. The high field strength spot or perhaps the electrodes will be destroyed by the powerful spark [24].

I.3.4. Dielectric barrier discharges (DBD)

(Figure I.3) shows a sample of a planar DBD setup. Due to the existence of at least one dielectric barrier, these discharges need alternating voltages to function. The dielectric, being an insulator, cannot pass a DC current. Its dielectric constant and thickness, in combination with the time derivative of the applied voltage, dU/dt, determine the amount of displacement current that can be passed through the dielectric(s). To transport current (other than capacitive) in the discharge gap the electric field has to be high enough to cause breakdown in the gas. In most applications, the average current density in the gas region is limited by the dielectric. It thus acts as a ballast which, in the ideal case, does not consume energy. Glass or silica glass, thin layers of enamel or polymer, and ceramic materials are preferred materials for the dielectric barrier. In rare circumstances, glass or silica glass may also be used. Some applications include the application of extra protective or practical coatings. The dielectric's ability to limit current is less effective at very high frequencies. For this reason, DBDs are normally operated between line frequency and about 10 MHz. In most gases, a significant number of micro discharges are seen when the pressure is in the range of 105 Pa and the electric field in the discharge gap is high enough to produce breakdown. This pressure range is recommended for ozone production, excimer creation, flue gas treatment, and pollution reduction [28].

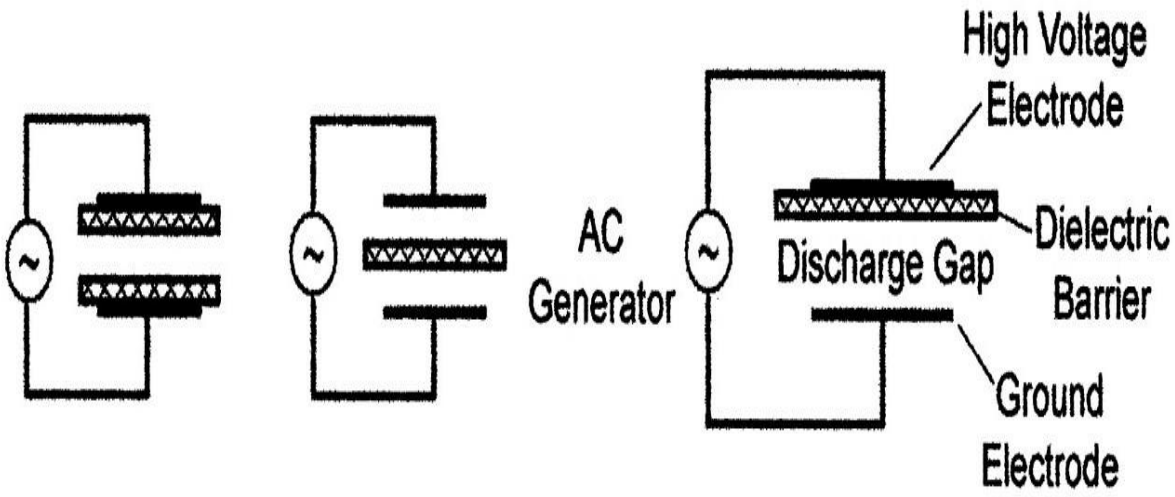

Figure I-3: Dielectric-barrier discharge configurations.

I.4. Electrostatic field properties

It is necessary to look at both the general characteristics and particular instances of electrostatic fields in order to completely describe their behaviour. The concept of superposition, which is essential to the study of multiple charge systems, will be introduced at the beginning of this section. The idea of electrostatic field lines as a graphic representation of field behaviour will next be discussed. Lastly, we will concentrate on certain configurations that are significant instances in electrostatic theory, such as electric dipoles and uniform fields.

I.4.1. Superposition principle

A witness charge Q is placed in a given position P, and an ensemble of N punctually placed charges q_i ($1 \leq i \leq N$) exerts electrostatic forces on it (Figure I.4). These forces are calculated separately for each charge and added vectorially. This is a physical principle known as the superposition principle [29].

$$\overrightarrow{F_Q} = \sum_{i=1}^{n} \overrightarrow{F_{q_i/Q}} = \sum_{i=1}^{n} \frac{1}{4\pi\varepsilon_0} \times \frac{q_i Q}{r_i^2} \times \overrightarrow{u_i} \qquad (I\text{-}1)$$

With:

r_i: is the distance between the charge q_i and Q.

$\overrightarrow{u_i}$:is the unit vector in the direction of the force exerted by q_i on Q.

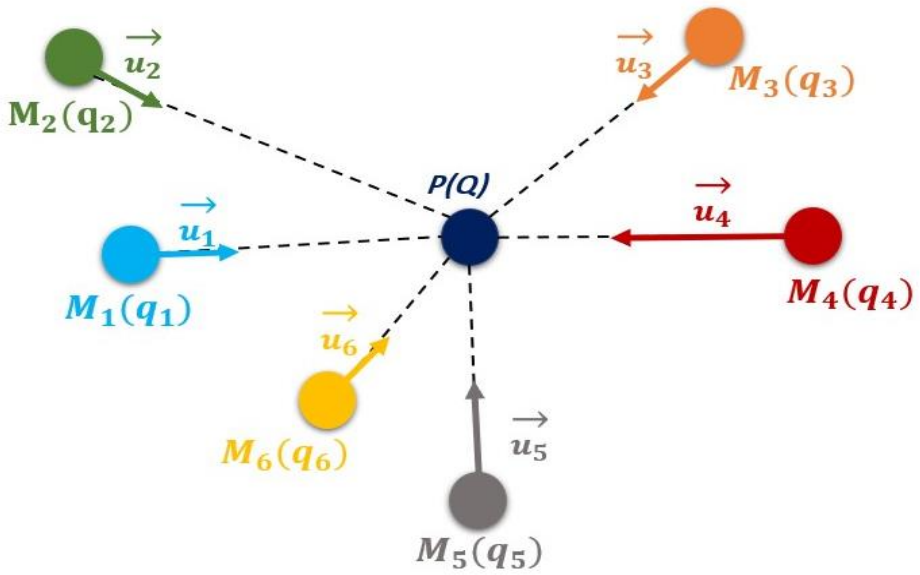

Figure I-4: Superposition principal.

I.4.2. Electrostatic filed lines

A line of field is a curve that has the electrical field carried by the line's tangent at each of its points. There are an infinite number of field lines in the space, and one line passes through each point in the space. Each field line is oriented in the vector's direction. The field lines diverge from positively charged sources (Figure I.5) and point in the direction of negatively charged sources [30].

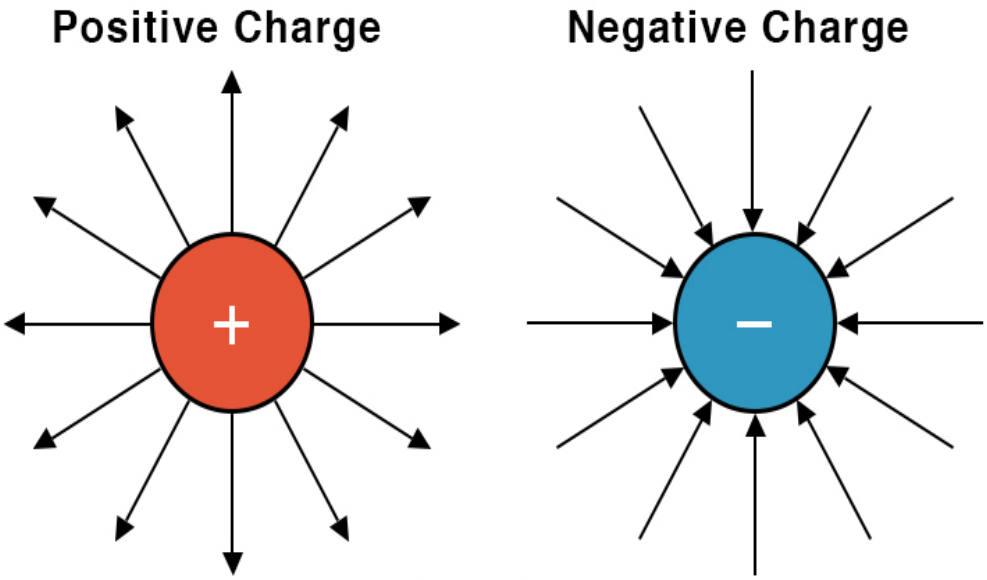

Figure I-5: Electrostatic field lines.

An imaginary surface known as a tube is created by a collection of field lines acting on a closed curve (For example, a cylinder when parallel field lines press against a circle). Due to the dielectric polarization effect, it is possible to materialize the field lines using semolina or iodine grains that face the direction of the field.

I.4.3. Uniform field

The electrical filed is uniform if the vector $\vec{E}$ maintains the same sign, direction, and value across the whole field (Figure I.6) [30].

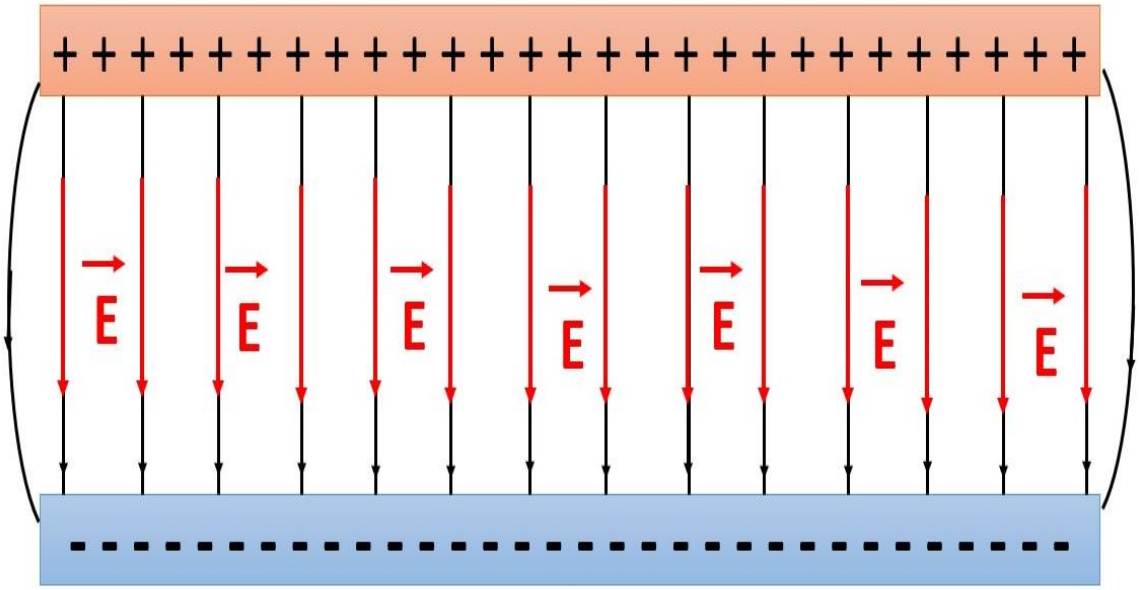

Figure I-6: Lines of field produced by two parallel electrodes.

A flat capacitor can be used to create an even electrical field. It refers to an electrical component that consists of two parallel metallic plates, or armatures, that are separated from one another by an insulator (air, vacuum, or plastic). A positive +q charge is present on one of the capacitor's armatures, while a negative -q charge is present on the other. As a result, the electrical field is essentially uniform between the two armatures; it is perpendicular to each and directed from the positively charged to the negatively charged armature.

I.4.4. Dipole moment

The dipole moment is a physical property that reflects the polarity of a molecule [31]. When a barycentre for positive charges (point P) separates from a barycentre for negative charges (point N), a molecule exhibits a dipole moment. These barycentre's P and N exist when there is a distinct difference in electronegativity between each liaison's two atoms and when the molecule's symmetry causes the dipole moments to annihilate (Figure I.7).

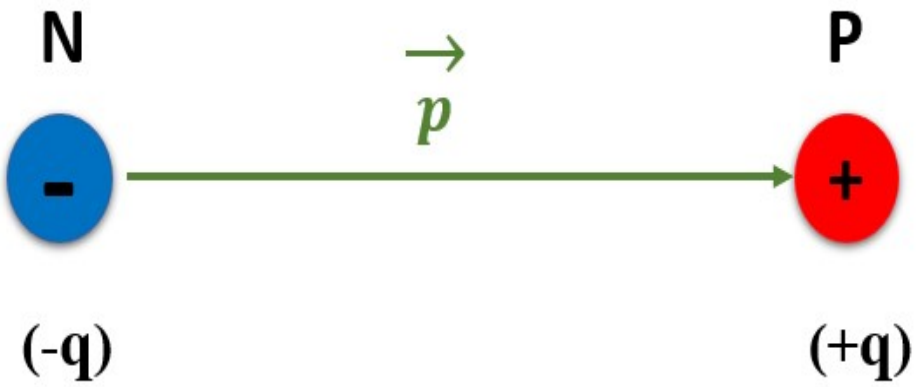

Figure I-7: Dipole moment.

I.5. Forces acting on particles

There are many kinds of forces that acting on particle: electrostatic force, mechanical force, adhesion force and dielectrophoretic force

I.5.1. Electrostatic forces

The force between charges in electrostatics can take on several shapes based on the system's structure and the surroundings. Two basic forms of electrostatic force: the Coulomb force, which is applicable to point charges in free space, and the image force, which appears when charges are close to conducting boundaries will be discussed in the ensuing subsections.

I.5.1.1. Coulomb Force

When a charged particle is close to charged surfaces or other charged particles, an electrostatic force is applied to the particle. The force of Coulomb proportional to the charge is experienced by particles that have acquired an electrical charge when an electric field (E) is present (Figure I.8).

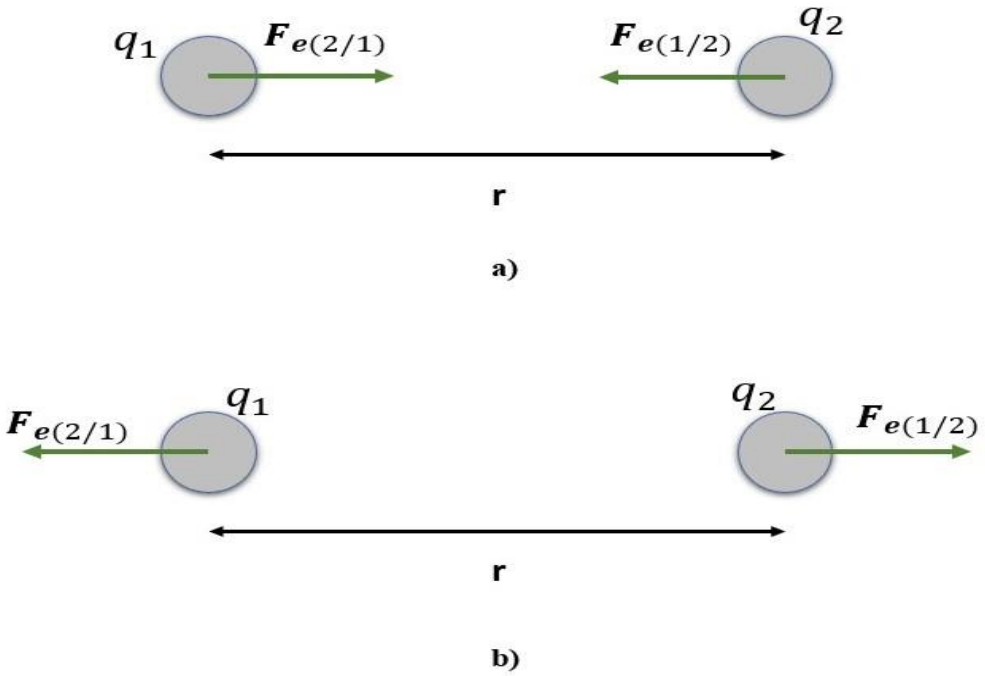

Figure I-8: Coulomb force between two charged spherical particles.

a) Attraction ($q_1.q_2$<0)

b) Repulsion ($q_1.q_2$>0)

The following equation represents the scalar formulation of the Coulomb law in electrostatics [32- 33].

$$F_e = K.\frac{|q_1.q_2|}{r^2} \qquad (I\text{-}2)$$

Where:
F_e: Electric force in Newtons (N)
q_1: First charge that applies electrical force to the second charge in Coulombs (C)
q_2: Second charge that applies electrical force to the first charge in Coulombs (C)
r: Distance between the two punctuating charges in meters (m)
K: Colomb law constant, $K = \frac{1}{4\pi\varepsilon_0} = 9.10^9\ Nm^2/C$; ε_0: Permittivity of the void.

I.5.1.2. Image force

A charged particle induces an image charge on a surface when it approaches. The size of the particles and the composition of the conveyor's isolating film both affect the electrostatic image force. However, the most important factor is the particle's charge, which often decreases with time. As a result, in practice, the image's force may be overlooked. This force is provided by [34–39].

$$F_i = \frac{1}{4\pi\varepsilon_0}\sum_{n=1}^{N}\left(\frac{q_i q_n}{2z}\right)^2 \frac{z}{|z|} \qquad (I\text{-}3)$$

With:
q_i: Particulate charge.
q_n: Film isolating charge (negligible).
z: Distance between the conveyor's surface and the particulate.

I.5.2. Mechanical force

According to classical mechanics, a number of forces control how bodies behave when they are moving or stationary. Among these, the gravitational force, centrifugal force, and friction force are crucial to many physical systems. These forces will be defined and discussed in the ensuing subsections, along with their causes, consequences, and typical applications.

I.5.2.1. Gravitational force

The physical reaction known as gravitational force is what draws two bodies together mutually. This force is in charge of the bodies falling and the movement of the dead bodies. It is expressed through the following relationship [40]:

$$F_g = m \,.\, g \qquad (I\text{-}4)$$

Where:
m: the body's mass.
g: the gravitational constant.

I.5.2.2. Centrifugal force

The concept of centrifugal force is widely understood. In spinning systems, the well-known outward-acting force is produced. It has several useful technical uses, and its mathematical formula is essential for planetary orbital calculations [41]:

$$F_c = m.r.\omega^2 \qquad (I\text{-}5)$$

Where:
F_c: the centrifugal force.
m: the mean body mass.
r: the circle radius.
ω: the angular velocity.

I.5.2.3. Friction force

Frictional force is the force generated by two surfaces that contact and slide against each other. the maximum amount of friction force that a surface can apply upon an object can be easily calculated with the use of the given formula [42]:

$$F_f = \mu \, . N \qquad \text{(I-6)}$$

With:
μ: the co-efficient friction.
N: the normal force.

I.5.3. Adhesion force

The particles that are deposited on the surface of the conveyor are affected by gravitational and adhesion forces. There are three main categories of adhesive forces:

- Capillary force
- Van-der-Waals-force
- Electromagnetic force

The force of Van der Waals is frequently the strongest force for small particles and can cause the adhesion of particles to surfaces or to other particles. Instantaneous polarization of atoms and molecules due to the effects of quantum mechanics causes the Van der Waals force [43]. The main attractive forces are Van-Der-Waals and electrostatic forces as the operation of the electrodynamic field is restricted to dry conditions for practical uses by conveyors.

I.5.3.1. Capillary force

In general, we call ‘capillary forces’ interactions between particles, which are mediated by fluid interfaces. The interest in these forces has grown due to their recognized importance for the self-assembly of macroscopic and microscopic particles and even of protein molecules and viruses (Figure I.9). In certain situations, a capillary bridge between two particles or substances is formed during the liquid phase. When that happens, the capillary force is generally oriented towards the planes of the contact lines on the particle surfaces.

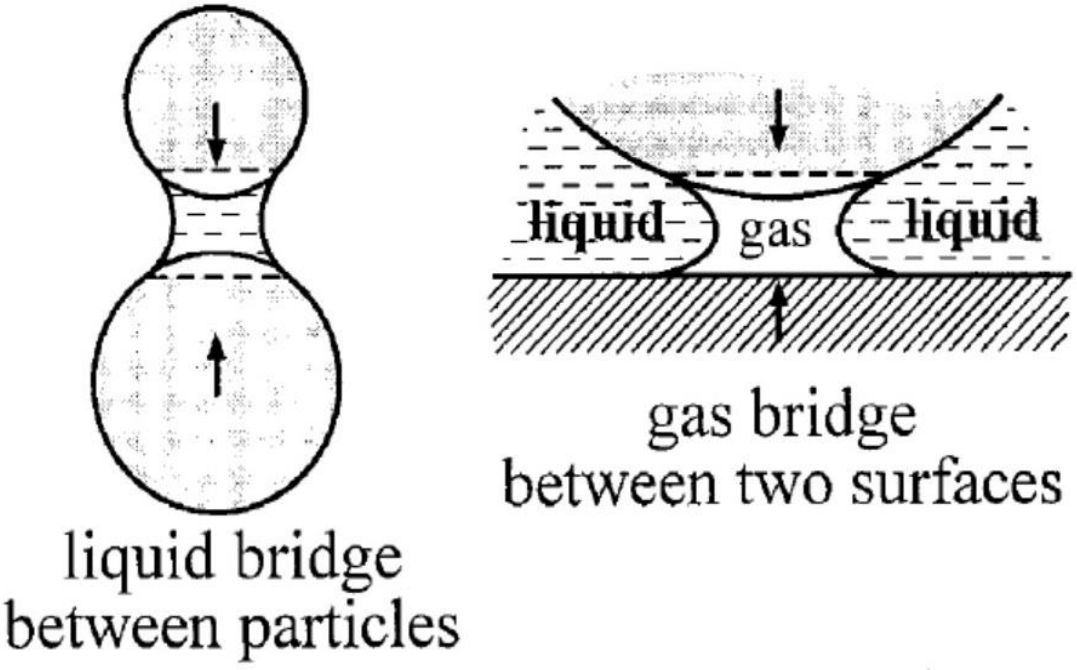

Figure I-9: Capillary forces.

A high ambient humidity will increase the force of adhesion's effect since the force of adhesion of liquids is proportional to the distance between two particles and the amount of liquid available [44, 45].

I.5.3.2. Van Der Waals force

Van der Waals forces are specific intermolecular interactions observed in liquids and solids. They are electrostatic in nature, arising from the interactions of positively and negatively charged species [43, 46].

There are three different types of Van der Waals forces:

a) Permanent dipole-permanent dipole interactions:

Two polar molecules can interact by electrostatic forces. For example, in (Figure I.10) the positive pole of one molecule attracts the negative pole of a neighbouring molecule.

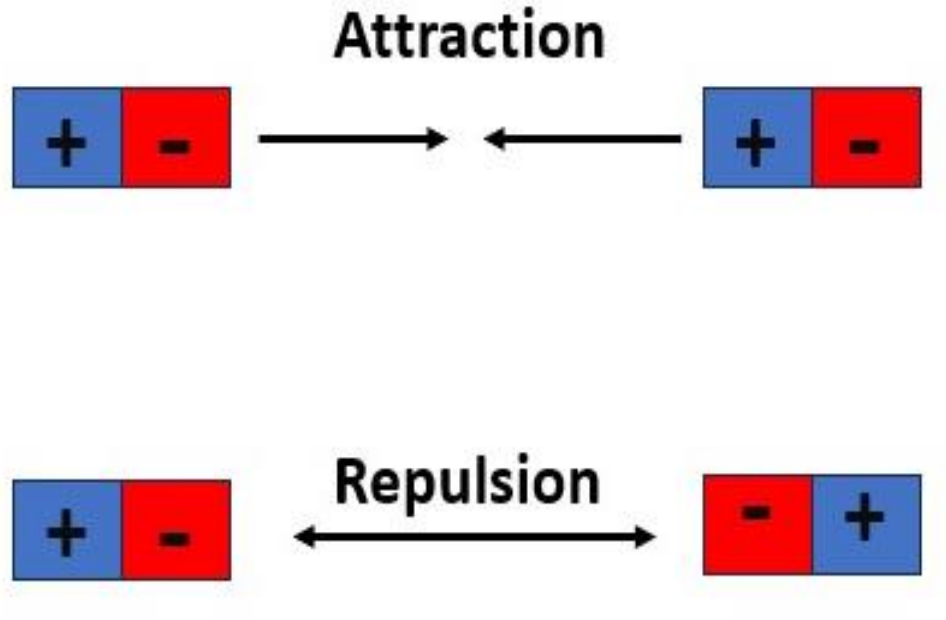

Figure I-10: Permanent dipole-permanent dipole interactions.

b) Permanent dipole – induced dipole interactions:

A polar molecule can interact with a non-polar molecule in a similar way. The polar molecule generates an electromagnetic field around it. The negative charges from the non-polar (neighbouring) molecule are attracted to the pole + of the polar molecule (Figure I.11).

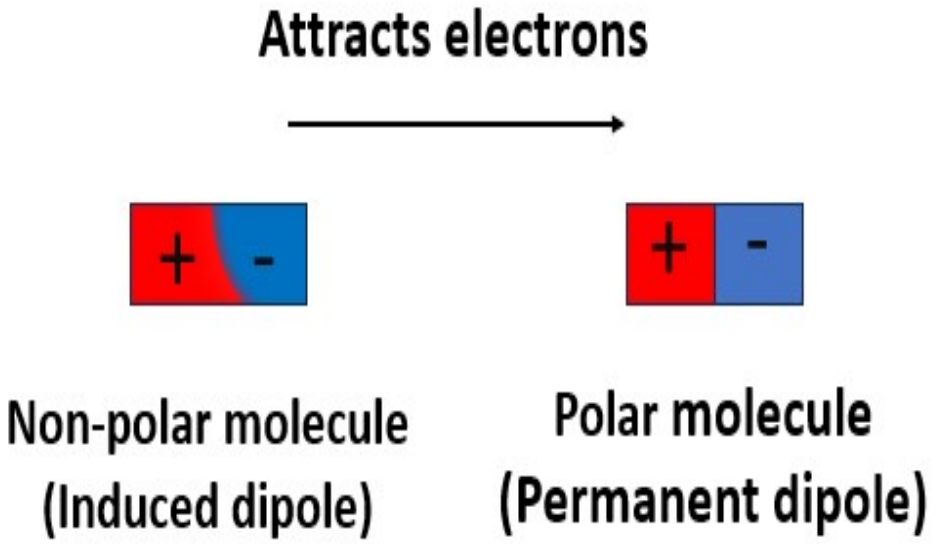

Figure I-11: Permanent dipole – induced dipole interactions.

c) Instantaneous dipole-instantaneous dipole interactions:

The electrons move in neutral atoms and non-polymeric molecules, resulting in instantaneous dipoles. These dipoles may interact and contribute to the molecule's cohesion.

I.5.3.3. Electromagnetic force

The electromagnetic force is the force of interaction between electrically charged particles, like electrons and protons, either stationary or moving. It consists of two distinct forces: electric force and magnetic force (Figure I.12). The electric force originates from the interaction between charged particles, whether they are stationary or moving. Oppositely charges attract each other, while like charges repel. Charged particles give rise to an electric field. However, when the particles start to move, they generate a magnetic field, which gives rise to a magnetic force. The electromagnetic force is manifested when the electric and magnetic fields interact with the charged particles. It is an exchange force, and the particles that carry the force are known as photons.

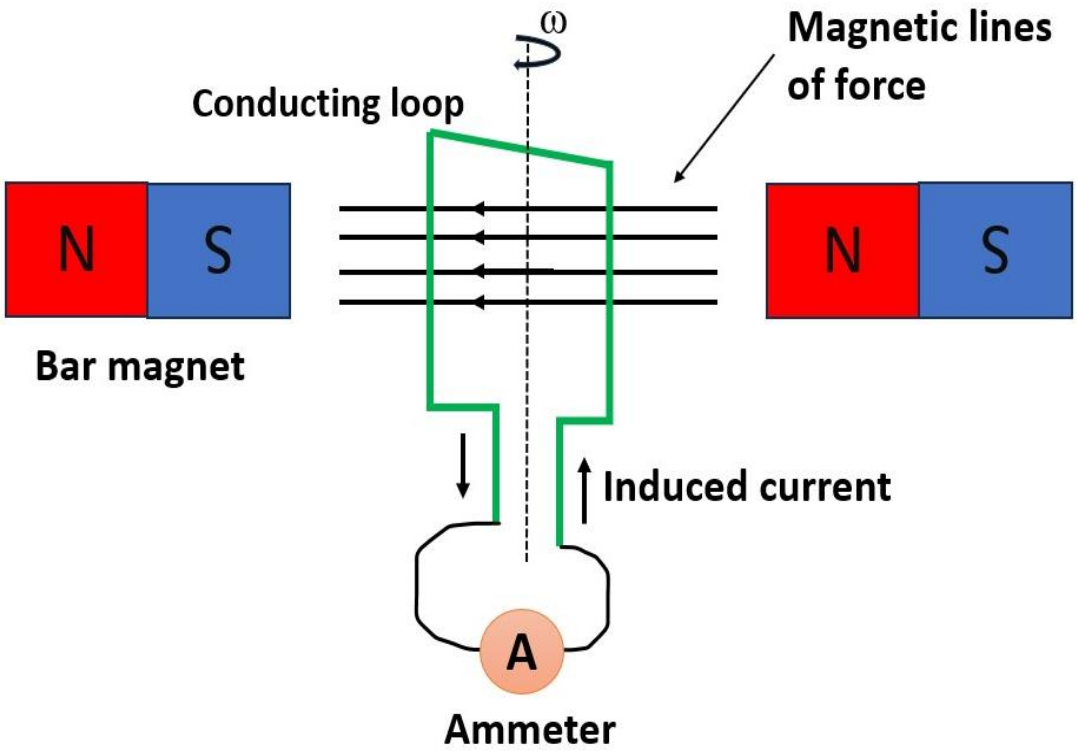

Figure I-12: Electromagnetic force principle.

I.5.4. Dielectrophoretic force

In non-uniform electric fields, polarisable particles encounter forces that result in dielectrophoretic phenomena. In order to provide a better understanding of this phenomenon, the subsequent subsections will first outline the fundamental dielectrophoretic phenomena before outlining the dielectrophoretic mathematical formulation and properties.

I.5.4.1. Dielectrophoretic phenomena (DEP)

The dielectrophoretic phenomenon is the movement of polarized material within an electric field. It is necessary for the applied electrical field to be non-uniform, and this phenomenon is increasingly used in microsystems to manipulate or move particles without mechanical touch. Two features define the DEP:

- It pertains to both neutral and charged matter, whether it is solid or liquid.
- Alternating electrical fields can reduce electrochemical reactions to electrodes.

The particle moves either towards the strongest field (the DEP is positive) or away from the weakest field (the DEP is negative).

I.5.4.2. Dielectrophoretic force

Dielectrophoretic force (DEP) is a result of the interaction between a dielectric particle's dipole moment and the no-uniform electrical field. This force can only be observed when there is a no-uniform electric field.

The following relationship describes DEP force:

$$F_{DEP} = 2.\pi.r_p^3.\varepsilon_0.\varepsilon_{rm}.F_{CM}.\nabla(E^2) \qquad (I\text{-}7)$$

With:

$$F_{CM} = \frac{\varepsilon_{rp}-\varepsilon_{rm}}{\varepsilon_{rp}-2\varepsilon_{rm}} \qquad (I\text{-}8)$$

Where:

ε_{rp}: the dielectric constant of the particle.

ε_{rm}: the dielectric constant of the medium.

r_p: the radius of the particle.

E: the electric field.

F_{CM} is the Clausius-Mossotti factor, which makes it possible to determine the direction of the force. When a particulate is more polarizable than the surrounding environment, $F_{CM} > 0$, the DEP force is directed towards the electrodes; when the particulate is less polarizable than the surrounding environment, $F_{CM} < 0$, the DEP force is directed towards the less intense electrical fields (between the electrodes) [47].

I.6. Electrostatic separators

Electrostatic separation encompasses a range of material processing technologies that use electrical forces acting on charged or polarized particles to achieve selective sorting of solid materials. When particles are introduced into the electrostatic separator, they acquire an electric charge and behave differently depending on whether they are conductive or insulating. There are three types of separation for millimetre-sized granular particle combinations. The first, known as

the plate-type electrostatic separator, is used to separate "conductive-conductive" particles. The second is known as the tribo-electrostatic separator is used to separate "insulator-insulator" particles (for example, ABS and HIPS), whereas the corona discharge separator is used to separate granular "insulator-conductor" combinations (for example, PVC/copper) [48–62].

I.7. Traveling wave conveyors

Traveling wave conveyors (TWCs) are frequently used to make movement of micronized insulating components through the interaction between phase shifted electric field and polarized particles. A TWC contains parallel electrodes with two, three, or four phase shifted alternative high voltage [63]. There are two factors that classify the conveyors: the number of phases and the geometry of the electrodes [64].

➢ **Factor of Phases Number:**

There are several different variations of the series of electrodes used in mobile conveyors (Figure I.13):

- **The biphasic conveyors:** consist of two intercalated electrodes powered by periodic voltages in two phases, with a displacement of π.
- **The triphasic conveyors:** consist of three interconnected series of electrodes, each connected to a periodic voltage source, with a phase difference of 2π /3 between them.
- **The four-phase conveyors:** consist of an electrode network made up of four interconnected series powered by voltage sources with a phase difference of π /2.

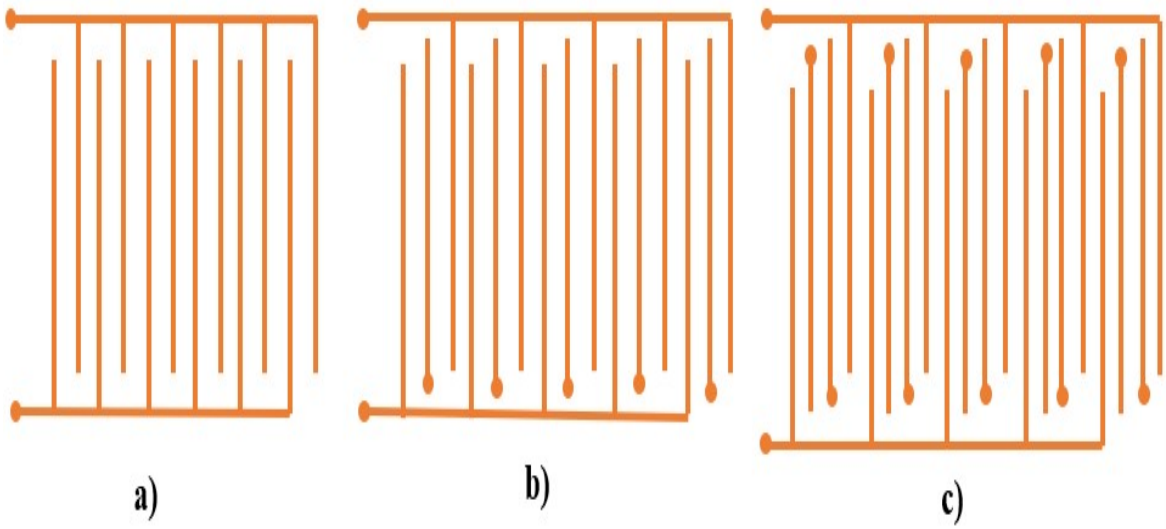

Figure I-13: Schematic illustrating several types of conveyers (2,3 and 4 phases).

➢ **Factor of electrodes geometry:**

The configurations of the conveyer's electrodes might be 2D or 3D. The conventional photolithography and metallization processes are used to manufacture the planar 2D electrodes.

The created field mostly affects surface-bound particles (Figure I.14).

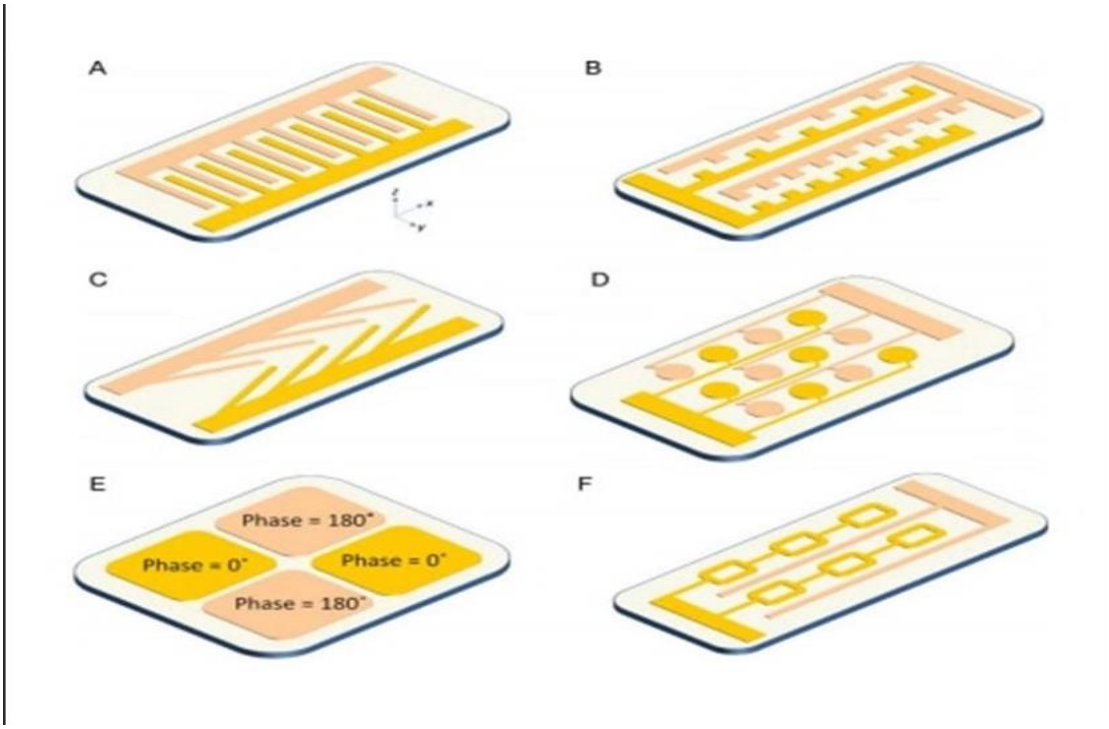

Figure I-14: 2D configuration.

The manufacturing of 3D electrodes involves more intricate procedures that enable the creation of an electrical field inside the fluid's volume. Therefore, a greater number of particles get a more intense application of the force (Figure I.15).

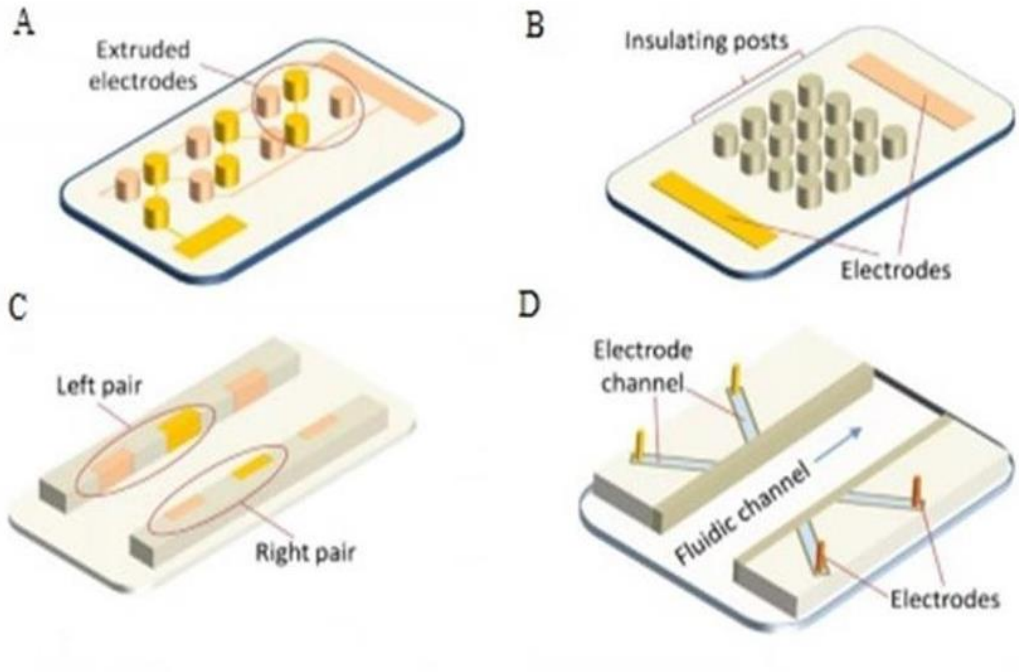

Figure I-15: 3D configuration.

I.7.1. Applications of the traveling wave technique

In a number of systems, the travelling wave technique provides a workable way to regulate the displacement of particles or fields. Its precision and adaptability have made it an essential instrument in many modern technological applications. This section seeks to outline the main uses of this method while highlighting its application and working principles.

I.7.1.1. Electrostatic dust removal from solar panels

Electrostatic dust removal devices for cleaning solar panels have arisen, using the properties of the dielectrophoretic force created by a traveling wave conveyor contained in the ITO (Indium Tin Oxide) electrodes. Unlike copper or aluminium, ITO is transparent, allowing photons of light to pass through without affecting the efficiency of a solar panel. NASA has chosen electrostatic conveyors over traveling waves as his preferred method to clear dust on future missions to Mars and the Moon.

Several studies have been conducted on the subject, including those of Kawamoto, who successfully recreated lunar atmospheric conditions in an isolated chamber to remove lunar dust (Regolith) deposited on a solar panel [37, 38]. Gaofa completed the same work [65]. Other research has enabled the implementation of a method for moving six types of earth and sand for solar panel cleaning in desert regions where a hydraulic system is not always feasible due to water scarcity. To achieve this, a combination of the conveyor electrostatic and panel tilting is required; this device works effectively despite a huge sand accumulation [66].

I.7.1.2. Application of traveling wave technology to agriculture

This technology is also used in agriculture to separate an agri-food product from its by-products (derivatives of agricultural products), such as sunflower meal and cottonseed, from undesired items such as cockles [67-68].

I.7.1.3. Traveling wave separation

In terms of separation using traveling waves, it is used for the separation of micronized particles in a liquid or air environment. It is based on the effect of the dielectrophoretic force. The dielectrophoretic force enables manipulation of materials with dielectric characteristics, such as biological cells, micro-fabricated inorganic components etc. Electrodes and an alternating voltage source are needed to generate dielectrophoretic force. Several research works in biochemistry have emerged, such as the separation of leukocytes and erythrocytes, or the response of these two particles to traveling waves, which causes the leukocytes to follow the mobile wave created differently than the erythrocyte, and thus there is a separation [69]. Other researchers have used two types of conveyors to move a fluid in two opposite directions of movement with different frequencies; there are in fact two directions of movement in a fluid for low and high frequencies. According to research, the electrophoresis force at a specific frequency influences the movement of particles suspended in a fluid. Using traveling wave technology, some researchers developed a concentrator for bio-agent collecting [70–73].

In biology, the dielectrophoretic force generated by the traveling waves technique has an important effect on biological cells because it enables the manipulation and movement of biological cells for a variety of applications such as counting, sorting cells, delivering genes, and creating new cell hybrids using a non-uniform electric field [74-75]. For example, scientists have developed a bio-particle separator capable of separating cells, viruses, and proteins [76]. Others have separated living cells from a combination of debris cells and non-living cells in the presence of dielectrophoretic force [77]. In earlier research, this method has been used to separate a combination of human and bacterial cells [78].

I.8. Separation of insulating-conductive particles using adhesive force

Several investigations have examined the separation of insulating-conductive particles employing adhesive force, and the results have been favourable. A travelling wave conveyor separator is used to recover industrial waste that requires fine grinding to completely separate metal and plastic particles [79]. A new separation process of metal/plastic granular mixtures using a cylindrical TWC was developed; the functioning principle of the separation technique is based on the attraction force applied on the metal particles [80-81]. This force was influenced by the applied voltage, frequency, and signal waveform [82-83]. The biggest issue with employing an electrical curtain for separation is the breakdown sparks between electrodes and particles when a high voltage value is applied. This difficulty was reduced by the development of a new double-sided electrical curtain [84]. Particle charge is a phenomenon that improves separation efficiency by increasing the speed of plastic particle movement [85]. by placing an aspirator above an actuator, a new device was invented to ensure the separation process of a metal-plastic mixture [86].

I.9. Conclusion

Electrical field properties and a thorough review of particle charging techniques were covered in this chapter. Additionally, various forces acting on the particle were discussed. An overview of electrostatic separators and a travelling wave conveyor with their uses were also provided. The possibility of separating a metal/plastic mixture using a travelling wave conveyor was finally covered in extensive works.

The next chapter will be provided a detailed account of the experimental materials and methodology used to address the thesis objectives.

Chapter II:
Material and methods

Chapter II: Material and methods

II.1. Introduction

In this chapter, we will provide a detailed account of the experimental materials and methodology used to address the thesis objectives. The main focus of this study is to explore the functionality of a new electrostatic separator featuring a rotating disk design. To achieve this goal, we have devised a comprehensive experimental approach incorporating various techniques and protocols. The chapter begins by presenting an overview of the materials employed in our investigation. It then proceeds to introduce the components of the separator, offering detailed explanations of the two main investigative aspects: adhesion force and separation process. Finally, the chapter wraps up by outlining the analytical techniques and computational tools utilized to interpret the experimental results.

II.2. Materials and software

The following materials and Proteus software were used to create and manipulate the new electrostatic separator that was the subject of this work.

II.2.1. Materials

The choice of materials plays a critical role in the success and reliability of experimental setups. This section introduces the different materials utilised in the study and describes their electrical and physical characteristics that are pertinent to the experimental work.

II.2.1.1. High-voltage sources

Three different kinds of high-voltage supplies are employed to power the actuator in order to examine the signal form effect:

- The high-voltage amplifier (TREK 2220).
- Continuous high voltage power supply (SPELLMAN SL300).
- Midpoint transformer (ZM 20/14, Siemens).

Other high voltage supply is used to power the midpoint transformer called: Autotransformer (ALT7-PE))

a) The high-voltage amplifier (TREK 2220)

TREK's Model 2220 (2kV – 20 mA) is one of the several models within the 2200 series of high voltage 40 W, provided at an attractive price and offering high performance.

The unit incorporates DC stability, wide bandwidth and well-regulated/controlled AC output signals. It also features a full four-quadrant class AB all-solid-state output stage, DC offset adjustment with front panel metering, and protection to prevent the output from being overpowered. The instrument sinks or sources current into reactive or resistive loads throughout the output voltage range, making it ideal to achieve the accurate output response and high slew rates demanded by reactive loads (Figure II.1).

Figure II-1: The high-voltage amplifier (TREK 2220).

b) DC high voltage power supply (SPELLMAN SL300)

(Figure II.2) shows the high-tension supply (Spellman, 30 kV, 9 mA) that is being used provides a continuous high voltage 30 kV with a 9 mA output.

Figure II-2: DC high voltage power supply (SPELLMAN SL300).

c) Midpoint transformer (ZM 20/14, Siemens)

Transformers are essential devices in electrical systems, enabling voltage transformation and current conversion. They consist of primary and secondary windings that transfer electrical energy through electromagnetic induction. A mid-point HV transformer, also known as a centre tapped transformer, is a special configuration that offers a unique advantage: the ability to provide both higher and lower voltage outputs This is achieved by introducing a centre tap at the midpoint of the high-voltage winding. By splitting the high-voltage winding into two equal sections and connecting the centre tap to a ground or neutral point, we can obtain two output voltages. These voltages include a higher voltage between either end of the winding and the centre tap, and a lower voltage between the two ends of the winding. The midpoint high-voltage transformer (ZM 20/14, Siemens) used, operating at a frequency of 50 Hz, has two secondary HV-windings that can each provide a maximum voltage of 7 kV and a current of 20 mA (Figure II.3). The two sinusoids high voltages have the same amplitude and are phase shifted by an angle of 180◦.

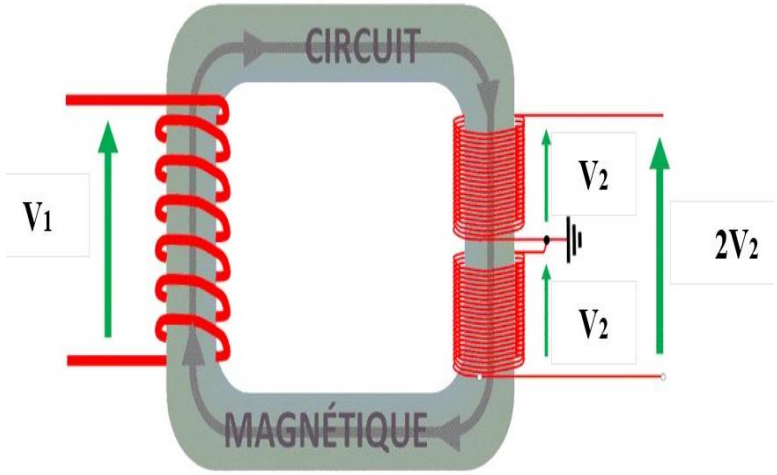

a)

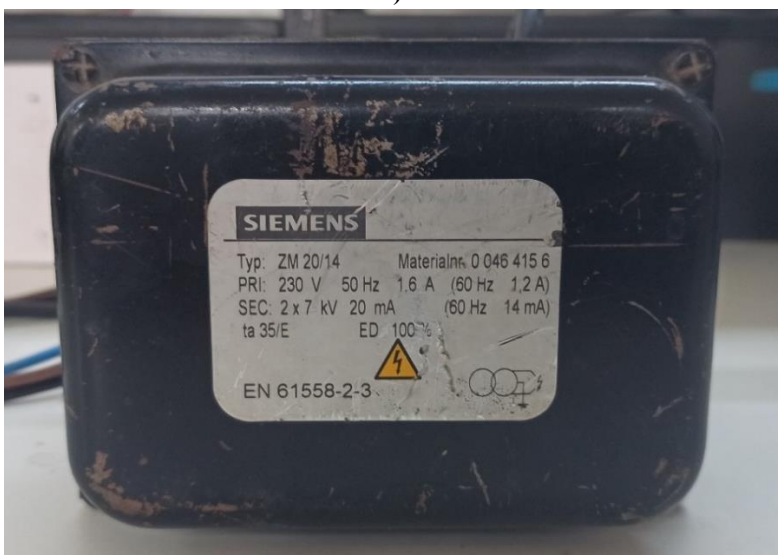

b)

Figure II-3: Midpoint transformer (ZM 20/14, Siemens).

a) Descriptive schematic of a midpoint transformer**. b)** Photography of the transformer used.

d) Autotransformer (ALT7-PE)

The autotransformer consists of only one single-coil winding which is used as primary as well as secondary windings. In autotransformer, primary and secondary windings are connected electrically as well as magnetically. The autotransformer can be used as a step up and step-down transformer. (Figure II.4) presents the autotransformer (ALT7-PE) that is used for voltage variations in various applications such as powering our device's DC motor, midpoint transformer, and vacuumblower.it is characterized by: Power (1,89 kVA), primary voltage (220/240 V) and secondary voltage (0-260 V).

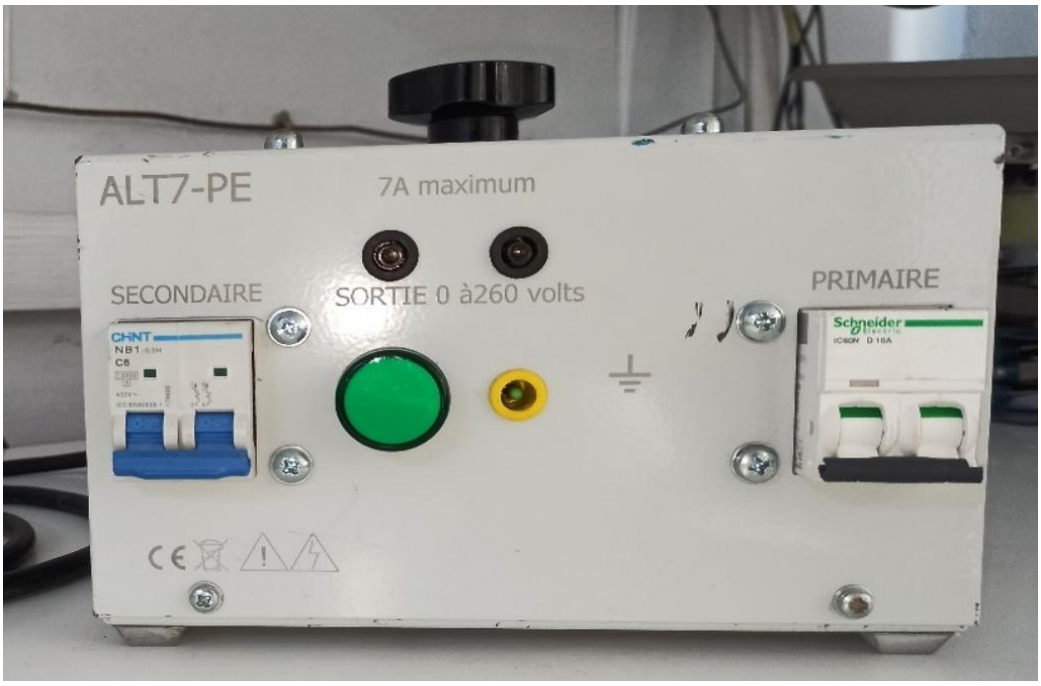

Figure II-4: Autotransformer (ALT7-PE).

II.2.1.2. High voltage probe

A high voltage probe is an electrical measurement tool used to safely measure high voltages in various applications. It is designed to withstand and accurately measure voltage levels that exceed the capabilities of standard multi-meter or oscilloscope probes. High voltage probes typically consist of a probe tip, a co-axial cable, and a voltage divider network. The probe tip is the part that makes contact with the high voltage source, and it is insulated to prevent electrical shock. The co-axial cable connects the probe tip to the measuring instrument, such as an oscilloscope or a multi-meter. The voltage divider network within the probe reduces the high voltage to a lower, measurable level that the measuring instrument can handle (Figure II.5). The PVM-1 high voltage probe that was utilized was characterized by (Table II.1).

Table II-1: The high voltage probe characteristics.

Model	Max DC/Pulsed V (kV)	Max Freq. (MH)	Cable Impedance (Ω)	DC - 2 Hz accuracy	2 Hz - 200 Hz accuracy	200 Hz - 5 MHz accuracy	Input R/C (MΩ/pF)	Cable Length (ft/m)
PVM-1	40/60	120	50	<0.1%	<1%	<1.5%	400/13	400/13

Figure II-5: High voltage probe.

II.2.1.3. Function generator (SIGLENT SDG 5122)

The SDG 5122 is a dual-carnality generator that can simultaneously emit two distinct forms of waves. These shapes appear on the device's LCD screen, allowing users to make adjustments and change the frequency, amplitude, and other parameters as needed. (Figure II.6).

Figure II-6: Function generator (SIGLENT SDG 5122).

II.2.1.4. Memory oscilloscope (GWINSTEK GDS-3154)

The GDS-3000 Series digital storage oscilloscope is a full-featured and powerful tool that allows you to tackle complex measurement issues with ease. The GDS-3000 Series, carrying a maximum bandwidth of 500MHz, is equipped with a real-time sampling rate up to 5GSa/s and an equivalent-time sampling rate of GSa/s. The large 8-inch SVGA TFT LCD screen, combined with the advanced digital signal processing technology VPO, provides meticulous detail and clarity for the displayed waveforms. The GDS-3000 Series gives you confidence not to miss any part of the test signal in the product verification and debugging stages and allows you to speed up your task without hesitation (Figure II.7).

Figure II-7: Memory oscilloscope (GWINSTEK GDS-3154)

II.2.1.5. Direct current motor

A DC motor was used to train the actuator because it's speed can be controlled over a wide range, using either a variable supply voltage or by changing the strength of current in its field windings (Figure II.8).

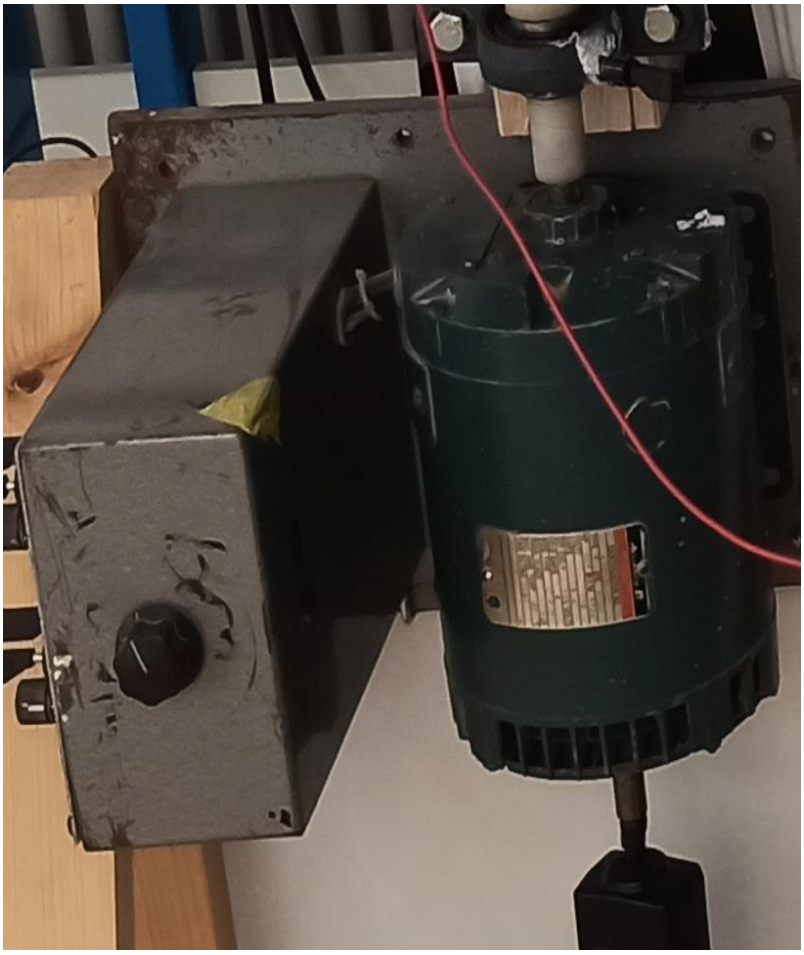

Figure II-8: Direct current motor.

II.2.1.6. Vacuum blower (Crown 550W CT17002)

(Figure II.9) presents the Crown 550W CT17002 that was the vacuum blower used in separator construction. This device guarantees you remarkable results thanks to its powerful air flow of 3.5 m^3/min and a no-load speed of 14,000 rpm. The Crown 550W CT17002 electric blower makes your work easier. Its performance guarantees good work efficiency.

Figure II-9: II.2.1.6. Vacuum blower (Crown 550W CT17002).

II.2.1.7. Vibrating Feeder

A vibrating feeder is an industrial machine that allows products to be conveyed along a corridor from point A to point B of a production line. This equipment is becoming more and more important in our industries due to its ease of use and the possibility of automating its process. There are many applications for using a vibrating feeder.

- Conveying of materials, small particles.
- Transport of powders.
- Product dosage.

The vibrating feeder type used in this work was LEV2-220V-50/60 Hz-S3000-0,25A-37W max-IP66 (Figure II.10).

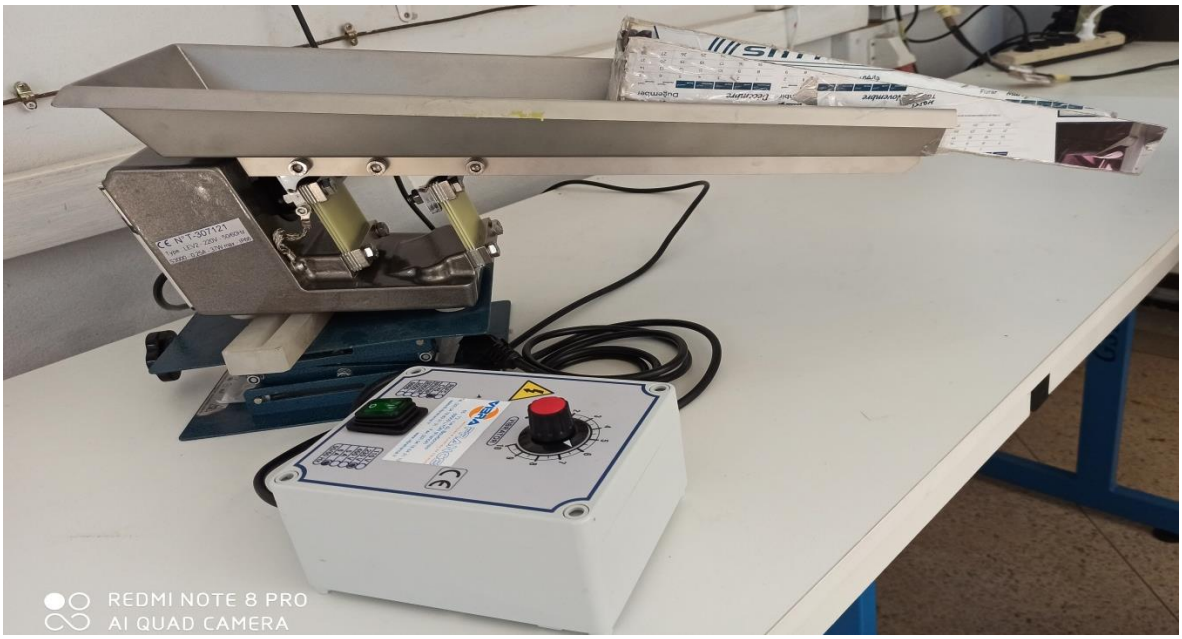

Figure II-10: Vibrating feeder.

II.2.1.8. Analytical scale ABJ 220-4NM

Laboratory analytical scale ABJ 220-4NM is intended for determining the mass of material to be weighed (Figure II.11). The weight value can be read when a stable weight value is obtained. The weighing object is carefully placed in the middle of the weighing plate using a laboratory weighing vessel (weighing vessel, glass and flask).

Figure II-11: Analytical scale ABJ 220-4NM.

II.2.1.9. Electronic Digital Tachymeter (Lutron Dt-2236)

To measure the motor speed an electronic tachometer (Lutron Dt-2236) used (Figure II.12). it was characterized by:

- **Measurement parameters:** photo tachometer, contact tachometer, surface speed.
- **Display:** 5-digit LCD display, 10 mm (1 cm).
- **Time base:** crystal quartz.
- **Operating temperature:** 0 ◦Cto50 ◦C
- **Operating humidity**: less than 80% RH.
- **Battery:** 1.5V AA batteries; Power consumption: photo type: approx. 153 mA DC, contact type: approx. DC 10mA.
- **Accessories:** user manual, reflecting tape marks, rpm adapter board, wheel speed test surface.

Figure II-12: Electronic Digital Tachometer (Lutron Dt-2236).

II.2.1.10. Hygrometer (TFH 610)

(Figure II.13) shows the hygrometer (TFH 610) used to measure relative humidity and temperature simultaneously. The TFH 610 is equipped with an air probe or sword probe. TFH 610 device elements:

- Display panel (LCD).
- ON/OFF key
- Probe.

Figure II-13: Hygrometer (TFH 610).

II.2.2. Proteus Professional Software

For design the different actuators chapes, the Proteus Professional was used.

II.2.2.1. Proteus presentation

Proteus is a widely used software tool in the field of electronics and computer-aided design (CAD). It is primarily known for its simulation capabilities and is commonly used by engineers, students, and hobbyists for designing and testing electronic circuits before building them physically (Figure II.14).

This software is developed by Lab Center Electronics Ltd. and provides a comprehensive set of tools for designing, simulating, and testing electronic circuits. It offers a virtual environment where users can simulate and analyse the behaviour of circuits without the need for physical components. This helps in reducing costs, time, and effort associated with building and testing circuits in the real world.

Proteus consists of two main components: ISIS (Intelligent Schematic Input System) and ARES (Advanced Routing and Editing Software). ISIS allows users to draw and design electronic circuit schematics using a vast library of components, including microcontrollers, sensors, transistors, integrated circuits, and more. ARES, on the other hand, enables the design and layout of printed circuit boards (PCBs) for the circuits created in ISIS.

One of the key features of Proteus is its simulation capability. Users can simulate the designed circuits and observe the behaviour of components and signals in real-time. This allows

for testing and debugging of circuits before their physical realization, ensuring their functionality and performance. The software provides various analysis tools, including transient analysis, AC analysis, and digital simulation, to perform in-depth investigations of circuit behaviour.

Proteus also supports micro controller simulation, allowing users to program and test microcontroller-based systems within the software environment. It provides a wide range of microcontroller models and peripherals that can be integrated into circuit designs, enabling the development and testing of embedded systems.

In addition to simulation, Proteus facilitates PCB design and layout. ARES offers a user-friendly interface for designing custom PCBs, arranging components, and routing traces. It supports various auto-routing and design rule checking features to ensure a well-optimized and manufacturable PCB layout. Overall, Proteus is a powerful and versatile tool for electronic circuit design, simulation, and PCB layout. Its capabilities make it a valuable asset for electronics engineers, students, and hobbyists involved in various projects and applications.

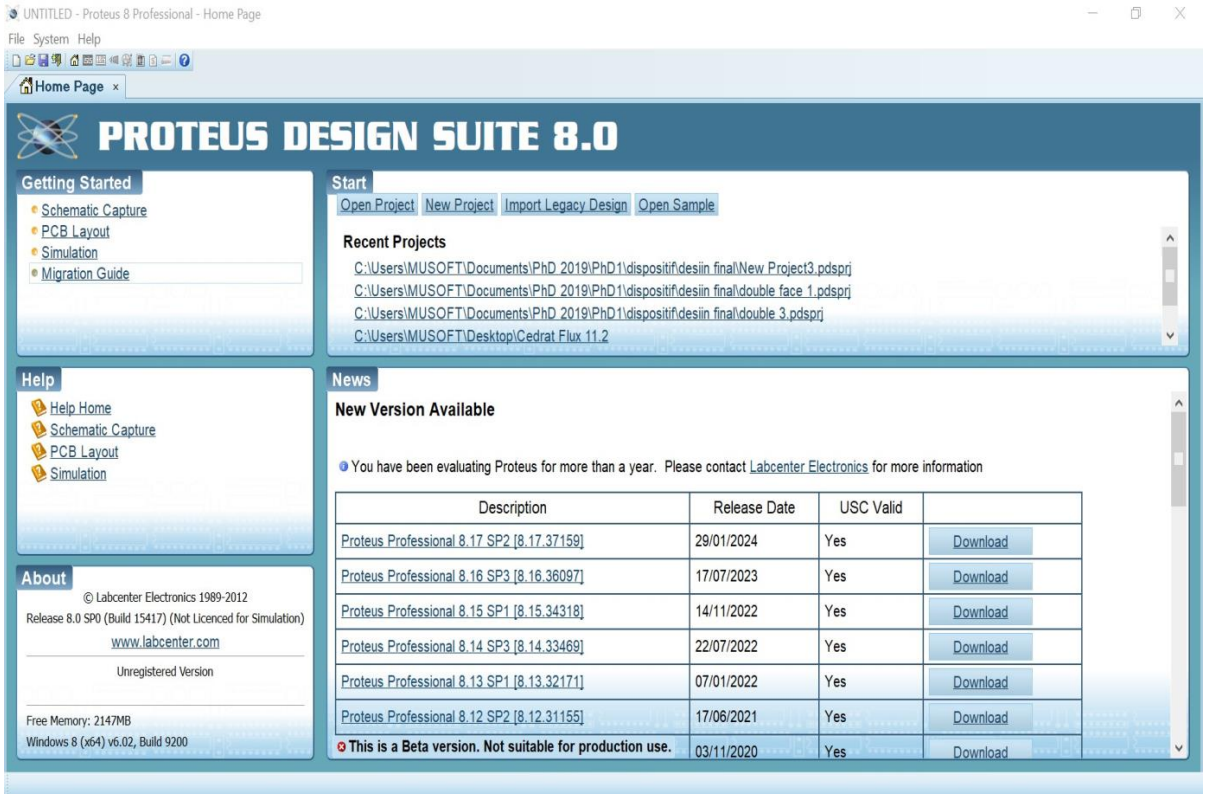

Figure II-14: Proteus interface.

II.2.2.2. Proteus window

(Figure II.15) presents the Proteus window that has many sections such as:

- **Editing Window:**

In the above figure, you can see that the dotted portion is called an editing window. This is a drawing portion of proteus where you simulate your engineering circuits and projects.

- **Overview Window:**

In the overview window, you see the complete view of your complete design.

- **Object Selector:**

This section has 2 buttons P and E. P is used to select different components and shown in this box. The E button is for editing something for example you want to vary any value of components then you can use this edit button.

- **Zoom Option:**

By using this option, you can easily zoom in and zoom out your layout and can observe the complete simulation very clearly.

- **Tool Option:**

By using this option, you can select different devices like voltmeter, ammeter, oscilloscope, etc.

- **Run Buttons:**

At the left bottom, there are 4 buttons Run, stop, pause, and step. These buttons are like the remote control and are on and off your circuit.

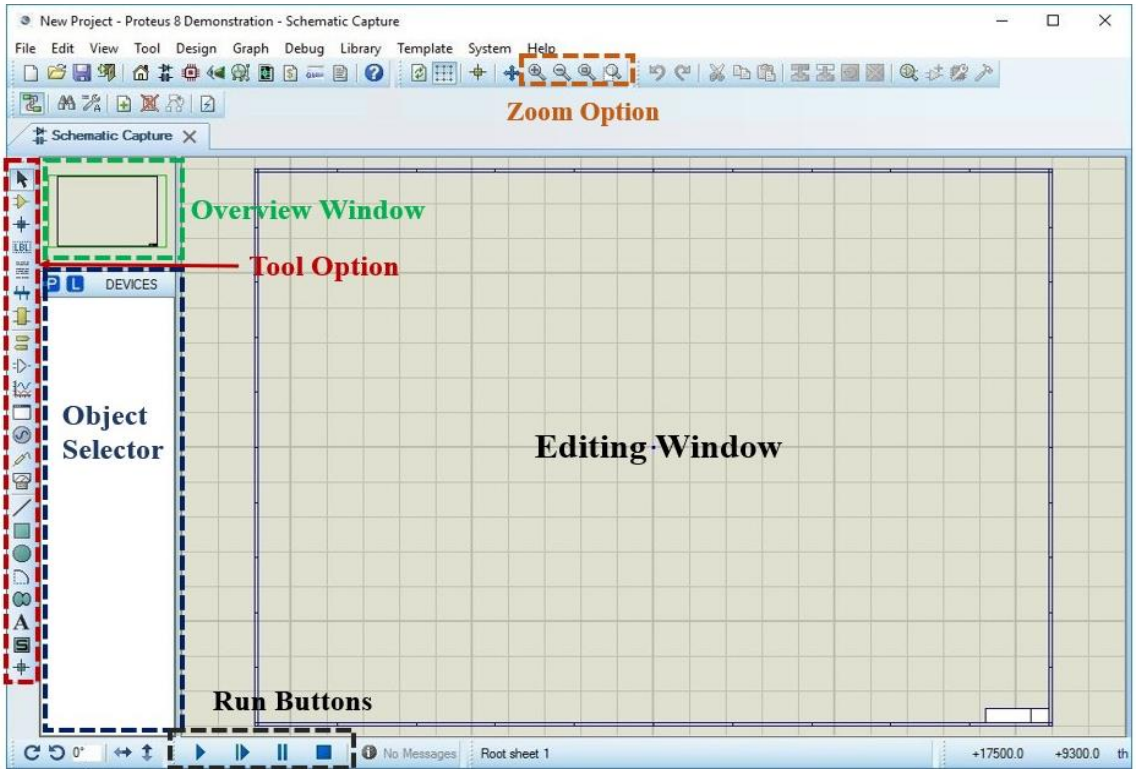

Figure II-15: Proteus window.

II.3. Printed Circuit Board (PCB)

The Printed Circuit Board (PCB) was used to realize the actuators studied in this work.

II.3.1. PCB presentation

Printed circuit boards (PCB) are the most frequently used interconnection technology for components in electronic products. The increasing packing density of contemporary mechanical and electrical components has led to changes in PCB requirements. They now have thinner

laminates and finer conductor tracks spread across an ever-increasing number of layers. Integrated circuits have advanced significantly, particularly in the past ten years. New design specifications have thus been made in order to put them on the boards. Surface mount technique is currently being used more often, despite insertion being widespread with DIP (Dual Inline-Package) technology in the 1970s.

Furthermore, the sizes of the holes are quickly reducing, the number of conductors between through-holes is growing, and the dimensions of the lines and spaces are decreasing. The use of micro vias as blind-vias or through-holes is becoming more common as a result of these needs. PCBs will be more useful and denser, more reliable, and less expensive in the future because to better, more tightly regulated, and more economical production. Additionally, the business will shift to PCBs that are more ecologically friendly. Furthermore, the benefits of contract manufacturing on a worldwide scale will successfully guarantee that PCB design and production are of a calibre that is recognized across the world.

II.3.2. Components of a PCB

Fundamental components of a printed circuit board are:

- **The base**, which is a thin board of insulating material, rigid or flexible, which supports all conductors and components.
- **The conductors**, normally of high purity copper in the form of thin strips of appropriate shapes firmly attached to the base material.

All copper areas and components attached to the copper are mechanically supported by the base. The dielectric characteristics of the base material determine the electrical properties of the full circuit; thus, these characteristics need to be understood and properly controlled. In addition to providing electrical connections between components, the conductors offer solderable attachment points for those same components.

The conductors offer solderable attachment sites in addition to electrical connections between components (Figure II.16).

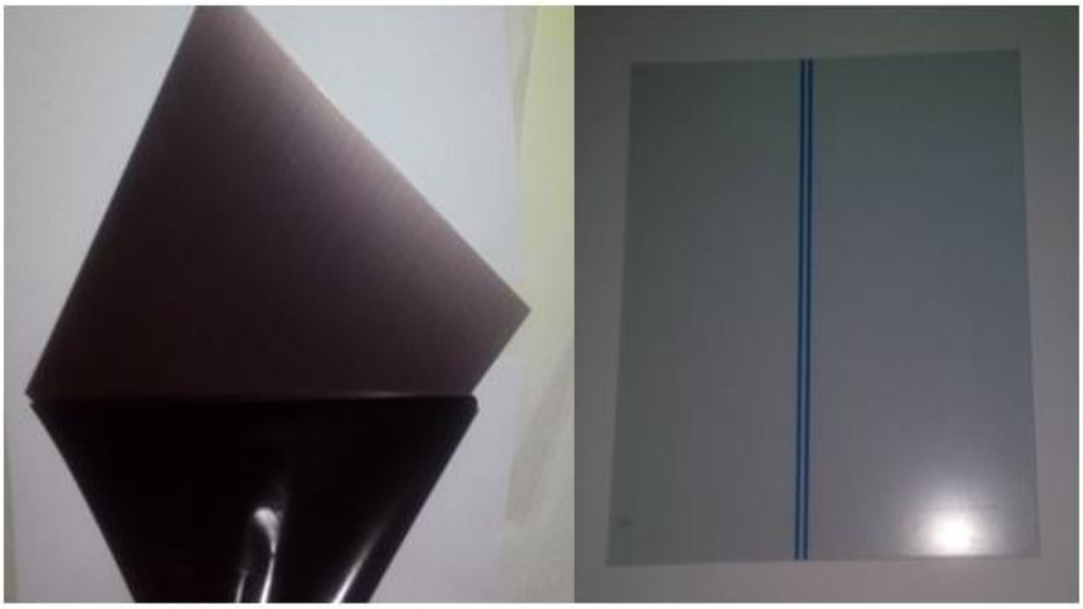

Figure II-16: Printed Circuit Board (PCB).

II.3.3. Classification of PCB

Printed circuit boards can be categorized based on the total number of conductor planes or layers that make up the wiring assembly or structures. One benefit of this board classification scheme is that it is directly linked to the board specifications. The key features that set PCBs apart are described in more depth below:

II.3.3.1. Single Sided Printed Circuit Board

A single sided board is made from rigid laminate consisting of a woven glass epoxy base material clad with copper on one side of varying thickness (Figure II.17).

Figure II-17: Single Sided Printed Circuit Board.

II.3.3.2. Double Sided Printed Circuit Board

Double sided boards are made from the same type of base material clad with copper on two sides of varying thickness (Figure II.18).

Figure II-18: Double Sided Printed Circuit Board.

II.3.3.3. Multi-Layer Board

Multi-layer boards are made from the same base material with copper layer on the top and bottom and one or more “inner layer” cores. The number of “layers” corresponds to the number of copper foil layers (Figure II.19).

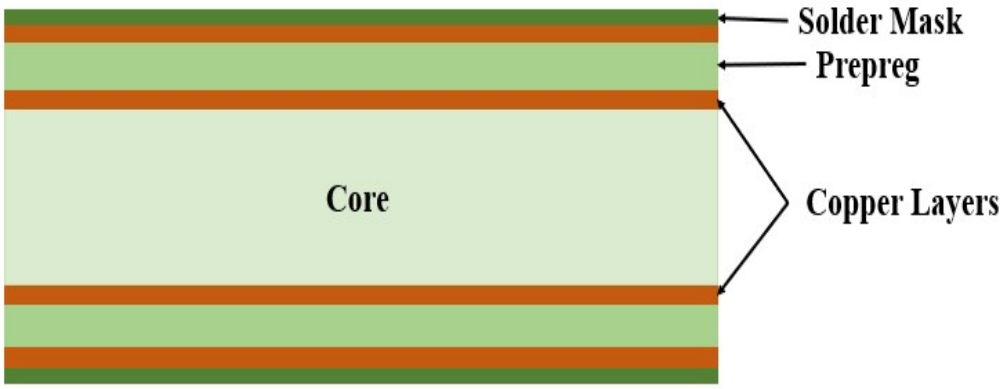

Figure II-19: Multi-Layer Board

II.4. Actuators realized

To study the electro-adhesion force and separation process, two different actuators were realized: a single-sided rotating disk-shaped actuator (SS-RDSA) and a double-sided rotating disk-shaped actuator (DS-RDSA).

II.4.1. Single-Sided Rotating Disk Shape Actuator (SS-RDSA)

The Single-Sided Rotating Disk Shape Actuator (SS-RDSA) realized has a circular shape, and it’s built up using a single-sided Printed Circuit Board (PCB) of thickness 2 mm and diameter 200 mm. On the upper side of the PCB, two interdigitated copper electrodes in the shape of helices, measuring 35 mm in thickness and 1 mm in width, were placed. There is a space of 2 mm between them. In order to avoid electrical breakdown and short circuits between electrodes, an insulating coating of acrylic varnish is also applied on the upper surface of the actuator (Figure II.20).

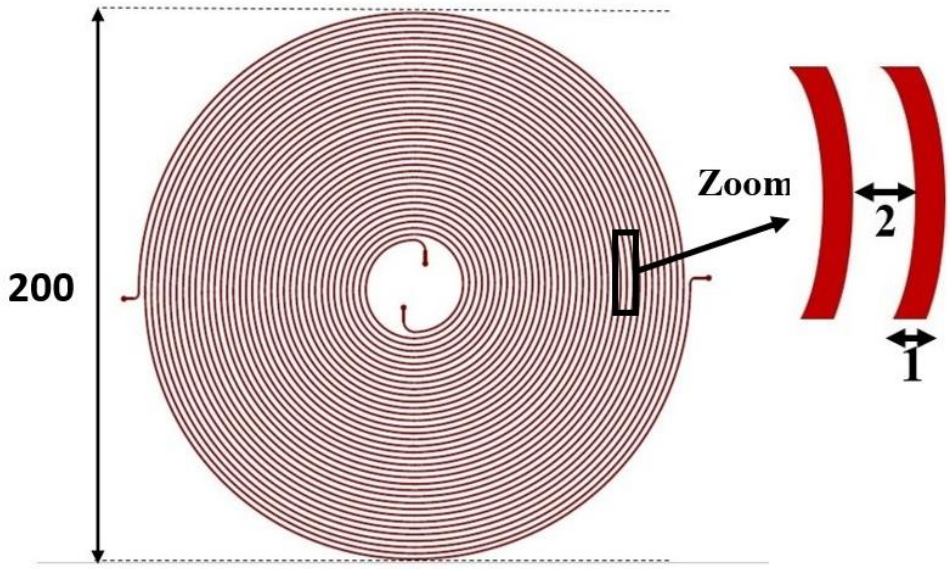

a)

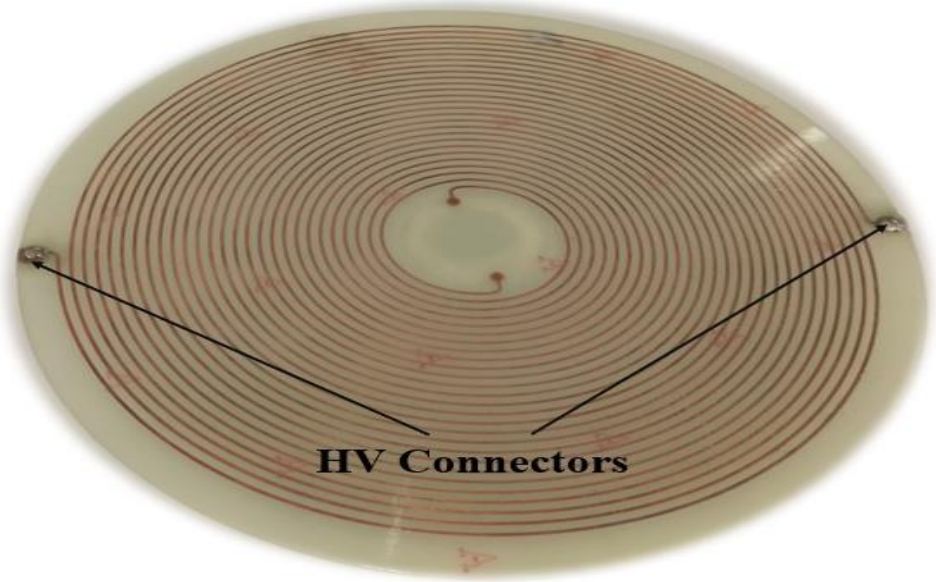

b)

Figure II-20: The Single Sided Rotating Disk Shape Actuator (SS-RDSA).

a) Descriptive schematic (dimensions in mm).

b) Photography of the SS-RDSA.

II.4.2. Double-Sided Rotating Disk Shape Actuator (DS-RDSA)

The Double-Sided Rotating Disk Shape Actuator (DS-RDSA) is made of a double-sided Printed Circuit Board (PCB) that was sliced into a circular shape with a diameter of 200 mm and a thickness of 2 mm (Figure II.21). His top side was covered by a helical shaped electrode of 1 mm width with a gap of 2 mm between adjacent circles, and on his bottom side, a circular plan electrode was used (Figure II.22). The two sides of the actuator were then covered by an insulating acrylic varnish layer to prevent electrical breakdown between the electrode and metal particles.

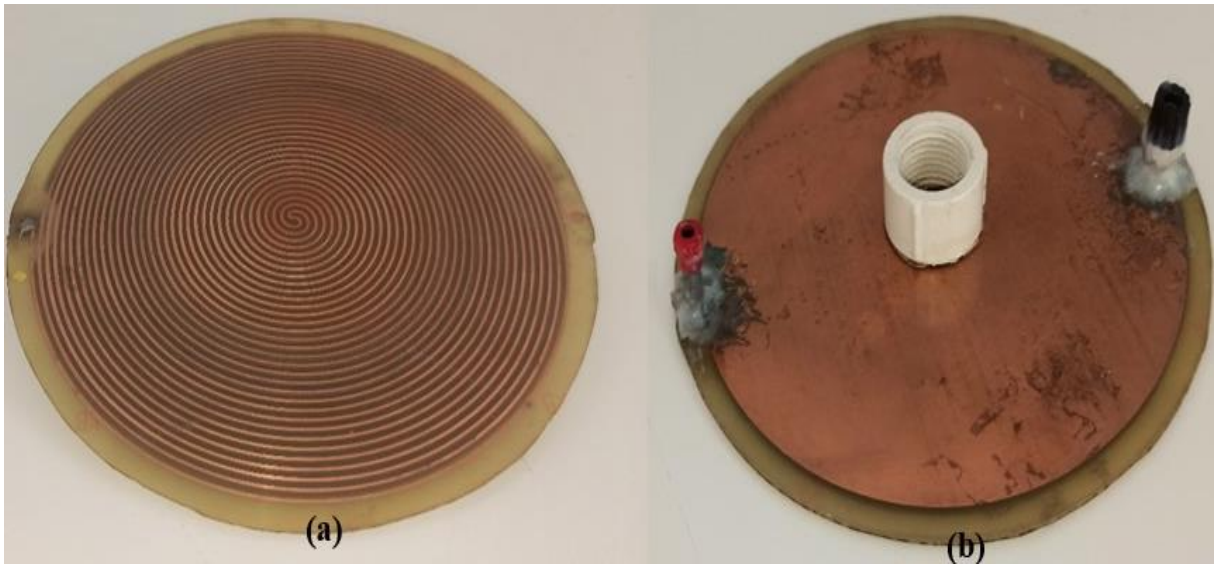

Figure II-21: Photography of the DS-RDSA

a) Top side. **b)** Bottom side.

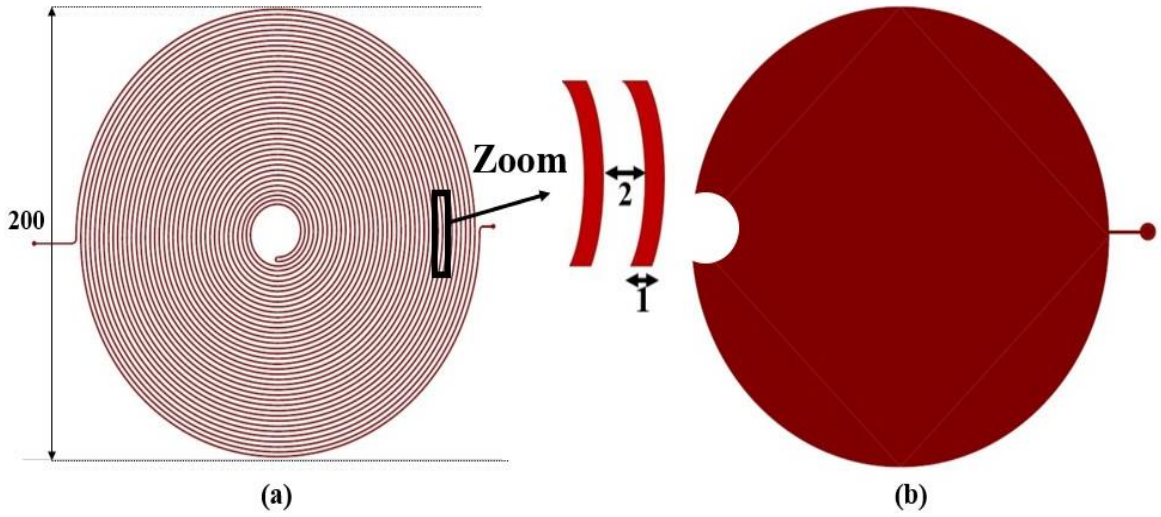

Figure II-22: Descriptive schematic of the DS-RDSA

a) Top side. **b)** Bottom side.

II.5. Employed products

The current study used a mixture of Polyvinyl Chloride (PVC) and Copper particles with an average granulometric size of 2-3 mm retrieved from electrical wire waste (Figure II.23).

In order to evaluate the effectiveness of the separator with larger particles, a larger PVC granular sample was utilized (Figure II.24).

Figure II-23: Smaller-size plastic/metal sample.

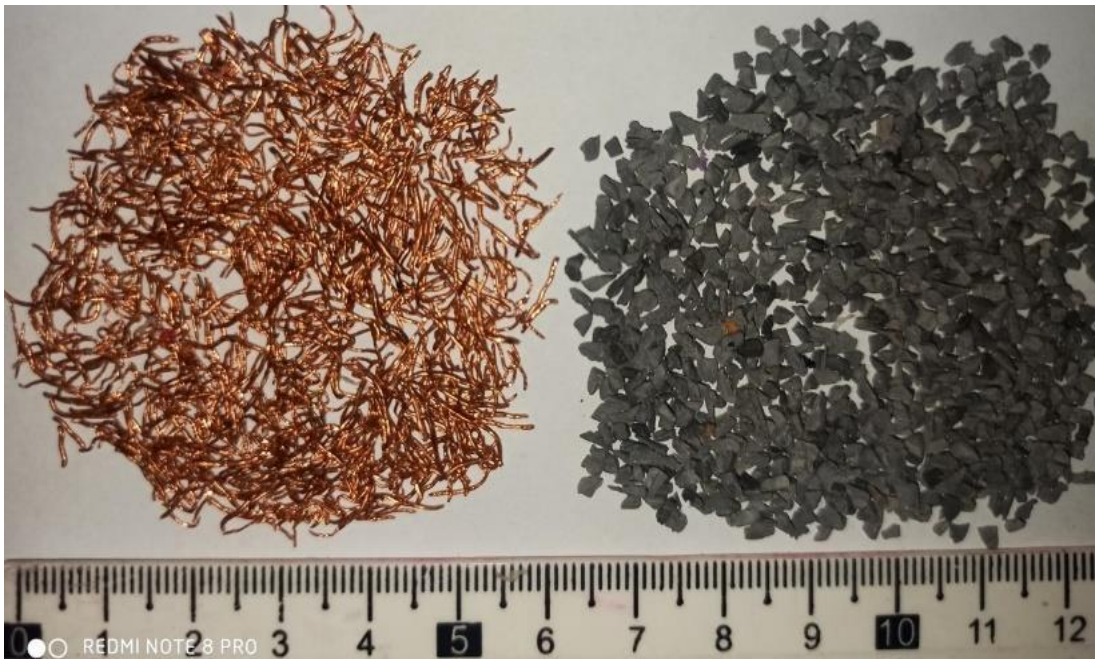

Figure II-24: Bigger size plastic/metal sample.

II.6. Experimental setup

As shown in the Figure II.25, the plastic/metal combination was deposited on the upper actuator's surface using a vibrating feeder with a regulated flow rate. During the separation process, the actuator was rotating using a controlled-speed DC electric motor, while a vacuum blower was employed to remove plastic particles. The metal particles stayed attached to the actuator surface due to the electro-adhesion force, and they were removed and collected in a box using a brush [87].

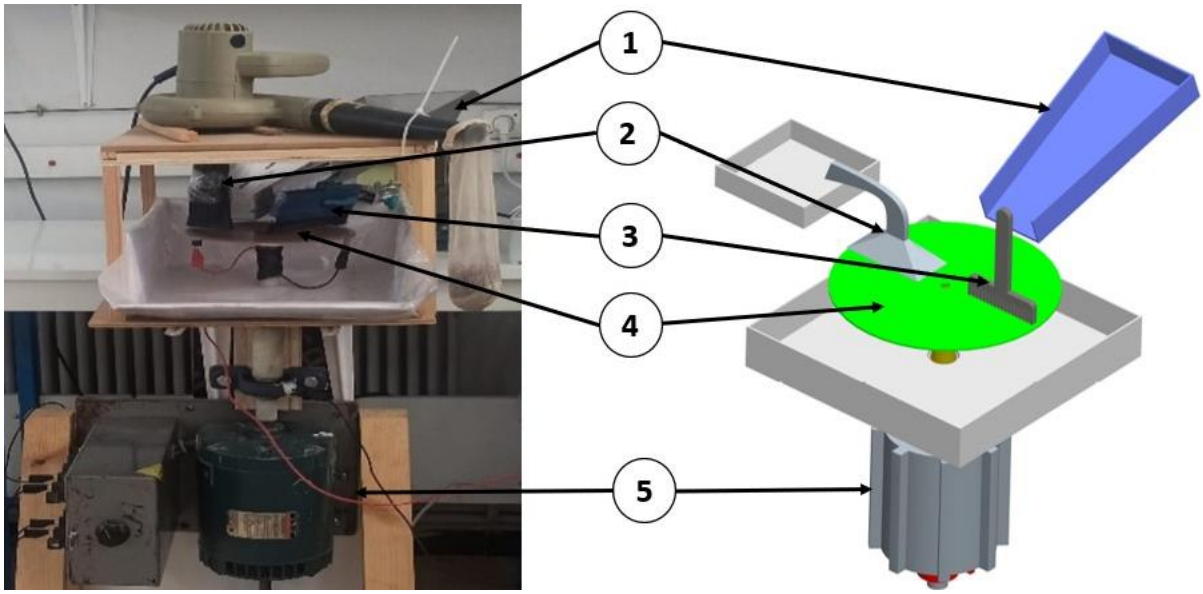

a) General description of the experimental setup.
(1-Vibrating feeder; 2-Vacuum blower; 3- Brush; 4- The actuator; 5-DC motor)

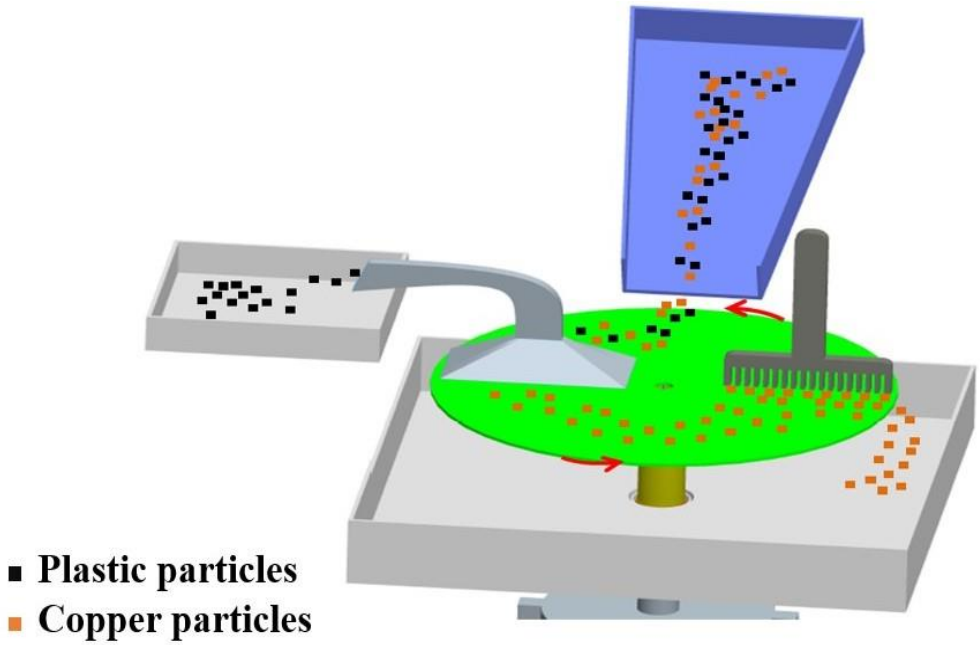

b) Schematic illustration of the separation process.
Figure II-25: The experimental setup.

Figure II-26: The separator device.

Figure II.26 provides a detailed photograph of the separator prototype developed within the APELEC laboratory (Applications of Plasmas, Electrostatics and Electromagnetic Compatibility). The figure offers a global view of the experimental configuration, emphasizing the distinct electrical supplies dedicated to each subsystem. Specifically, the supply of the vacuum blower is responsible for generating the airflow required to extract and transport the plastic particles, while the vibrating feeder supply ensures a continuous and homogeneous distribution of the particulate material onto the actuator surface. In parallel, the DC motor supply drives the mechanical components associated with the brushing and collection mechanism. Finally, the actuator is powered through high-voltage amplifiers, which deliver the electric field necessary to achieve efficient electrostatic separation of the metal and plastic particles.

II.7. Experimental procedure

This research included two sets of experiments. The first focuses on the electro-adhesion force given to copper particles, while the second investigates the possibility of separating metal/plastic particles using a rotating actuator. Each of the experiments were done twice, and the mean value was shown.

II.7.1. Electro-adhesion experiments (without vacuum blower)

In this section, studies were conducted to investigate the effect of the electro-adhesion force on metal particles without the use of a vacuum blower. As already mentioned, the vacuum blower in the experimental setup sucks up plastic particles. As a result, the vacuum blower was

not employed in this part because we were simply studying the electro-adhesion force given to the copper particle.

A 5 g sample of copper particles was initially manually deposited onto the actuator's surface. The actuator was then powered and operated for a duration of 2 minutes. At the end of the experiment, the mass of the copper remaining on the actuator was measured using a digital balance with a precision of 0.1 g and compared to the initial mass of 5 g. The electro-adhesion effect was quantified in percentage by calculating the recovery rate of the copper particles "R_m" using the following formula:

$$R_m(\%) = \left(\frac{M_m}{M_{mt}}\right) \times 100 \qquad \text{(II-1)}$$

where:

- ✓ M_m: Mass of the metal particles remaining on the actuator's surface.
- ✓ M_{mt}: Total mass of the metal particles deposited initially on the actuator's surface, equal to 5 g.

II.7.2. Separation experiments (with vacuum blower)

For these studies, a vibrating feeder was used to deposit a mixture of copper/plastic particles of total mass 10 g, consisting of 50% copper and 50% plastic, on the surface of the actuator. Note that the actuator and vacuum blower activated first, then the vibrating feeder.

The vacuum blower lifted the plastic particles, but the metal particles remained on the actuator's surface until a brush collected them in a collecting box located under the actuator. Because some copper particles may be sucked by the vacuum blower into the plastic product, the recovery rate of the copper collected in its box was compared to the original 5 g put on the actuator using the same previous formula "R_m". In addition, some plastic particles may fall into the copper collection box. We defined a second parameter "P_m" as the purity rate of copper using the following formula:

$$P_m(\%) = \left(\frac{M_m}{M_{mbox}}\right) \times 100 \qquad \text{(II-2)}$$

Where:

- ✓ P_m: Purity rate of the metal product.
- ✓ M_m : Mass of the metal particles collected in its box.
- ✓ M_{mbox}: Total mass of both metal and plastic particles in the collection box of metal.

Conversely, the recovery and purity rates of plastic particles were determined using the following formulas:

$$R_p(\%) = \left(\frac{M_p}{M_{pt}}\right) \times 100 \qquad (\text{II-3})$$

$$P_p(\%) = \left(\frac{M_p}{M_{pbox}}\right) \times 100 \qquad (\text{II-4})$$

Where:

- ✓ R_p : Recovery rate of plastic particles.
- ✓ P_p: Purity rate of plastic particles.
- ✓ M_p : Mass of the plastic sucked up by the vacuum blower.
- ✓ M_{pt}: Total mass of the plastic particles deposited on the actuator's surface (5 g).
- ✓ M_{pbox}: Total mass of both plastic and metal particles in the collection box of plastic.

II.8. Conclusion

In conclusion, this chapter provides an overview of the materials and methods used in this experimental study. first, a simple characteristic presentation of each martial was illustrated. Then, the Proteus software used to design the electrode shapes was presented. After that, the different Print circuit Board used to realize the actuators were described. Finally, the experimental methods and analytic formulas used to evaluate the separator efficiency were explained.

The next chapter will be studying the first actuator, which will be Single Sided Rotating Disk Shape Actuator (SA-RDSA).

Chapter III:
Single -Sided Rotating Disk Shape Actuator

Chapter III: Single Sided Rotating Disk Shape Actuator

III.1. Introduction

Applying electrical forces on charged or polarized particles to sort granular mixtures is a popular material processing technique known by the general name "electrostatic separation.". To meet the needs, several electrostatic separation devices were realized and developed. Each separator works differently under particular conditions and has its own property.
This work focuses on utilizing a rotating disk to realize a new electrostatic separator device. A Single Sided Rotating Disk Shape Actuator (SS-RDSA) will be constructed in this chapter and will be used to analyse the electro adhesion force applied to metal particles. After that, the effectiveness of the separation process will be investigated in order to separate a mixture of plastic and metal using the SS-RDSA.

III.2. Applied voltage waveshapes

III.2.1. TREK supply

(Figure III.1) explains how two high voltage amplifiers (TREK, Model 2220, ±2 kV, ±20 mA) supply the two phases of the SS-RDSA through HV connectors. These amplifiers are controlled by a function generator (SDG Siglent 1025) to alter the voltage level, waveform signal, and frequency applied to each electrode. The signals delivered by the HV amplifiers were visualized using a digital oscilloscope (Gwinstek GDS-3154).

Note that in this study the phase shift between both signals applied to actuator connectors were fixed at 180˚ (Figure III.2).

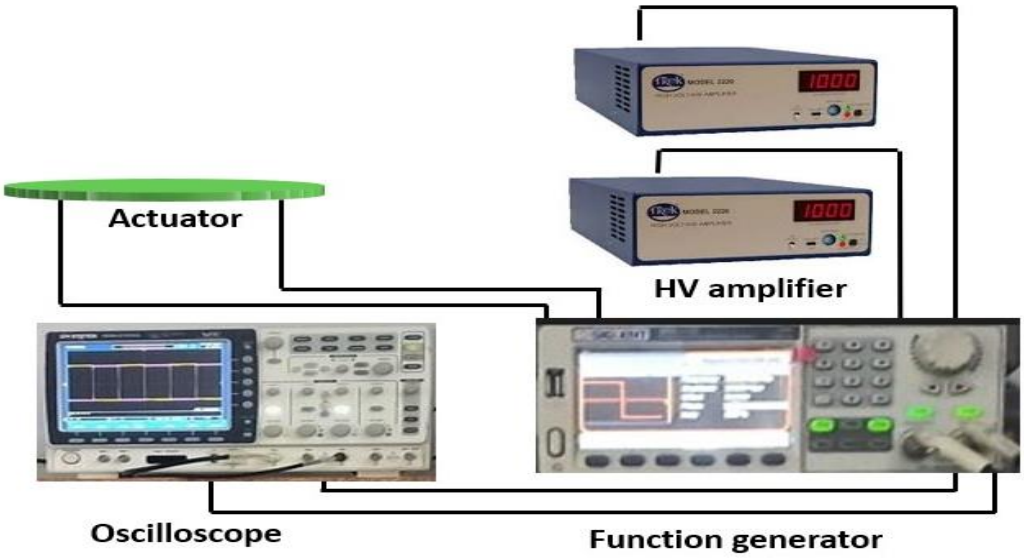

Figure III-1: TREK supply connectors schematic description.

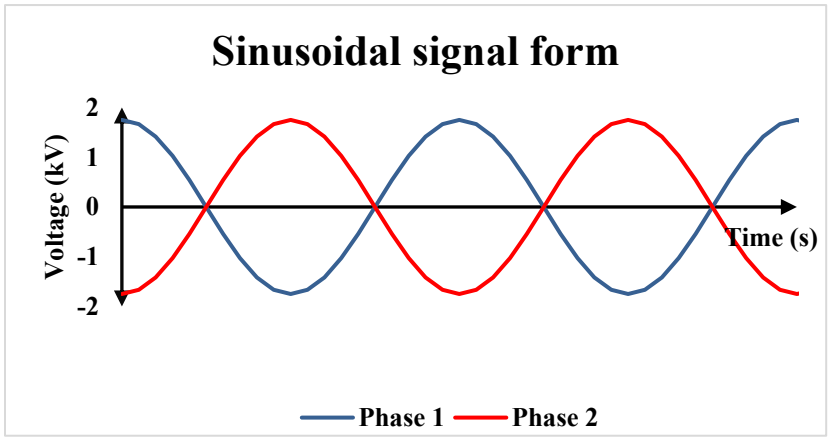

a)

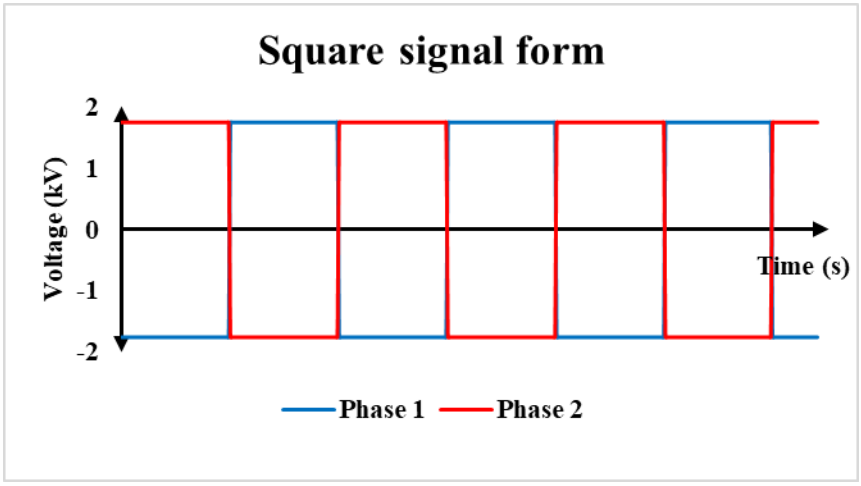

b)

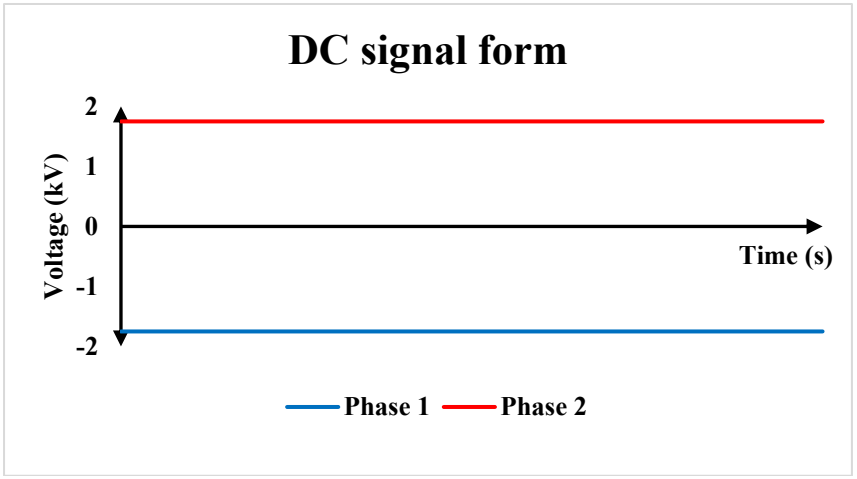

c)

Figure III-2: Voltage signals forms delivered by TREK.

a) Sinusoidal signal form, b) Square signal form and c) DC signal form

III.2.2. DC high voltage power supply

The two SS-RDSA electrodes are shown in (Figure III.3); the first electrode was grounded, while the second was powered by a DC high voltage (positive charge). With the use of a high voltage probe (PVM-1 high voltage probe) and a digital oscilloscope (Gwinstek GDS-3154), the signal produced by the DC high voltage was visualized.

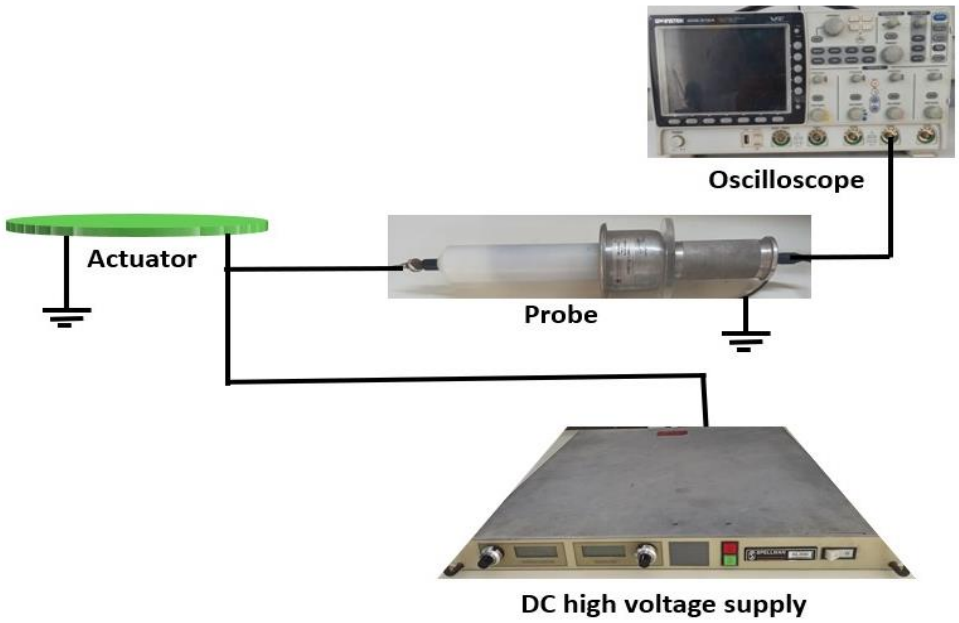

Figure III-3: DC high voltage supply connectors schematic description.

III.3. The SS-RDSA's zones

Due to the difference in centrifugal force, the SS-RDSA was separated into two zones that were examined independently. As shown in (Figure III.4), these zones present by the circular rings with widths of R_1=6cm (Zone 1) and R_2=4 cm (Zone 2).

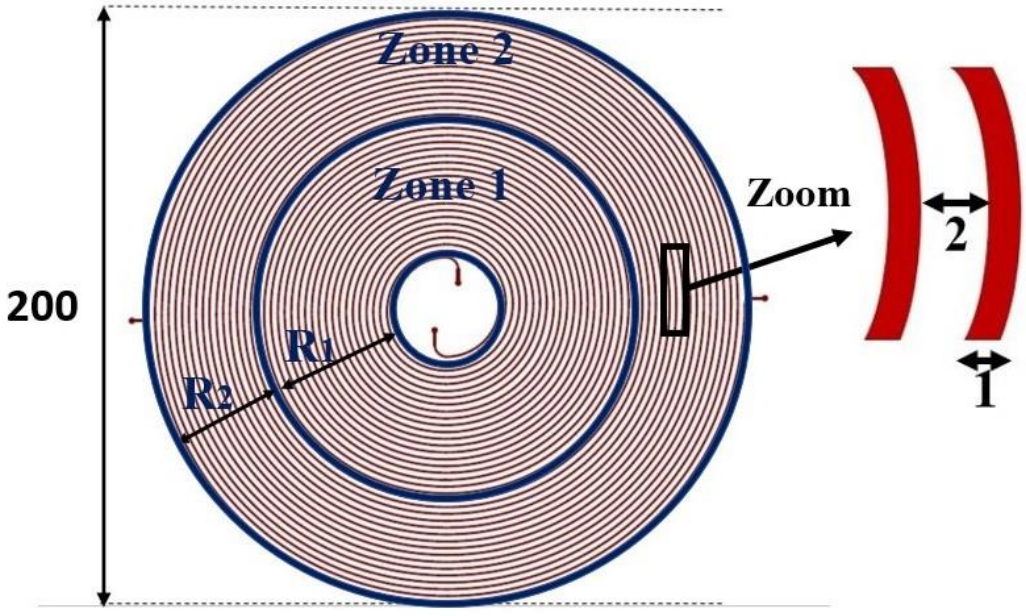

Figure III-4: The SS-RDSA's zones presentation.

III.4. Results and discussion

III.4.1. Electro-adhesion experiments (Without vacuum blower)

Experiments were conducted without the use of the vacuum blower in order to assess the role that electrostatic forces alone play in the adhesion process. Under regulated conditions, this method enables the isolation and evaluation of electro-adhesion's efficacy. The following presents the experimental setup, technique, and observed results.

III.4.1.1. HV amplifier

In this section, the HV amplifier was used to power the SS-RDSA. The frequency effect, applied HV level effect and the rotation speed effect were examined.

a) Frequency effect

In condition of rotation speed equal to 80 rpm, high square voltage of 1.5 kV and in Zone 2, the frequency effect was studied for two range: 1 to 10 Hz (Figure III.5.a) and 10 to 100 Hz (Figure III .5. b).

The plotted results show in Figure III .5 present the variation of the recovery rate (%) of the copper particles still on the SD-RDSA surface as a function of the frequency. These results show that for a square signal, the frequency has no effect on efficiency of adhesion force.

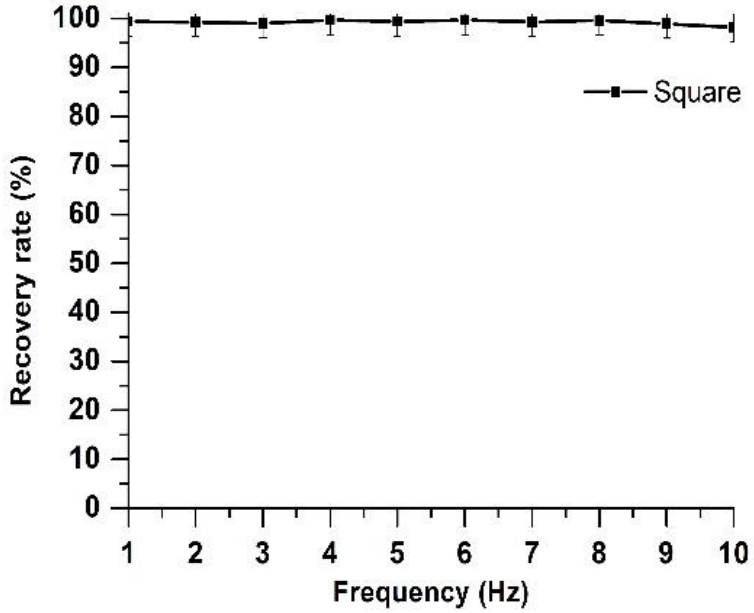

a)

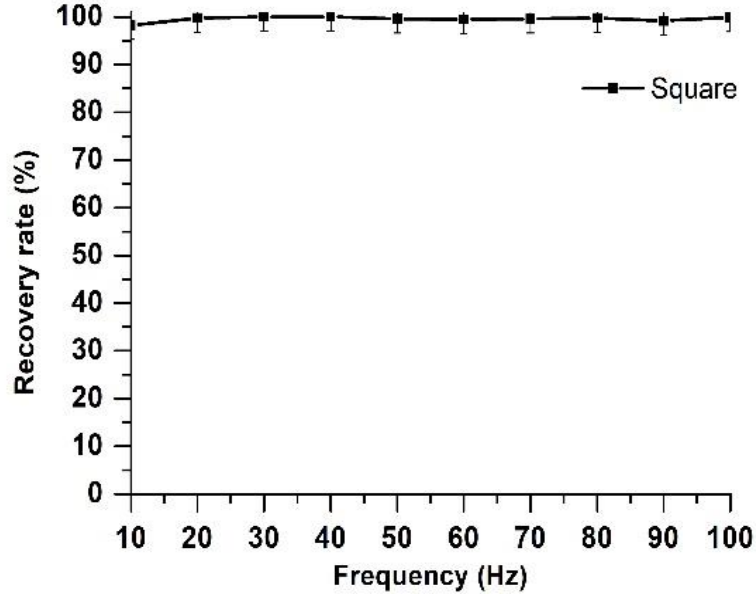

b)

Figure III-5: Variation of the recovery rate (%) of the copper particles still on the SD-RDSA surface as a function of the frequency.

a)1-10 Hz range. **b)** 10-100 Hz range.

b) Applied high voltage effect

In this section, three types of voltage waveform signal (square, sinusoidal and continuous) were applied and compared for two rotation speed values (80 and 120 rpm) for both SS-RDSA's zones (as described in Figure III.4). Note that the frequency was fixed at 30 Hz.

In both zone 1 (Figure III.6) and zone 2 (Figure III.7), the recovery rate variation of the

copper particles R_m that were still adhered on the SS-RDSA's surface was examined based on the applied voltage of three signal forms.

The electro-adhesion force has a considerable influence from the level of applied voltage that causes all copper particles to adhere, as can be seen from the results presented in (Figure III.6) relating to the experiments carried out in zone 1 of the SS-RDSA. regardless of what the voltage signal waveform is, at 80 rpm, the particles adhere at a voltage of 0.5 kV.

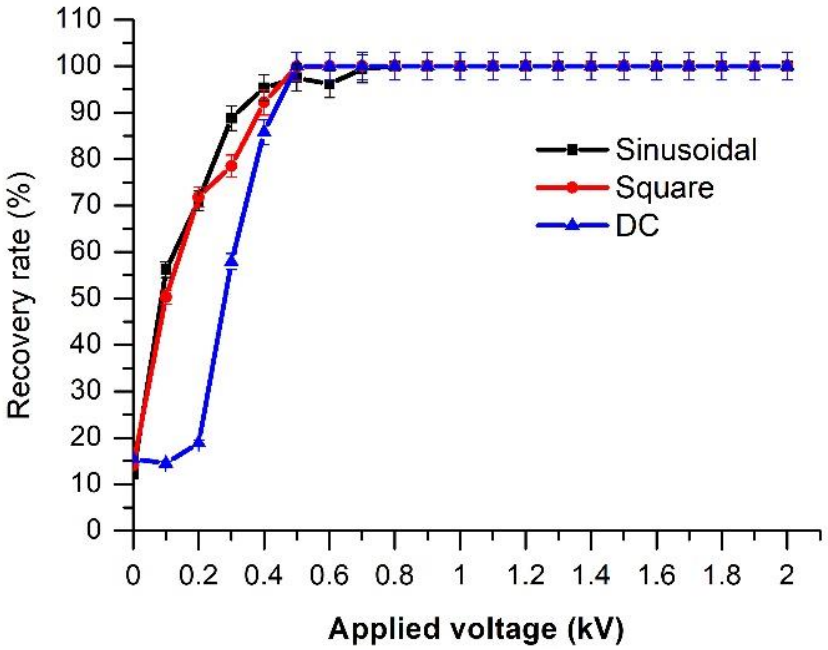

a)

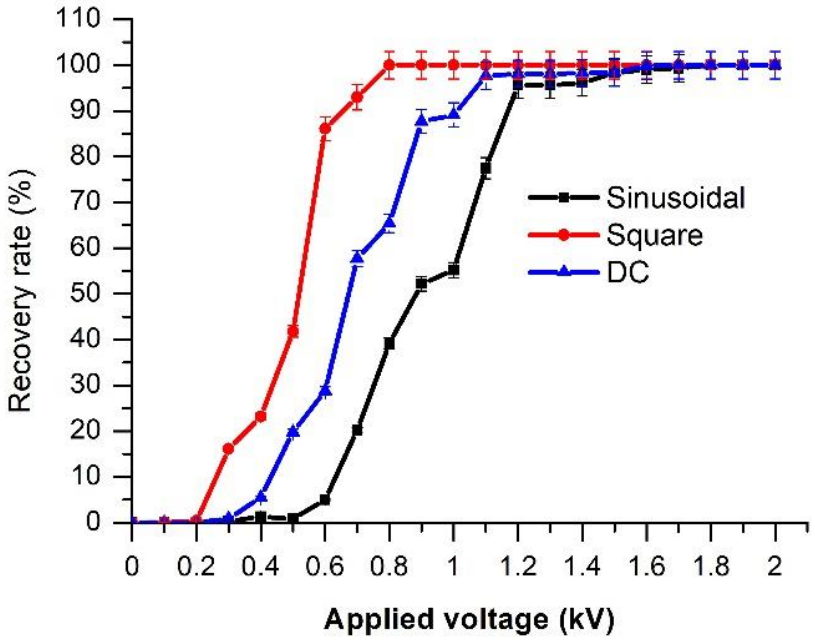

b)

Figure III-6: Variation of the recovery rate (%) of copper particles still on the SS-RDSA surface as a function of the applied voltage for two rotation speeds and the three voltage waveform signals (**Zone 1**).

a) n=80 rpm; b) n=120 rpm.

Fifteen percent of the copper particles on the SS-RDSA are still there at 0V, as seen in (Fig. III.6.a), this happens as a result of the reduced rotation speed in this case (80 rpm), which reduces centrifugal force to an amount that is not strong enough to counteract the pull of gravity exerted on the particles. At 120 rpm, the adhesion force depends on the waveform signal. When the voltage is squared, the electro-adhesion begins at 0.8 kV, giving greater results. The adhesion begins at 1.1 kV and 1.2 kV, respectively, for the DC and AC waveform signals.

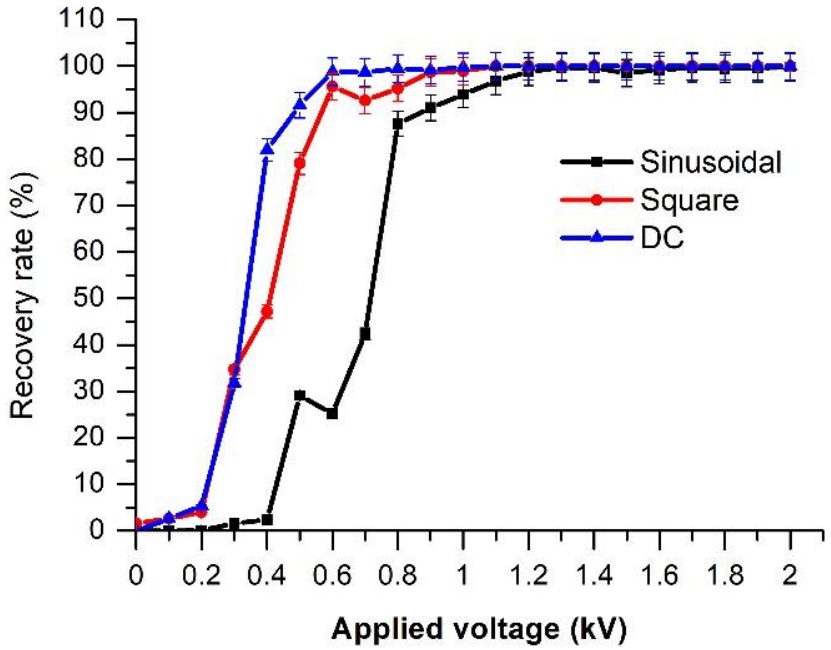

a)

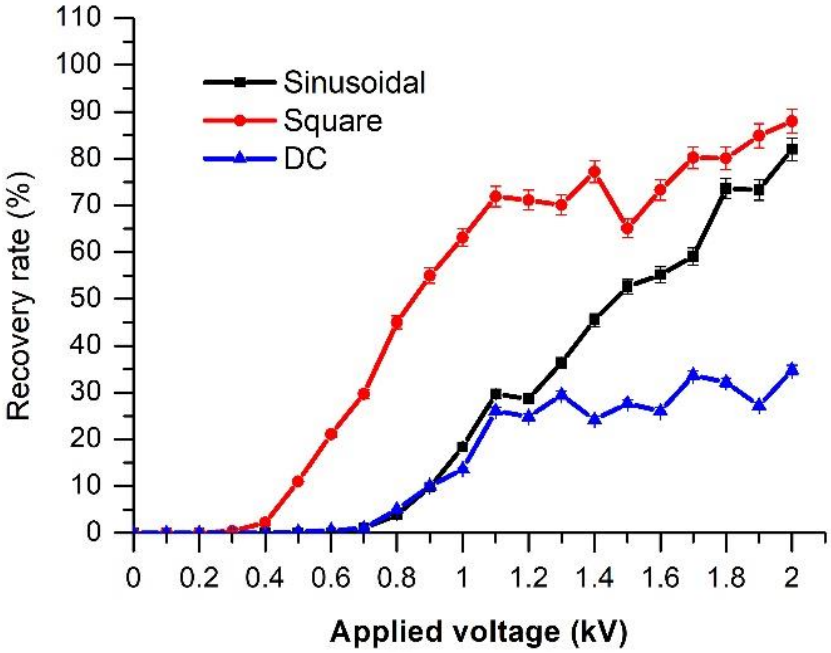

b)

Figure III-7: Variation of the recovery rate (%) of the copper particles still on the SS-RDSA surface as a function of the applied voltage for two rotation speeds and the three voltage waveform signals (**Zone 2**).

a) n=80 rpm; b) n=120 rpm.

Furthermore, it is clear from the results of the experiments executed in zone 2 of the SS-RDSA, which are shown in (Fig. III.7), that the electro-adhesion force plays an important role in this situation as well, but at greater voltages than in zone 1. At a rotation speed of 80 rpm, the influence of the voltage becomes noticeable at 1.2 kV, which permits the attachment of all copper particles. On the other hand, greater voltages would be needed to guarantee the particles adherence at a speed of 120 rpm. It should be mentioned that the actuator's capacitive charging behaviour which is caused by the separation of two electrodes by a dielectric layer is responsible for the decrease in copper particle recovery that was seen while employing DC high voltage.

The capacitor becomes electrically charged when a high DC voltage is given to the electrodes, which makes the metal particles less attracted to one another. This occurs as a result of the particles picking up the electrodes charge polarity. In contrast to the results presented in (Fig.III.6) and (Figure III.7.a), where the electro-adhesion of the particles is greater owing to the reduced centrifugal force, this impact is most visible in zone 2 and for high values of the rotation speed.

c) Rotation speed effect

The variation of the recovery rate of the copper particles that are still on the SS-RDSA surface is shown in (Figure III.8) for the three voltage waveform signals at constant voltage levels (0.6 kV and 2 kV) as a function of rotation speed.

Keep in mind that this portion of the experiment only looks at zone 1. The results show that in order to ensure the best recovery rate at a greater speed, a higher applied voltage level is required. At a voltage of 2 kV, the maximum speed increases to 120 rpm, while at a lesser voltage of 0.6 kV, it is only 80 rpm.

The intensity of the centrifugal force, which is proportionate to the particle's position and the disk's rotation speed, is what causes the influence on particle adhesion. The effectiveness of separation decreases significantly as the radius and rotation speed increase.

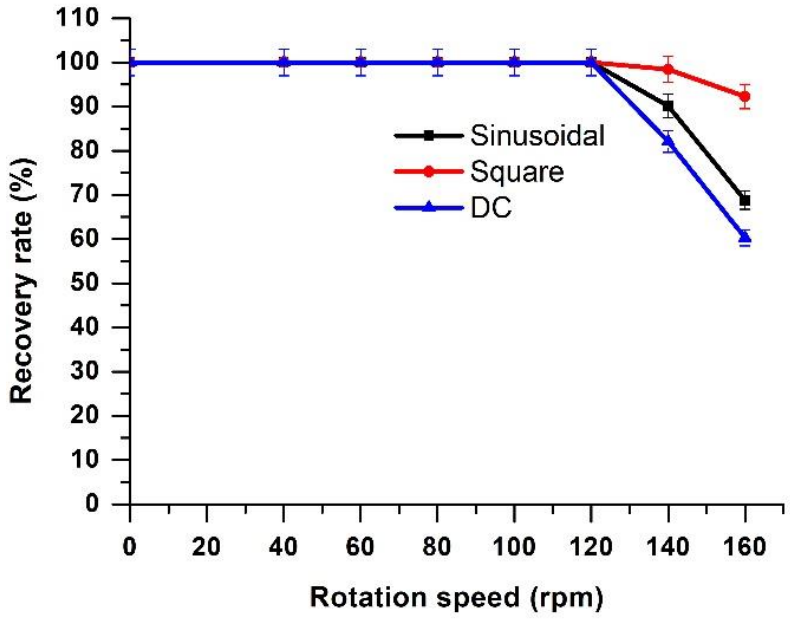

a)

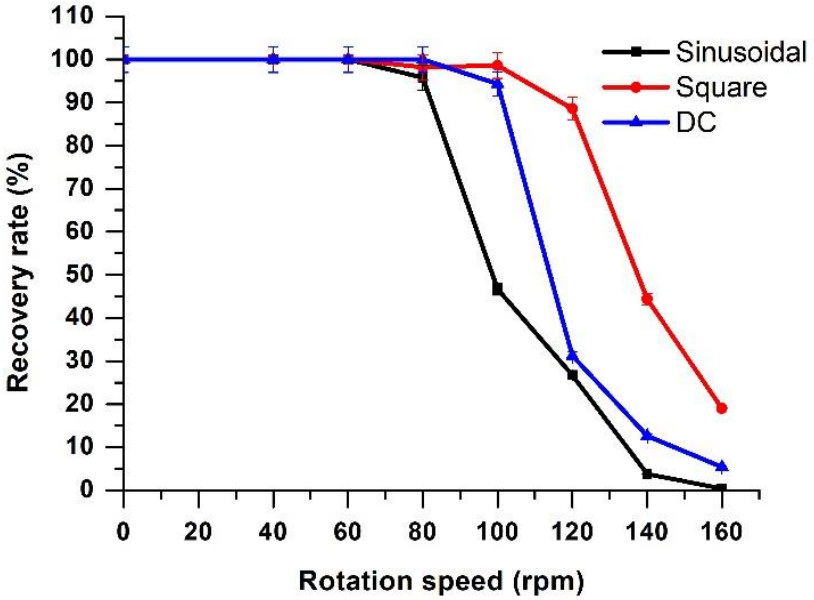

b)

Figure III-8: Variation of the recovery rate (%) of copper particles still on the SS-RDSA surface as a function of the rotational speed for two values of the applied voltage and three waveform signals (Zone 1).

a) V=0.6 kV; b) V=2 kV.

III.4.1.2. DC high voltage power supply

In this part of study, the SS-RDSA was supplied using a positive DC high voltage (SPELLMAN SL300) as described in (Figure III.3).

(Figure III.9) illustrates a variation in recovery rate of the copper particles R_m that remained stuck on the surface of the SS-RDSA in zones 1 and 2, depending on the supplied DC high voltage at two different rotation speeds: 80 and 120 rpm.

The obtained results indicate that in zones 1 and 2, respectively, a maximum recovery rate was achieved at 1 kV and 2 kV of applied DC high voltage for a speed of 80 rpm. Additionally, 2 kV and 3 kV were required in zones 1 and 2, respectively, at a speed of 120 rpm to achieve the maximum recovery rate. As previously mentioned, the intensity of the centrifugal force is the mean cause of particle detachment.

An electro-adhesion force is given to the metal particle when it is on the SS-RDSA due to the electric field created by the potential difference between the electrodes causing the induction of opposing charges on its surface. As seen in (Figure III.10), the action of the electric field produced by two layers of electric charges with opposing polarity causes the electro-adhesion of the copper particles.

Due to the free electron mobility in conductive materials, the adhesion force is only effective on metal particles. A far weaker polarization charge is generated in the case of a plastic particle, one that is insufficient to promote surface adhesion. Therefore, only conductive particles are affected by the attraction force since the polarization charge created in the plastic granules is significantly less. Because of the strong electric fields present at these locations, the particles adhere to the SS-RDSA surface at the contact spots where they make contact with the electrode segment edges [88].

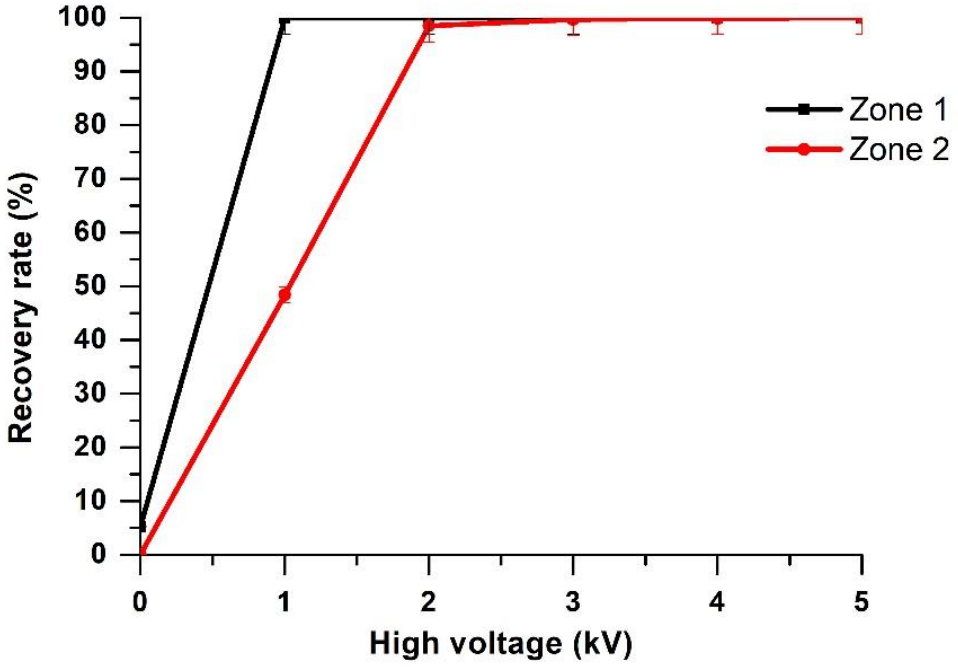

a)

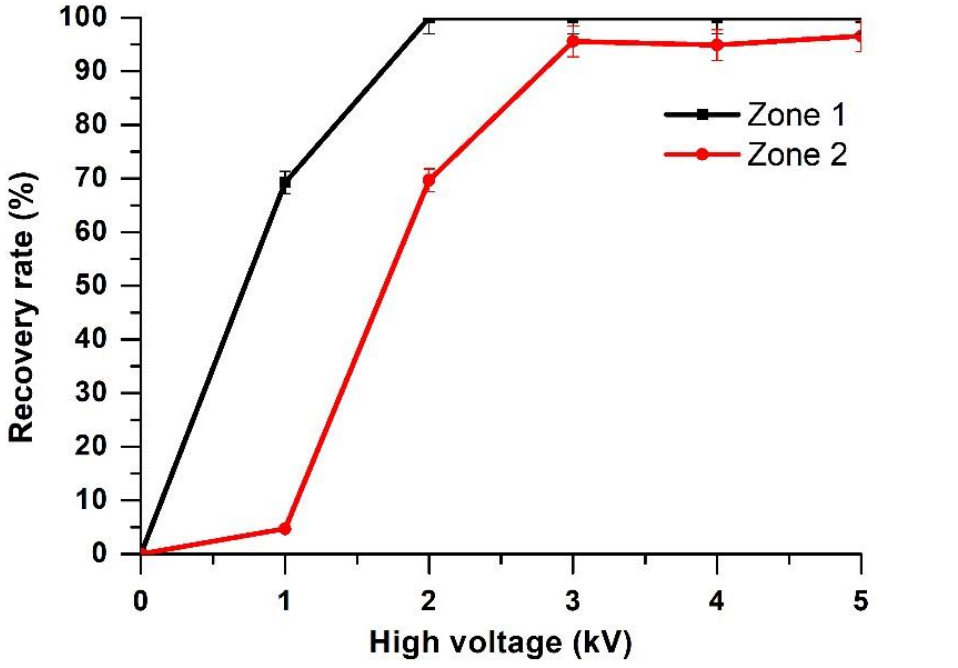

b)

Figure III-9: Variation of the recovery rate (%) of copper particles still on the SS-RDSA surface as a function of the applied DC voltage for two values of rotational speed and two zones.

a) n= 80 rpm; **b)** n= 120 rpm.

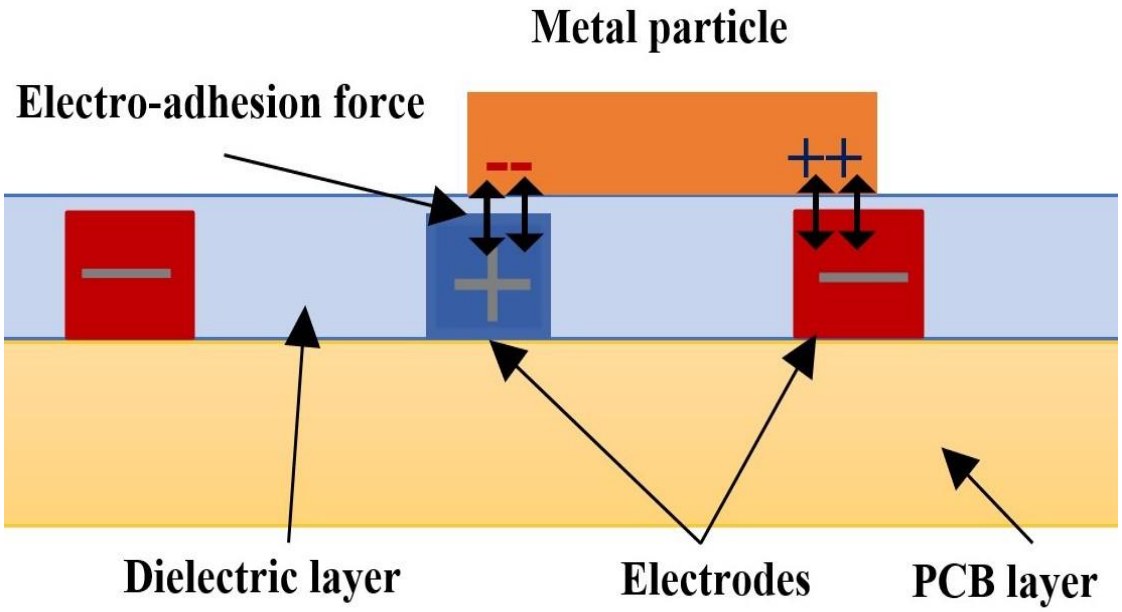

Figure III-10: The force of electro-adhesion exerted on conducting particles.

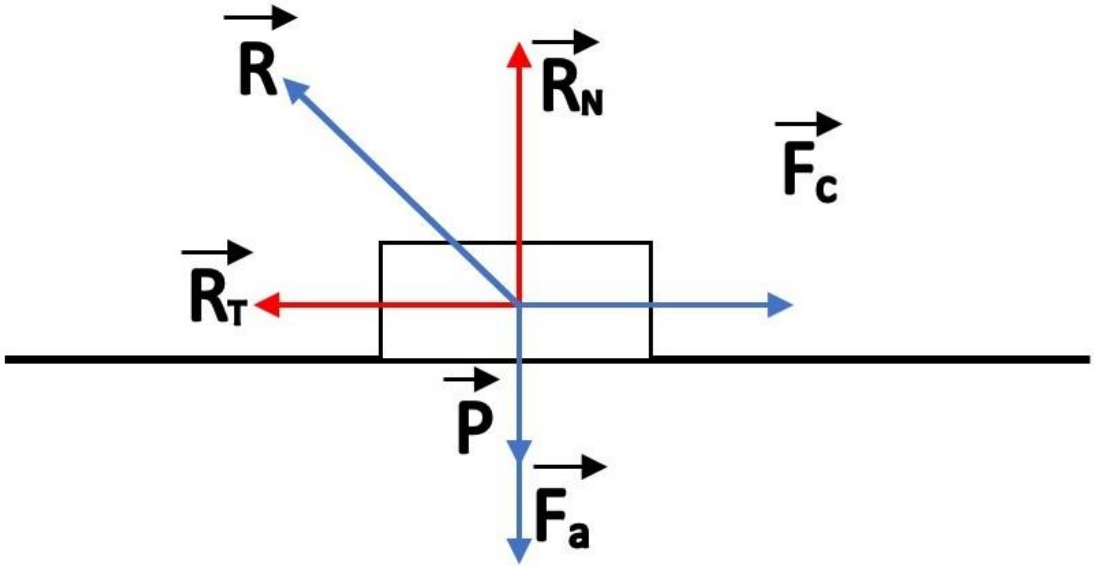

Figure III-11: The forces exerted on the particle.

Several forces are exerted to particle [89], as seen in (Figure III.11). These forces are listed below:

- $P = m.g$: Gravitational force

Were:

- ✓ m: Particle mass.
- ✓ g: Gravitational acceleration.

- R_N: Normal force (normal component of the reaction force).
- R_T: Friction force (tangential component of the reaction force).

The SS-RDSA's influence on the particle is known as its reaction force. In our case, the resultant of the friction force (R_T) and the normal force (R_N) is what represents this force, which

is a result of the contact forces that the SS-RDSA exerts at each place on the particle's surface.

- F_a: Adhesion force
- $F_C = m.r.\omega^2$: Centrifugal force.
  - ✓ ω: Angular velocity at the equilibrium just before detachment of metal piece and with electro-adhesion force (HV supply on).
  - ✓ ω_0: Angular velocity at the equilibrium just before detachment of metal piece and without electro-adhesion force (HV supply off).
  - ✓ μ: Friction coefficient.

Note that a solid enters translational equilibrium when the resultant force exerted on it equals zero, which is known as static equilibrium in physics. In our instance, consideration of the equilibrium condition came right before the particle detached.

In the absence of the adhesion force (the actuator's HV supply off):

$$R_T = F_C \qquad \text{(III-1)}$$

$$R_N = m \times g \qquad \text{III-2)}$$

From (III.1) and (III.2), the friction coefficient can be defined as:

$$\mu = \frac{R_T}{R_N} \qquad \text{(III-3)}$$

Thus:

$$\mu = \frac{r\omega_0^2}{g} \qquad \text{(III-4)}$$

The adhesion force formulas without vacuum blower can be defined by the following equations:

$$R_T = F_C \qquad \text{(III-5)}$$

$$R_N = mg + F_a \qquad \text{(III-6)}$$

$$F_C = \mu.(mg + F_a) \qquad \text{(III-7)}$$

$$F_a = m.g.\left(\frac{\omega^2}{\omega_0^2} - 1\right) \qquad \text{(III-8)}$$

III.4.2. Separation experiments (with vacuum blower)

The (Figure III.12) shows a side view of the experimental setup. The plastic/metal particle mixture was distributed out on the SS-RDSA using a vibrating feeder with a controlled flow rate, the metal particles were adhered to the SS-RDSA surface by the electro-adhesion force. The plastic particles were sucked out using a vacuum blower.

Take note that the zone 2 was used for all of the separation experiments.

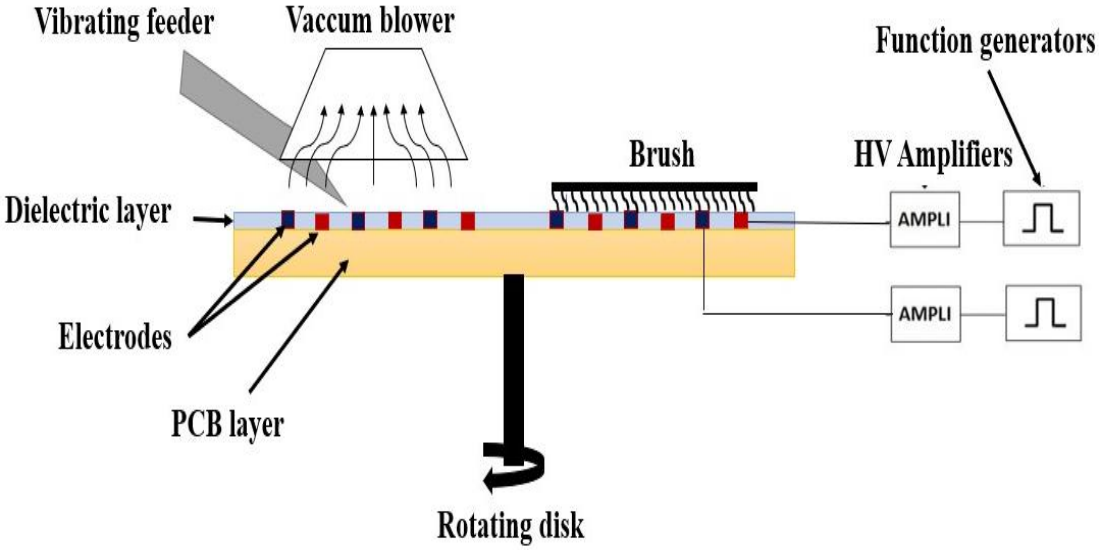

Figure III-12: Side view of the experimental setup.

III.4.2.1. Using a smaller-sized plastic particle

This section of the study used copper and plastic in a multimer size. The effects of the applied HV, ambient humidity, rotation speed, air suction rate, and vibrating feeding rate were examined.

a) Applied high voltage Effect

The following experiments were conducted using the experimental setup shown in (Figure III.12) to separate granular mixture samples with a total mass of 10 g that contained 50% plastic and 50% copper particles in order to analyse the separation efficiency. Fixed parameters for the vibrator feeding rate (D=0.08 g/s), air suction flow rate (Q=1.43 m^3/min), rotation speed (n=60 rpm) and humidity (R=35–40%) were used in this study.

In this section, we chose to use a square signal voltage with a fixed frequency of 30 Hz, in accordance with the earlier results of the electro-adhesion studies conducted with copper particles.

The variation in the recovery and purity rates of plastic and copper particles as a function of applied voltage is illustrated in (Figure III.13). The obtained results validate the impact of the electro adhesion force on the plastic purity and copper recovery, both of which rise with increasing applied voltage. The recovery of copper is seen to grow with voltage, achieving a value around 95% with a maximum purity at an applied voltage of 2 kV. Simultaneously, plastic purity rises to 90% depending on voltage, reaching a maximum at 2 kV. As a result, we observe that the copper purity and plastic recovery using this separation procedure are almost constant and equivalent to 100%.

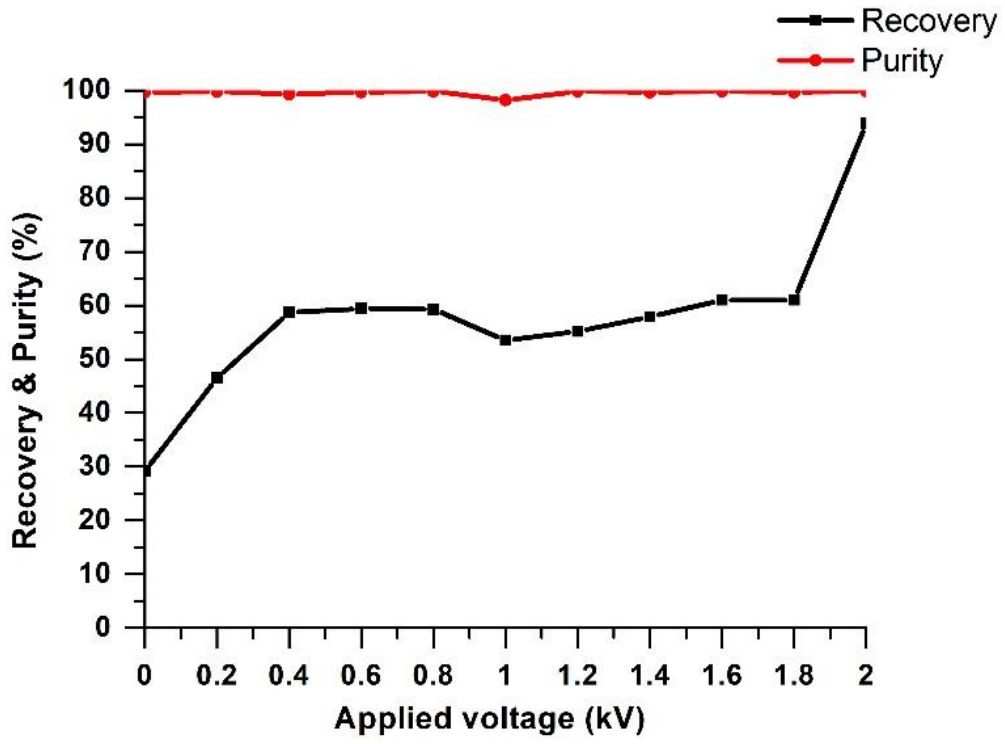

a)

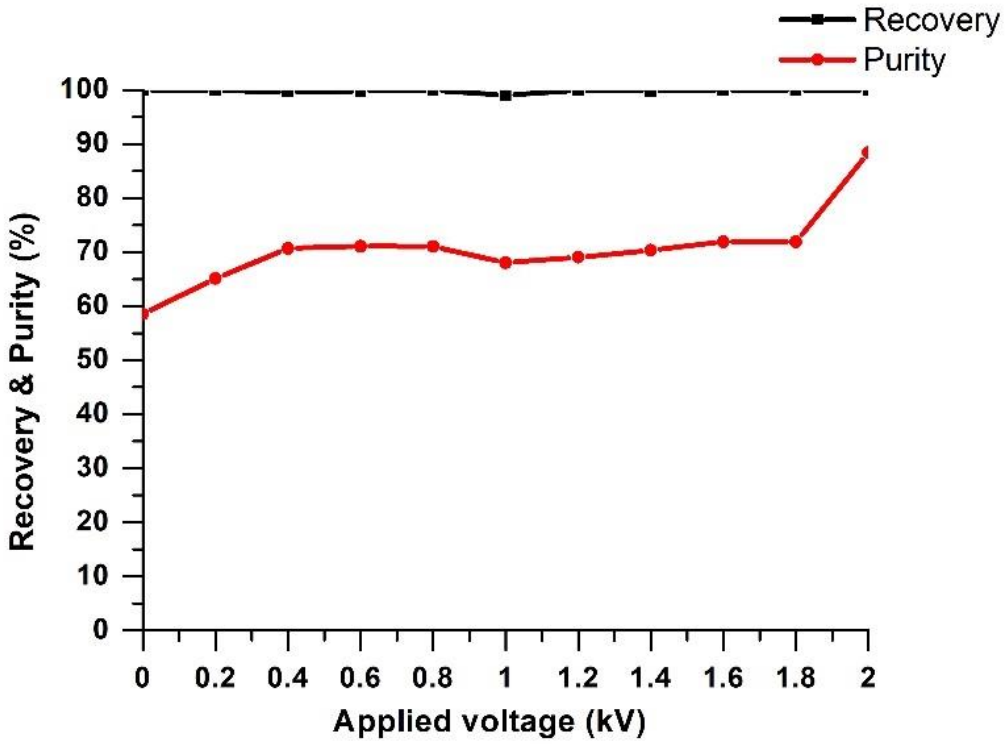

b)

Figure III-13: Variation of the recovery and purity rates of copper and plastic particles as a function of the applied voltage.

Experimental conditions: D=0.08 g/s; Q=1.43m^3/min; n=60 rpm; RH=35–40%.
a) Copper; **b)** Plastic.

This separation device is unique in that it recovers 100% of the plastic product using vacuum blower, making it a 100% recovery rate. But a tiny quantity of copper may also be extracted, which would merely have an impact on the plastic purity. Similarly, when the plastic

is completely recovered using vacuum blower, only the copper particles remain on the SS-RDSA surface, resulting in a 100% copper purity; nevertheless, this recovery may be less due to a tiny quantity of copper that may be sucked out along with the plastic.

It should be noted that the air suction flow rate in this part was larger (1.43 m^3/min) for showing the impact of the applied voltage and the variation between low and high voltage values. For the next experiments, the flow rate was reduced to 1.27 m^3/min in order to optimize separation performance.

b) Humidity Effect

Under identical previous experimental settings, the impact of surrounding humidity was examined to determine how it affected the copper separation process effectiveness, as it is widely recognized that humidity has a detrimental effect on electrostatic separation techniques.
Because it has been noted that vacuum blower recovers the entire amount of plastic, independent of the ambient humidity level, the results pertaining to the plastic product have not been published here.

It should be noted that the experiments were carried out on two distinct days with varying ambient conditions: one day was dry (35–40%), while the other was humid (55–60%).

Compared to electrostatic separators (tribo-electrostatic separator, corona separator), the influence of humidity is actually very advantageous for this separation device, as demonstrated by the results presented in (Figure III.14).

Given the capillary force acting between the particle and the SS-RDSA surface, the layer of water that recovers the surface of copper particles does, in fact, provide them a higher "mechanical" adherence. Observations reveal that even at zero voltage, the copper recovery is nearly at maximum, approaching 95%.

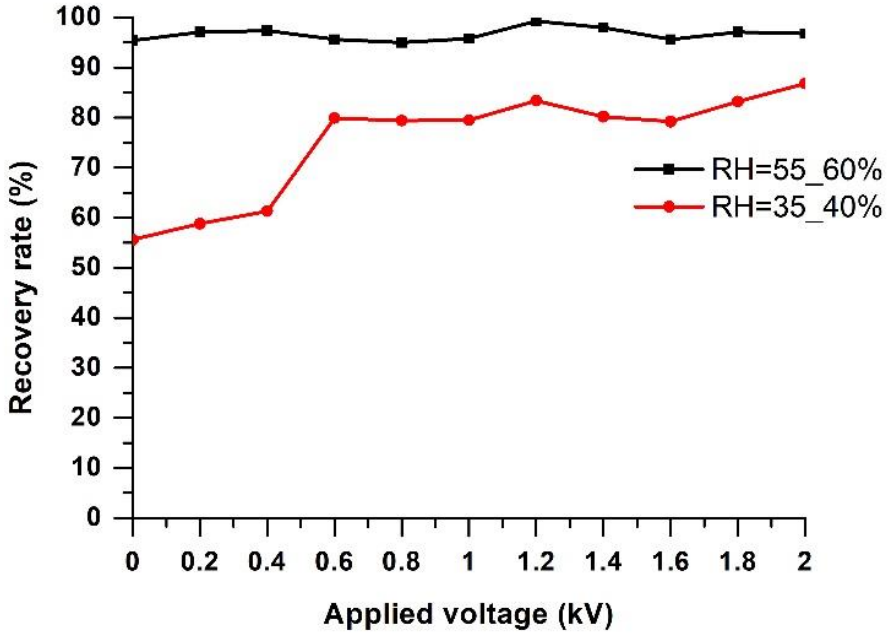

a)

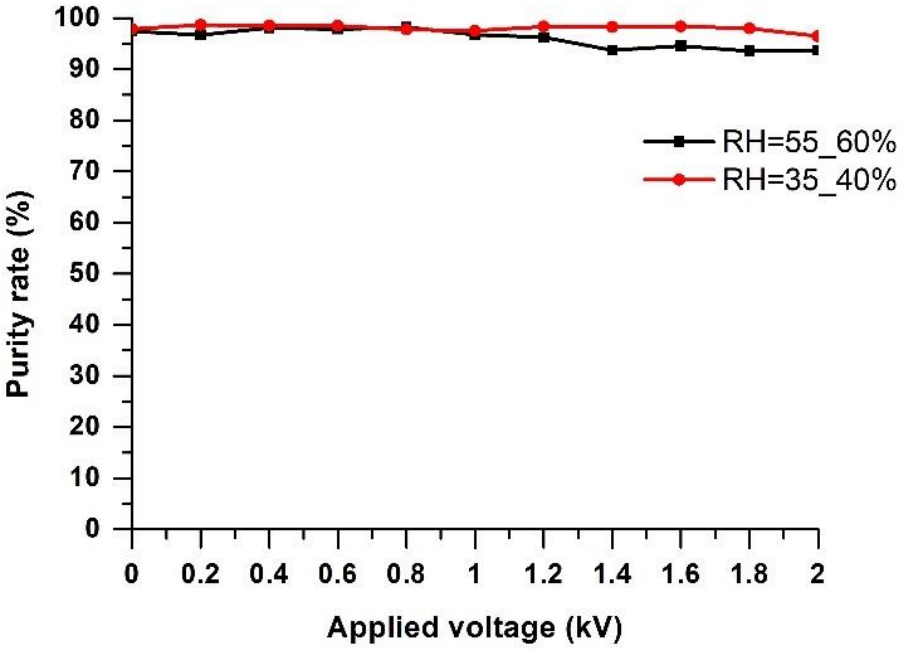

b)

Figure III-14: Variation of the recovery and the purity rates of copper particles as a function of the applied voltage for two values of humidity.

Experimental conditions: D=0.08 g/s; Q=1.27m^3/min; n=80 rpm.
a) Recovery; **b)** Purity.

c) Rotation speed Effect

The variation in the recovery and purity rates of copper and plastic particles as a function of rotation speed is shown in (Figure III.15), with other components (vibration feeding rate D=0.08 g/s; air suction flow rate Q=1.27 m^3/min; V=2 kV; RH=45–50%) held constant. The results that were plotted demonstrate that the separation performance is adversely affected by the rise in centrifugal force that follows from increasing the rotation speed. This is because the copper particles are more readily detached and drawn away by air suction.

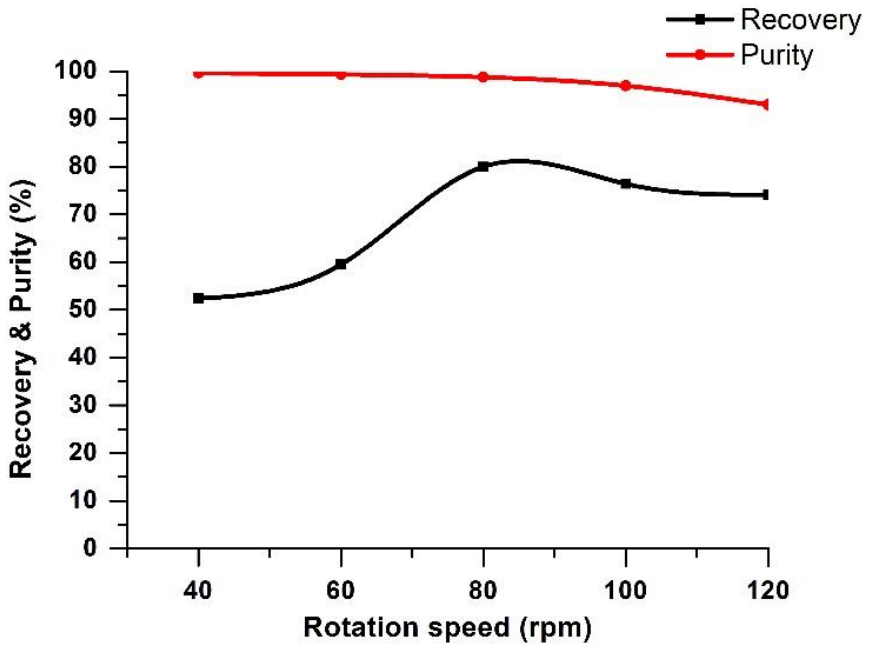

a)

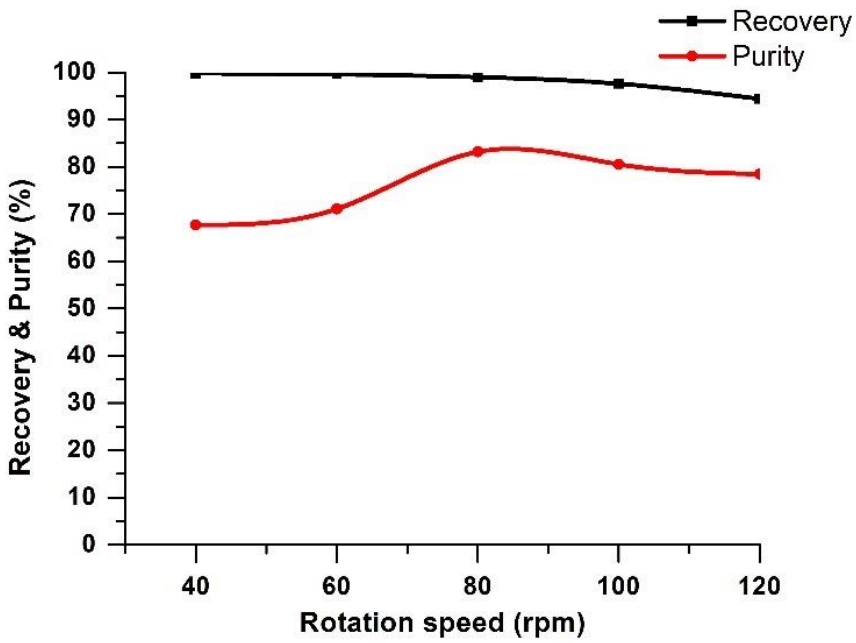

b)

Figure III-15: Variation of the recovery and the purity rates of copper and plastic particles as a function of the rotation speed.

Experimental conditions: D=0.08 g/s; Q=1.27m^3/min; V=2 kV and RH=45–50%.
a) Copper; **b)** Plastic.

d) Air suction flow rate Effect

The impact that the air suction flow rate has on the efficiency of separation was examined in this section. (Figure III.16) illustrates the results gathered, which show how the air suction flow rate affects the copper and plastic particle purity and recovery rates.

The plastic recovery and copper purity will both decline with a reduced air flow rate because some of the plastic product will remain on the actuator surface. The copper recovery and

plastic purity will both drop with a higher flow rate, though, since some copper product will be drawn out. Suction airflow rate should be set at a well-defined value in order to provide optimal separation for both metal and plastic particles at the same time. This ideal value should be sufficient to remove all plastic particles from the air without causing metal particles to aspirate.

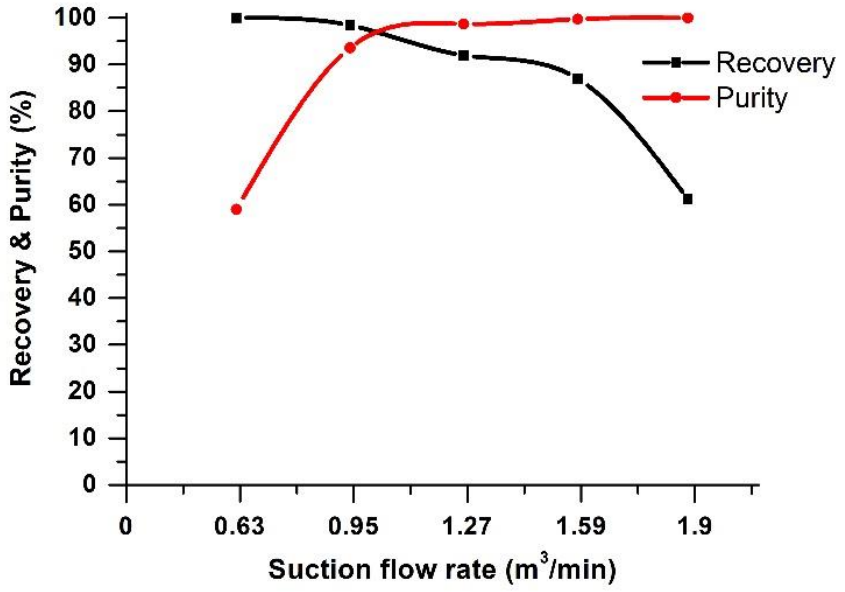

a)

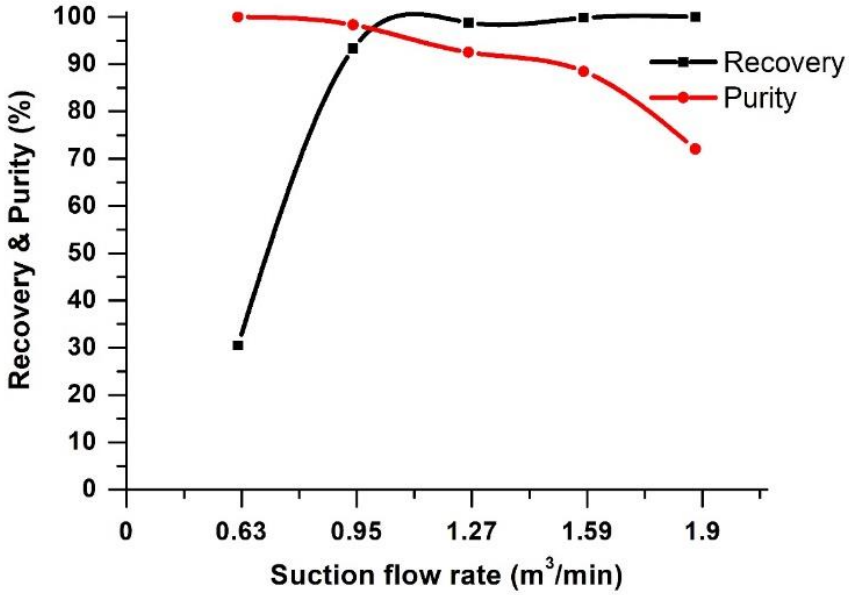

b)

Figure III-16: Variation of the recovery and the purity rates of copper and plastic particles as a function of the air suction flow rate.

Experimental conditions: D=0.08g/s; V=2 kV; n=80 rpm and RH=40–45%.
a) Copper; **b)** Plastic.

The particles typically range from 2 to 3 mm in size, and there is a 2 mm gap between each electrode. As a result, there is a good chance that the particles will make contact with at least one electrode. On the other hand, there can be situations in which the particle is positioned parallel to the electrodes and not in touch with them. The particles may get sucked up with the

plastic particles in these situations as they are not attracted to one other.

e) Vibrator feeding rate effect

Under constant values of other parameters (air suction flow rate Q=1.27m^3/min; rotation speed n=80 rpm; V=2 kV; RH=35–45%), the variation of the recovery and purity rates of copper and plastic particles is illustrated in (Figure III.17).

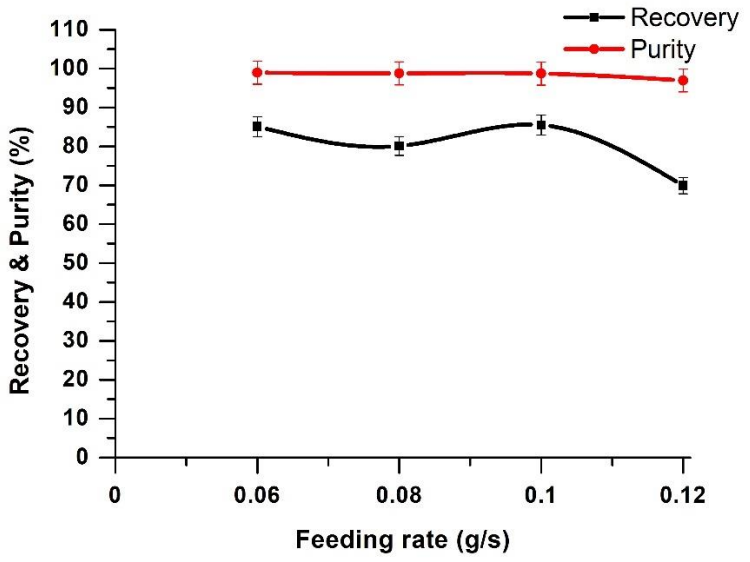

a)

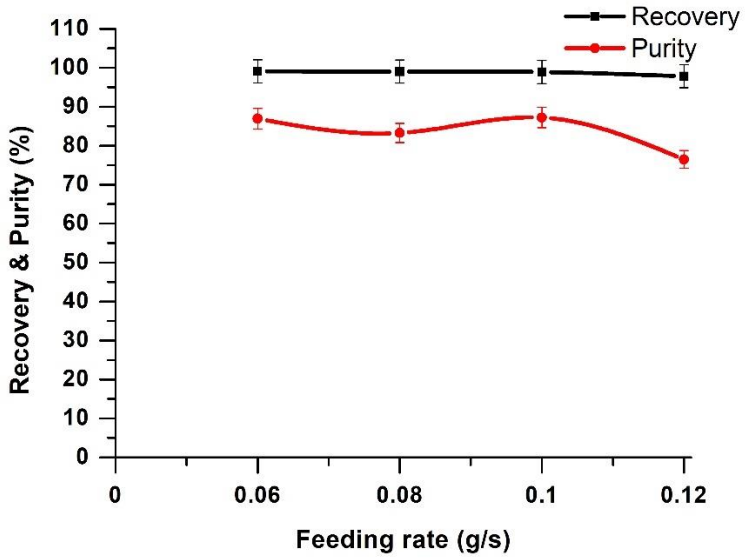

b)

Figure III-17: Variation of the recovery and the purity rates of copper and plastic particles as a function of the vibration feeding rate.

Experimental conditions: Q=1.27m^3/min; RH=40–45%; n=80 rpm; V=2 kV.
a) Copper; **b)** Plastic.

The results show that as flow has increased, performance has decreased noticeably. In fact, the product deposits in several layers as the vibrator feeding rate rises, rendering the separation ineffective.

III.4.2.2. Using a bigger-sized plastic particle

Using a larger plastic particle, more trials were conducted to supplement the earlier tests. This enabled us to compare results with those obtained for smaller particles and see how the electro-adhesion behaviour changed with increasing particle size.

a) Applied high voltage Effect

At condition of vibration feeding rate D=0.08 g/s; air suction flow rate Q=1.43m^3/min; rotation speed n=60 rpm; humidity RH=45–50%, the separation of metal/plastic bigger size particles possibility was examined.

(Figure III.18) presents the variation in the recovery and purity rates of copper and bigger size plastic particles as a function of the applied voltage. In proportion to the plastic purity rate, the metal recovery rate rises to 90% for an applied high voltage equal to 2 kV. Regardless of the voltage that was applied, the rates of plastic recovery and metal purity were set at 90%.

It should be mentioned that in order to suck in bigger plastic particle sizes, a higher air suction flow rate value was selected. Due to capillary force operating between the particle and the SS-RDSA surface discussed before in the humidity effect section, copper recovery was 70% at no voltage applied

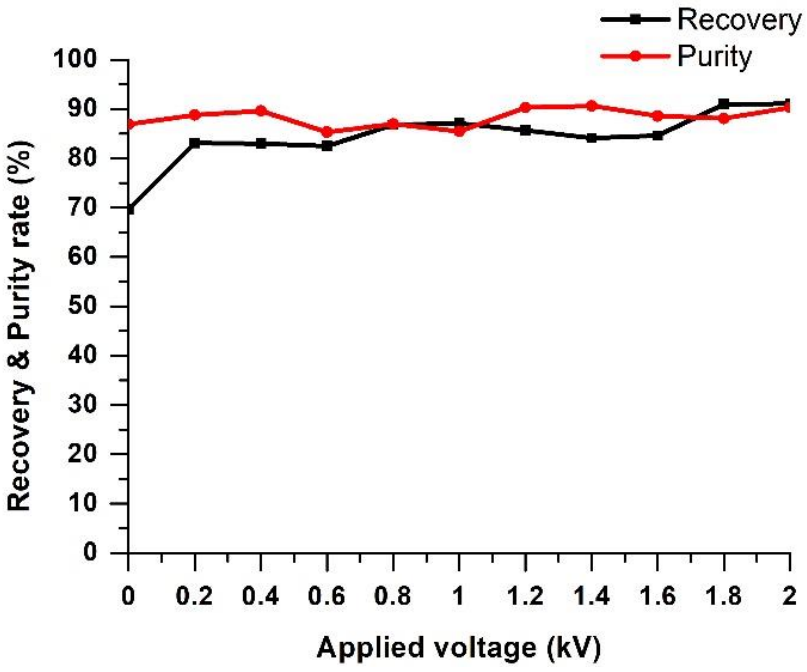

a)

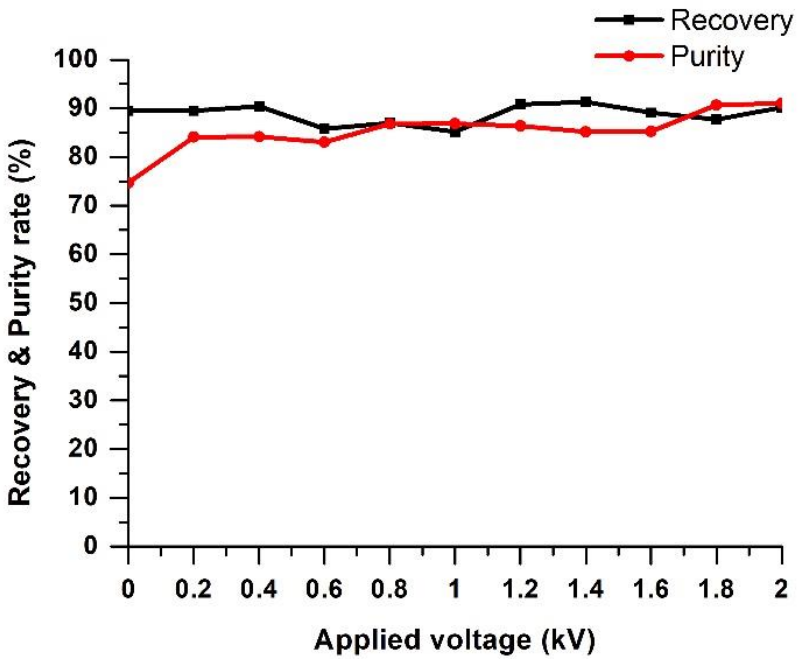

b)

Figure III-18: Variation of the recovery and purity rates of copper and plastic particles as a function of the applied voltage.

Experimental conditions: D=0.08 g/s; Q=1.43m^3/min; n=60 rpm; RH=45–50%.
a) Copper; **b)** Plastic (big size).

III.5. Conclusion

This chapter studied the electro adhesion force applied to metal particles and the efficiency of the separation process for both smaller and larger plastic particles with metal particles using a Single Sided Rotating Disc Shape Actuator (SS-RDSA). The following points were emphasized:

- ✓ More adhesion force is produced by the electric field created by a DC and square-shaped signal than by the sinusoidal signal.
- ✓ Electrostatic separation is carried out based on the air suction force acting on the plastic particles and the electro-adhesion force acting on the metal particles.
- ✓ Remarkable recovery and purity rates were attained, achieving up to 95% and 100%, respectively.
- ✓ The new separation technique is not sensitive to the surrounding humidity within the studied measurement range, compared with traditional electrostatic separation processes.

In the last chapter, a Double-Sided Rotating Disk Shape Actuator (DS-RDSA) will be realized and studied.

Chapter IV:
Double-Sided Rotating Disk Shape Actuator

Chapter IV: Double-Sided Rotating Disk Shape Actuator

IV.1. Introduction

In this chapter, a double-sided rotating disk shape actuator (DS-RDSA) was created using a double-sided printed circuit board (PCB) and it will be used in our separator device. In the first section, the electro-adhesion force will be examined in three zones (1, 2 and 3) and for three different actuator's supplies: TREK supply, midpoint transformer supply, and continuous high voltage supply. The frequency, applied voltage level, and rotation speed effect on the electro-adhesion force will be studied. while second section will be reserved to investigate the separation process of a millimetre and wider-size metal/plastic mixture. The applied voltage level, ambient humidity, rotation speed, suction flower rate and feeding rate effects will be analysed.

IV.2. Applied voltage waveshapes

In addition to the two prior high voltage supplies for the actuator, a midpoint transformer was also employed to power it.

IV.2.1. Midpoint transformer supply (ZM 20/14, Siemens)

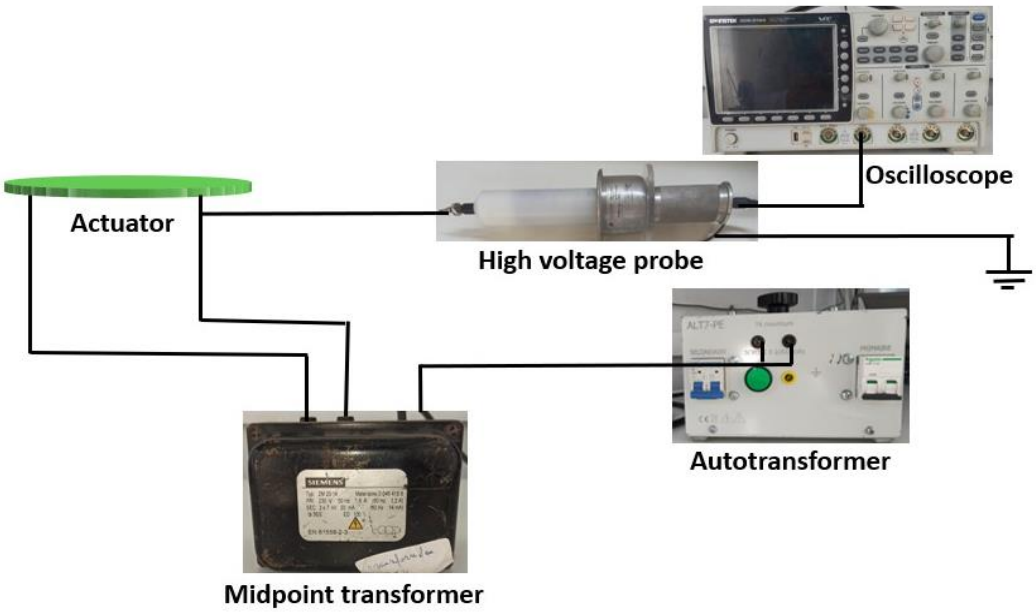

Figure IV-1: Midpoint transformer supply connectors schematic description.

(Figure IV.1) clarifies how a high voltage midpoint transformer (50 Hz ,7 kV and 20 mA) provides the two phases of the DS-RDSA via HV connections. The high voltage amplitude was controlled with an autotransformer (0-250 V) that powered the primary wounding. These signals were visualized with a memory oscilloscope (Gwinstek GDS-3154) employing a high voltage probe (Tektronix P6015A).

IV.3. DS-RDSA's zones

Because of the disparity in centrifugal force, the SS-RDSA was split into three zones and subjected to separate analysis. These zones are shown by the circular rings in Figure IV.2, which have radius of R1=4 cm (Zone 1), R2=3 cm (Zone 2) and, R3=3 cm (Zone 3).

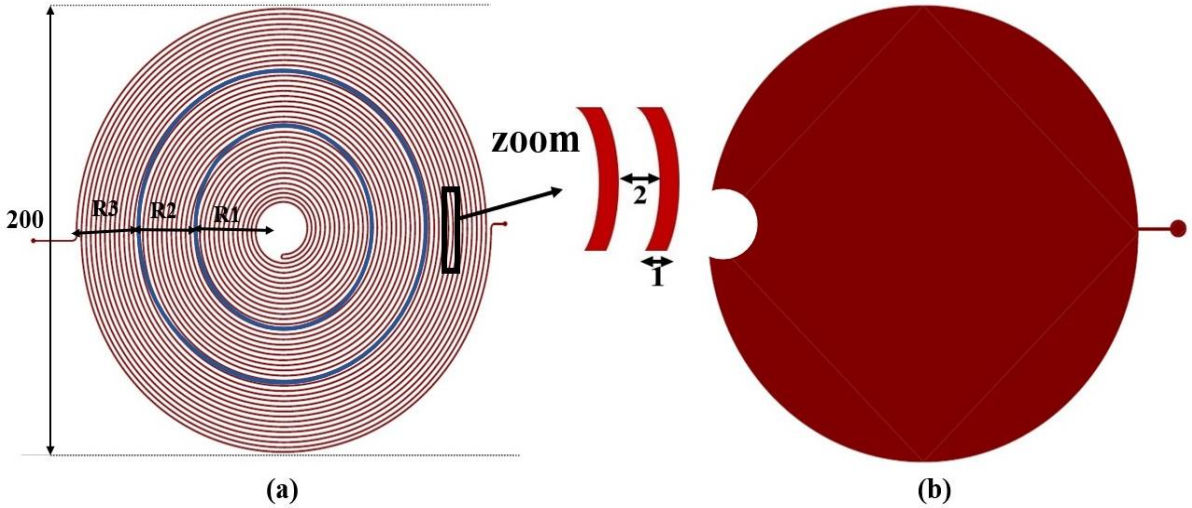

Figure IV-2: The DS-RDSA's zones presentation.

a) Top side; **b)** Bottom side.

IV.4. Results and discussion

IV.4.1. Electro-adhesion experiments (without vacuum blower)

Similar to the last time, the vacuum blower was removed in order to see how the electro adhesion force affected the metal particles.

IV.4.1.1. Experiments with HV amplifier

The DS-RDSA was powered by an HV amplifier during this experimental phase. The effect of frequency, HV level and rotation speed were studied.

a) Frequency effect

In zone 3, a rotation speed of 80 rpm and a hight voltage equal to 1,5 kV the frequency effect was studied for two range: 1 to 10 Hz (Figure IV.3.a) and 10 to 100 Hz (Figure IV.3.b).

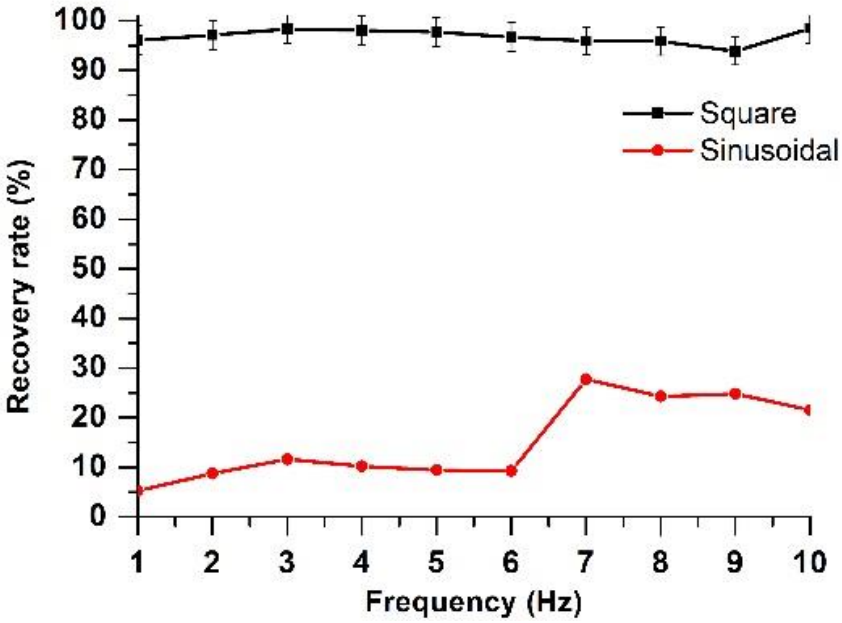

a)

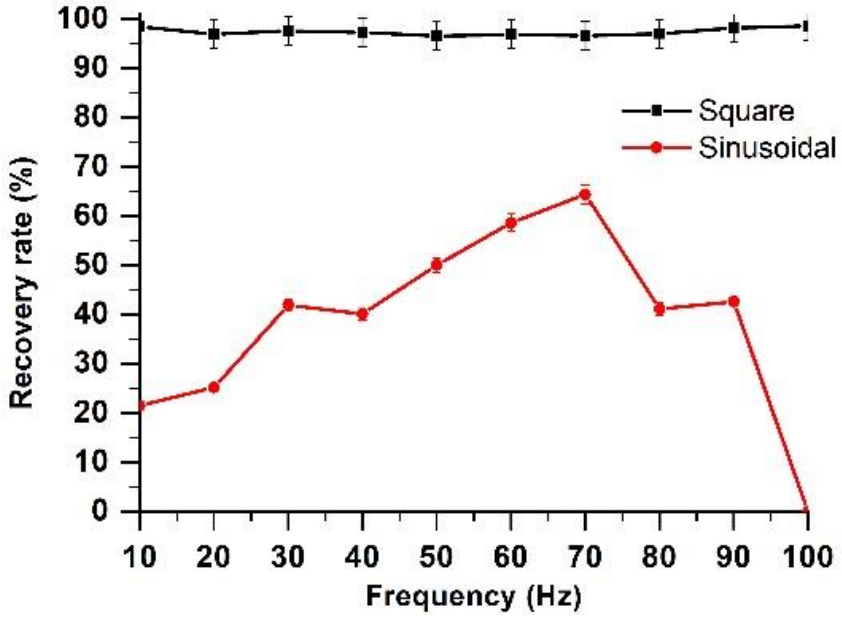

b)

Figure IV-3: Variation of the recovery rate (%) of the copper particles still on the DS-RDSA surface as a function of the frequency.

a) 1-10 Hz range; **b)** 10-100 Hz range.

The results plotted in Figure IV.3 shown that the metal was recovered completely regardless of the frequency value for a square signal. On the other hand, for a sinusoidal signal, the adhesion efficiency rises until 60 % for a frequency equal 70 Hz and then falls to 0%.
The decline in adhesion force observed at high frequencies for the sinusoidal signal can be explained by the signal's transition to a nearly triangular shape at very high frequencies. As the frequency increases, the time required for polarity inversion becomes comparable to the voltage period, leading to a reduction in the efficiency of copper particle attachment to the actuator [90].

b) Applied voltage effect

Based on the high voltage applied, the variation in the recovery rate of the copper particles that stayed attached on the DS-RDSA surface was investigated for two different rotation speeds, n = 80 rpm (Figure IV.4) and n = 120 rpm (Figure IV.5), as well as for three voltage waveform signals (square, sinusoidal and DC) in three zones, 1, 2, and 3 (as described in Figure IV.2). It should be noted that this study used a frequency equal to 30 Hz.

According to research conducted at a speed of 80 rpm, as shown in (Figure IV.4), regardless of the voltage signal waveform, 0.5 kV is required to establish all particle attachment when the product is placed in Zone 1. Furthermore, for square and DC waveform signals, 1.4 kV and 2 kV are needed with the Zones 2 and 3, respectively, to ensure full particle attachment.
Zone 1 and square voltage give the best results at a speed of 120 rpm (Figure IV.5), with electro-adhesion beginning at 1.1 kV.

The disparity in recovery rate of particles was explained by the centrifugal force intensity impact, which was related to the DS-RDSA's rotation speed and radius (Zones) where the product was placed. These factors will therefore have an effect on the separation efficiency [91-92].

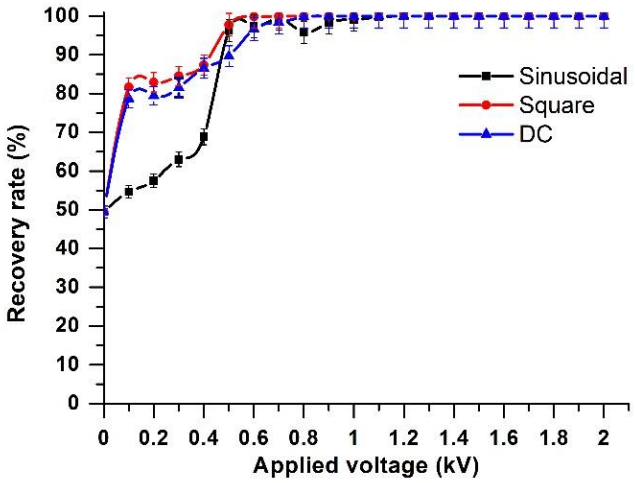

a)

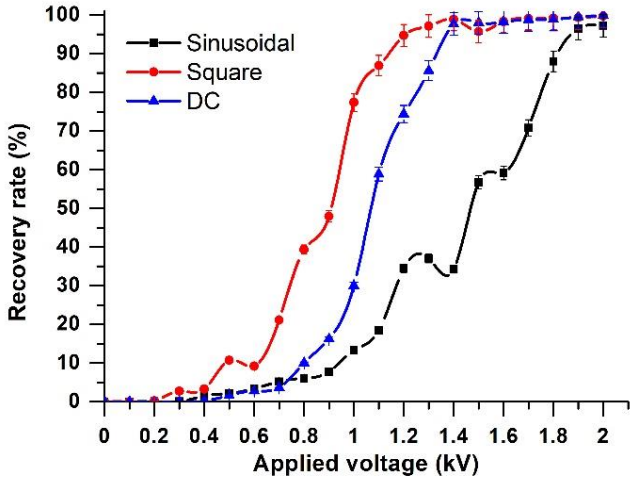

b)

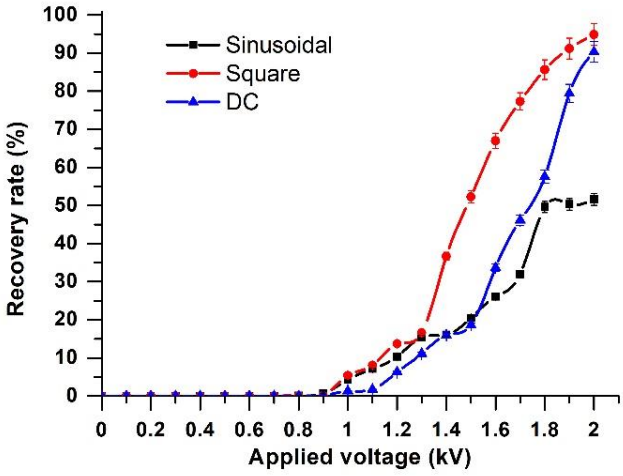

c)

Figure IV-4: Variation of the recovery rate (%) of the copper particles still on the DS-RDSA surface as a function of the applied voltage for three voltage waveform signals in the three zones (n = 80 rpm).

a) Zone 1 ; **b)** Zone 2 and **c)** Zone 3.

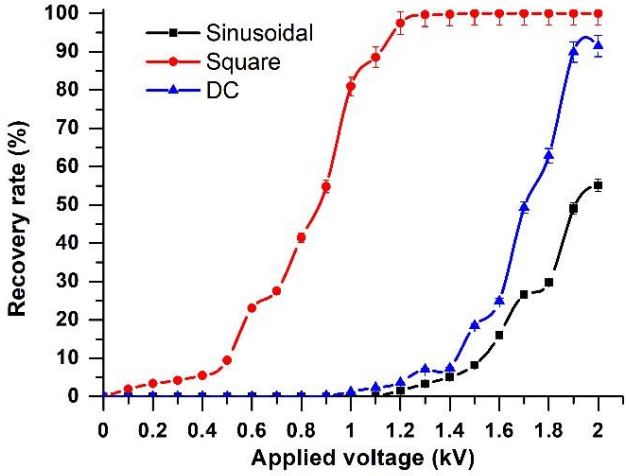

a)

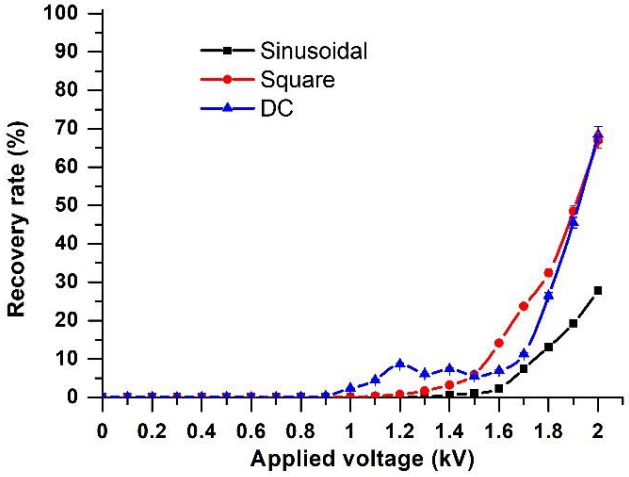

b)

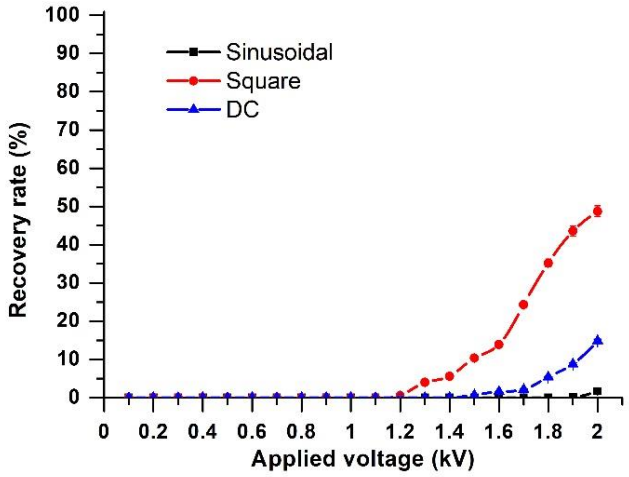

c)

Figure IV-5: Variation of the recovery rate (%) of the copper particles still on the DS-RDSA surface as a function of the applied voltage for three voltage waveform signals in the three zones (n = 120 rpm).

a) Zone 1 ; **b)** Zone 2 and **c)** Zone 3.

c) Rotation speed effect

To study the impact of rotation speed, two experiments were done for two square voltage values (0.6 and 2 kV). Note that these experiments were carried out in Zone 3 and under a frequency equal to 30 Hz.

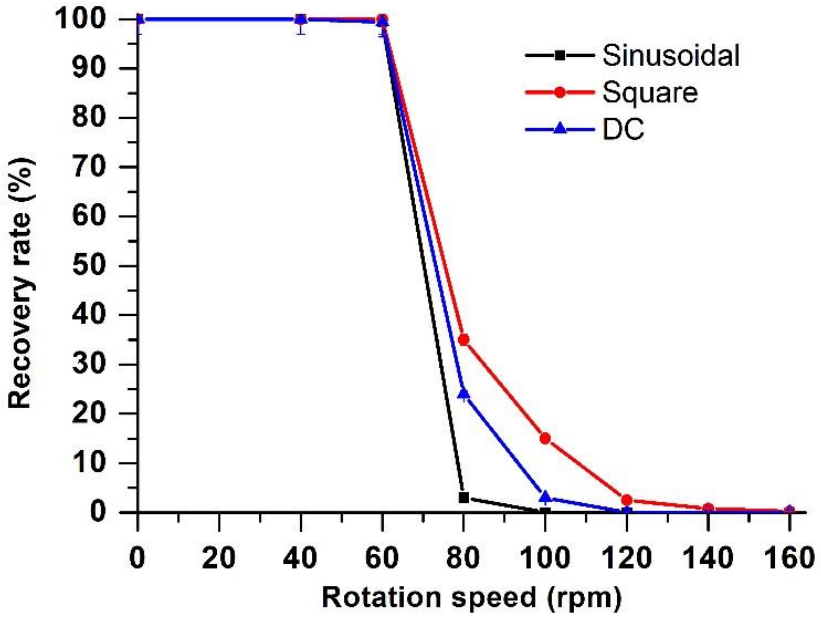

a)

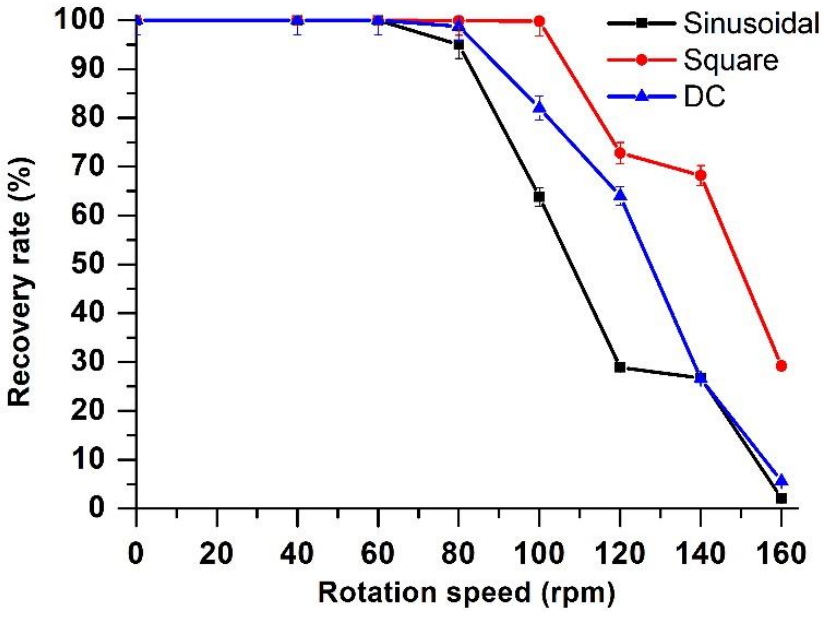

b)

Figure IV-6: Variation of the recovery rate (%) of the copper particles still on the DS-RDSA surface as a function of the rotation speed for three voltage waveform signals in Zone 3.

a) V=0.6 kV; **b)** V= 2 kV.

The results plotted in Figure IV.6 related to the variation of the recovery rate of the copper particles still on the DS-RDSA's surface as a function of the rotation speed for three voltage waveform signals in Zone 3 confirm that the centrifugal force has an impact negative to the metal recovery rate. Because when the centrifugal force increases the metal particles detached easily from the actuator's surface.

IV.4.1.2. Experiments with transformer

In order to see the sinusoidal HV effect, the DS-RDSA was powered by a transformer during these experiments phase.

a) Applied high voltage effect

This section was reserved to study the electro-adhesion force using a midpoint transformer supply (ZM 20/14, Siemens) that delivers a maximum sinusoidal high voltage equal to 7 kV with a frequency of 50 Hz.

(Figure IV.7) presents the obtained results of the recovery rate (%) of the copper particles still on the DS-RDSA surface as a function of the applied voltage delivered by the midpoint transformer for two rotation speeds of 80 and 120 rpm in three zones. These results show that for a rotation speed equal to 80 rpm, the metal particles were recovered totally for a maximum applied voltage of 0.5, 1, and 3 kV in zones 1, 2, and 3, respectively (Figure IV.7.a).

For a rotation speed of 120 rpm, the total recovery of metal particles was obtained for a maximal applied voltage of 2 and 5 kV in zones 1 and 2 (Figure IV.7.b). Note that the absence of results in zone 3 for an applied voltage of 5 kV was explained by the breakdown between metal particles and the bottom electrode of the actuator.

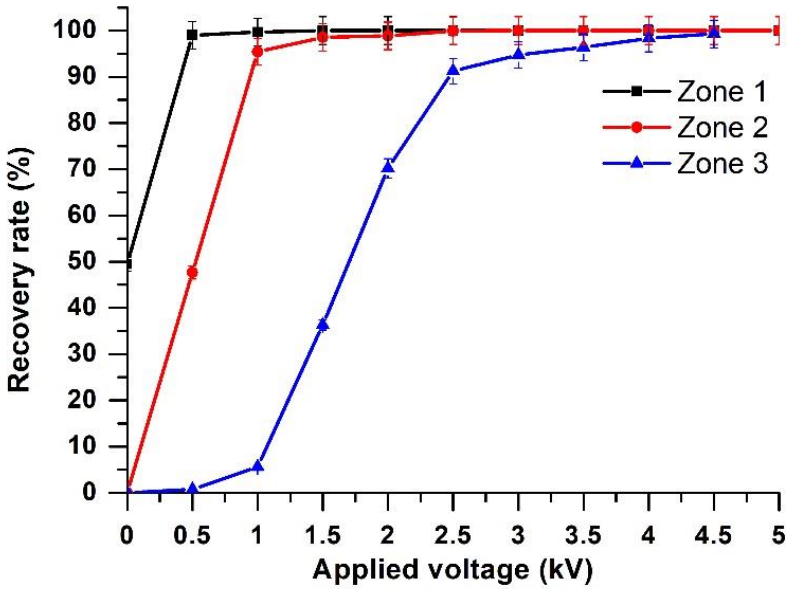

a)

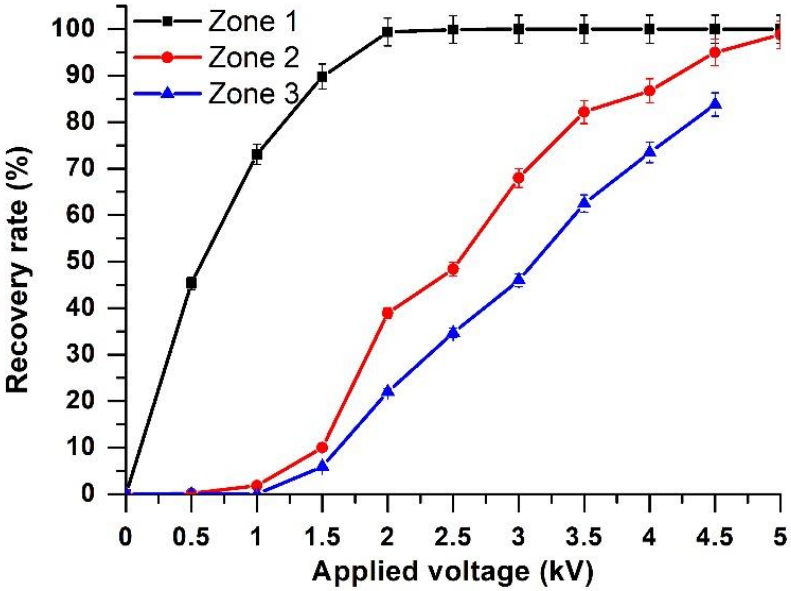

b)

Figure IV-7: Variation of the recovery rate (%) of the copper particles still on the DS-RDSA surface as a function of the applied voltage delivered by a midpoint transformer for two rotation speeds in three zones.

a) n= 80 rpm; **b)** n= 120 rpm.

IV.4.1.3. Experiments with HV DC-voltage

During this experimental phase, the DS-RDSA was powered by a DC supply to observe the DC applied voltage effect.

a) Applied high voltage effect

A continuous high-voltage power supply (Gwinstek GDS-3154) was used to see the impact of this kind of supply on the adhesion force delivered by DS-RDSA.

Note that the top electrode was supplied by a positive DC and the bottom electrode was grounded, so the maximum voltage values applied to the first electrode were used to plot the results presented in the following figure.

(Figure IV.8) represents the obtained results of variation of the recovery rate of the copper particles still on the DS-RDSA surface as a function of the applied voltage delivered by the Continuous high voltage power supply for two rotation speeds in three zones. At 80 rpm, metal particles remained fully attached to the actuator's surface at voltages of 2, 3 and 4 kV in zones 1, 2, and 3 respectively (Figure IV.8.a). At a rotation speed of 120 rpm, metal particles were recovered with a maximum applied voltage of 3 and 4 kV in zones 1 and 2 respectively (Figure IV.8.b). These results show that the voltage difference between both actuator electrodes affects the electro-adhesion force.

Similar to the preceding actuator (SS-RDSA), when a metal particle is on the DS-RDSA, the electric field formed by the potential difference between the electrodes causes the induction of opposing charges on its surface that result the electro adhesion force (Figure IV.9).

The electro adhesion force delivered by SS-RDSA is greater than that delivered by DS-RDSA due to the thickness and kind of the dielectric layer between electrodes. Therefore, in order to provide more context, future studies should figure out how to alter the PCB layer of a double-sided printed circuit board in order to test different thickness and material permeability configurations.

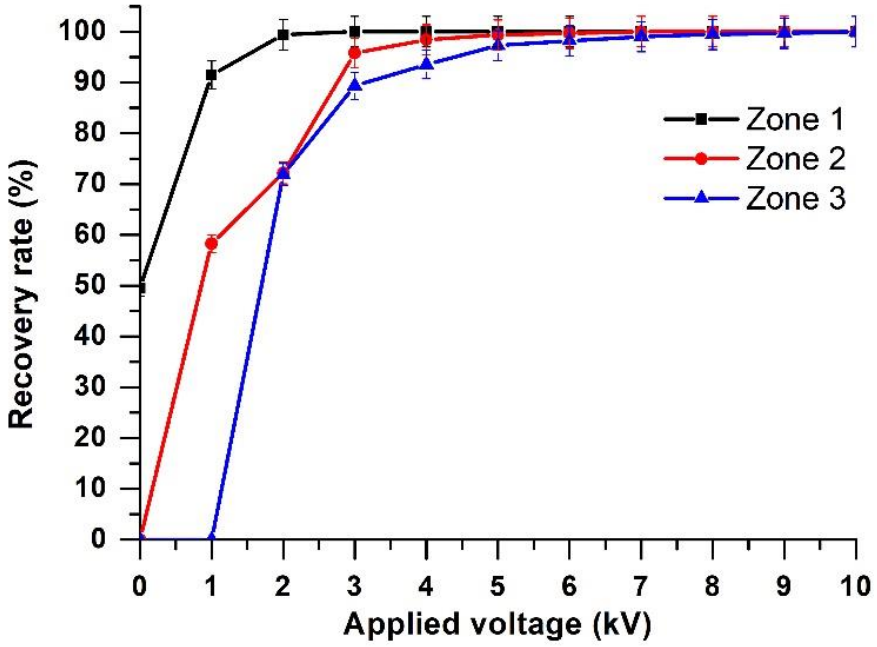

a)

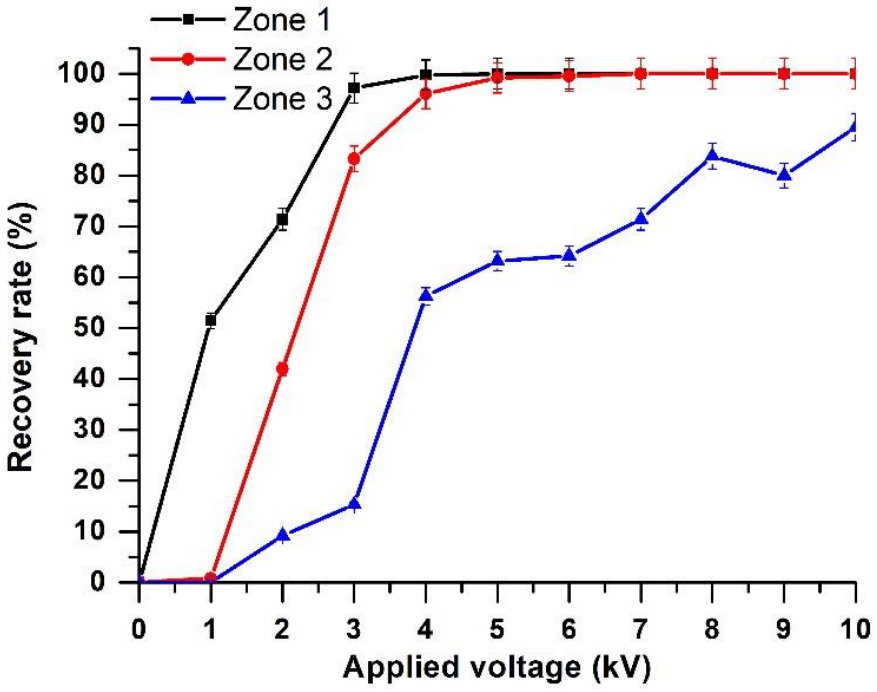

b)

Figure IV-8: Variation of the recovery rate (%) of the copper particles still on the DS-RDSA surface as a function of the applied voltage delivered by a continuous high voltage power supply for two rotation speeds in three zones

a) n= 80 rpm; **b)** n= 120 rpm.

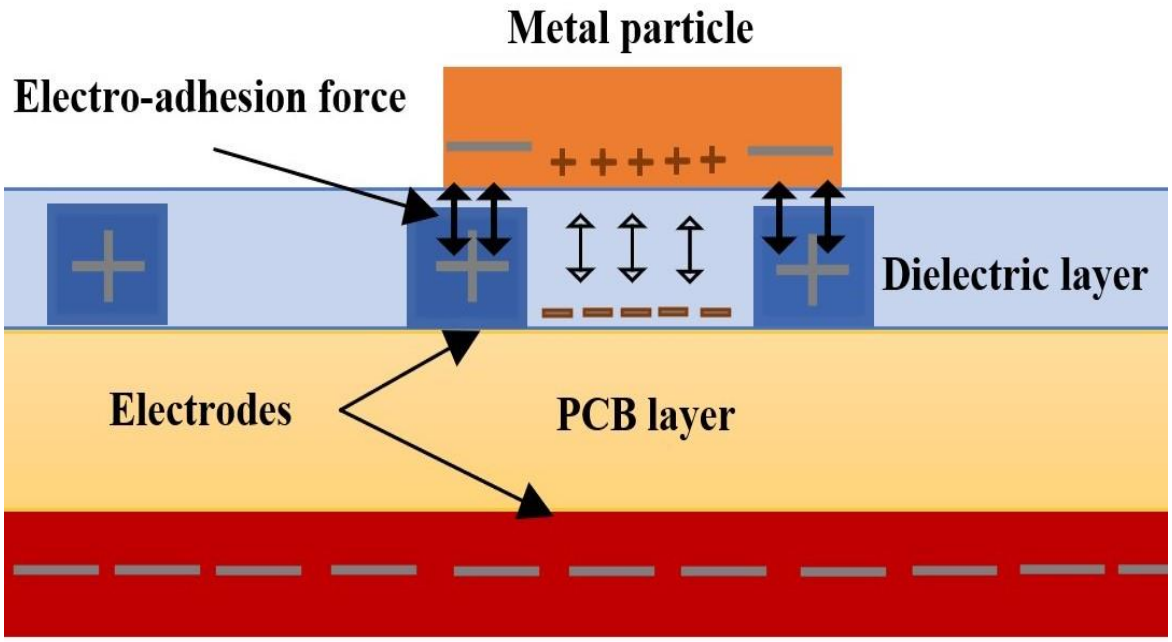

Figure IV-9: The force of electro-adhesion exerted on conducting particles by DS-RDSA.

IV.4.2. Separation experiments (with vacuum blower)

In this section, the same separation process was used, but the Simple-Sided Rotating Disck Shape Actuator (SS-RDSA) was replaced by a Double-Sided Rotating Disck Shape Actuator (DS-RDSA) (Figure IV.10).

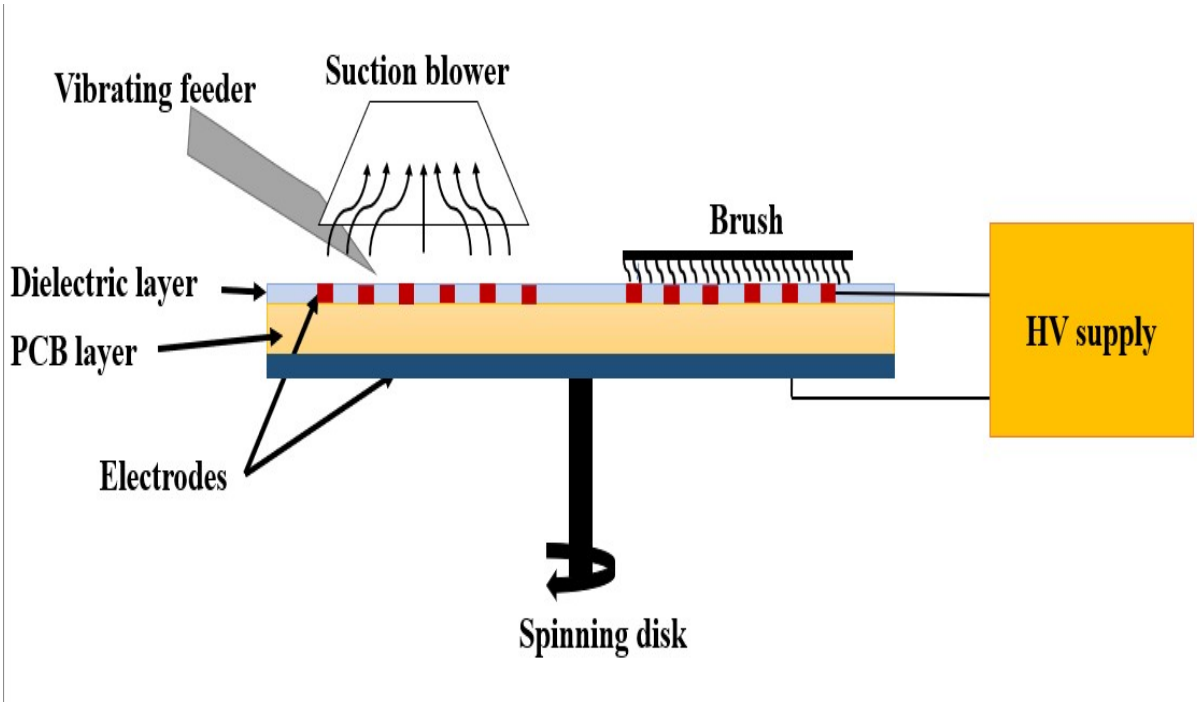

Figure IV-10: Side view of the experimental setup with a DS-RDSA.

IV.4.2.1. Smal-size plastic particles

Here, also, the DS-RDSA was assessed using smaller metal and plastic particles. The effects of the applied HV, the air suction rate, rotation speed, vibrating feeding rate, and ambient humidity were investigated.

a) Applied high voltage Effect

A transformer and an HV amplifier were employed to power the DS-RDSA in order to figure out how HV wave shapes affected the separation efficacy.

➢ Using a HV amplifier TREK supply

To analyse separation efficiency, the following tests were carried out using the experimental apparatus indicated in (Figure IV.10). A TREK supply was used to power the actuator to separate granular mixture samples with a total mass of 10 g, comprising 50% plastic and 50% copper particles. This study used fixed parameters for the air suction flow rate (Q=1.27m^3/min), rotation speed (n=80 rpm), vibrator feeding rate (D=0.08 g/s) and a humidity ambient (H= 60-65%).

It should be noted that a square signal operating at 30 Hz frequency and 180 º shift phase was employed.

(Figure IV.11) presents the variation of the recovery and purity rates of plastic and copper particles as a function of applied voltage delivered by a TREK supply. The results show a proportionate relationship between the applied high voltage value and copper recovery as well as plastic purity. At an applied voltage of 0.4 kV, the maximum recovery of copper and plastic purity were attained (100%). The maximum levels of copper purity and plastic recovery were achieved regardless of the applied voltage value.

All plastic was aspirated using a vacuum blower with a 0,27 m^3/min value rate, which explained the maximum copper purity rate and plastic recovery rate independent of the applied voltage. Copper recovery and plastic purity both increase with applied high voltage. This is because applied voltage increases the electro adhesion force that make the copper particles adhered to the surface of actuator.

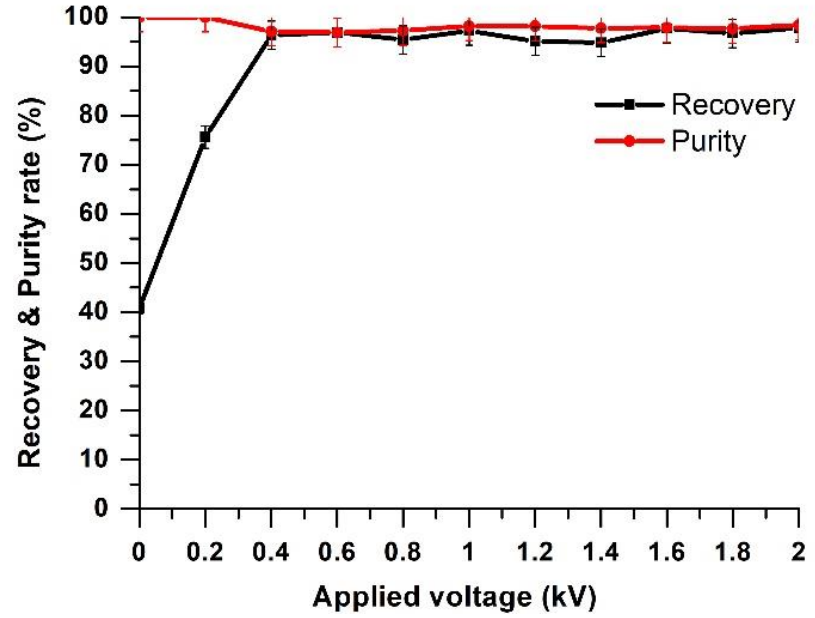

a)

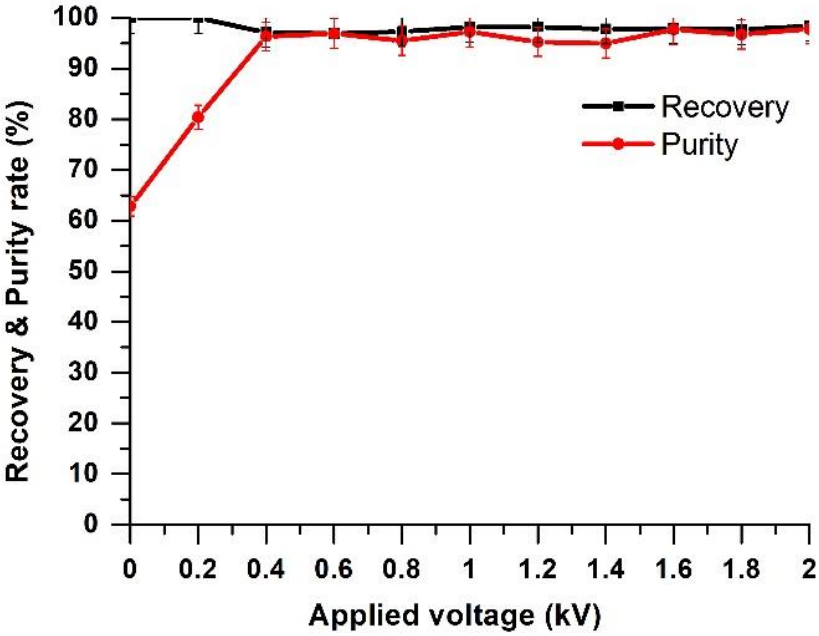

b)

Figure IV-11: Variation of the recovery and purity rates of copper and plastic particles as a function of the applied voltage delivered by TREK supply.

Experimental conditions: D=0.08 g/s; Q=1.27 m^3/min; n=80 rpm; RH=60–65%.
a) Copper; **b)** Plastic.

➢ Experimental with transformer

In conditions of vibration feeding rate equal to 0.08 g/s; air suction flow rate of 1.27m^3/min; rotation speed of 40 rpm; humidity between 35 and 45%, the following experiments were done.

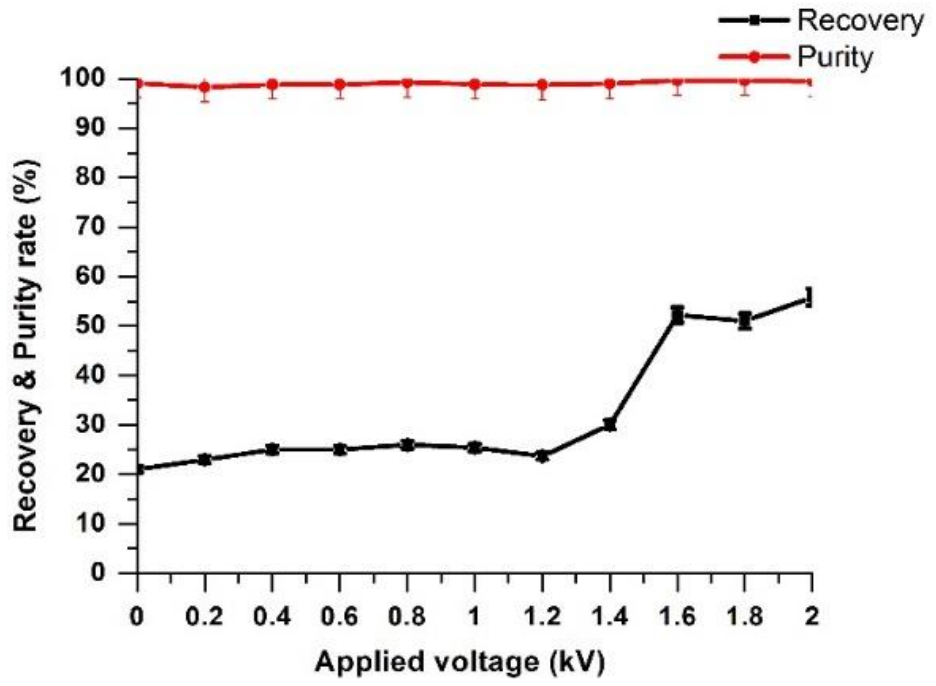

a)

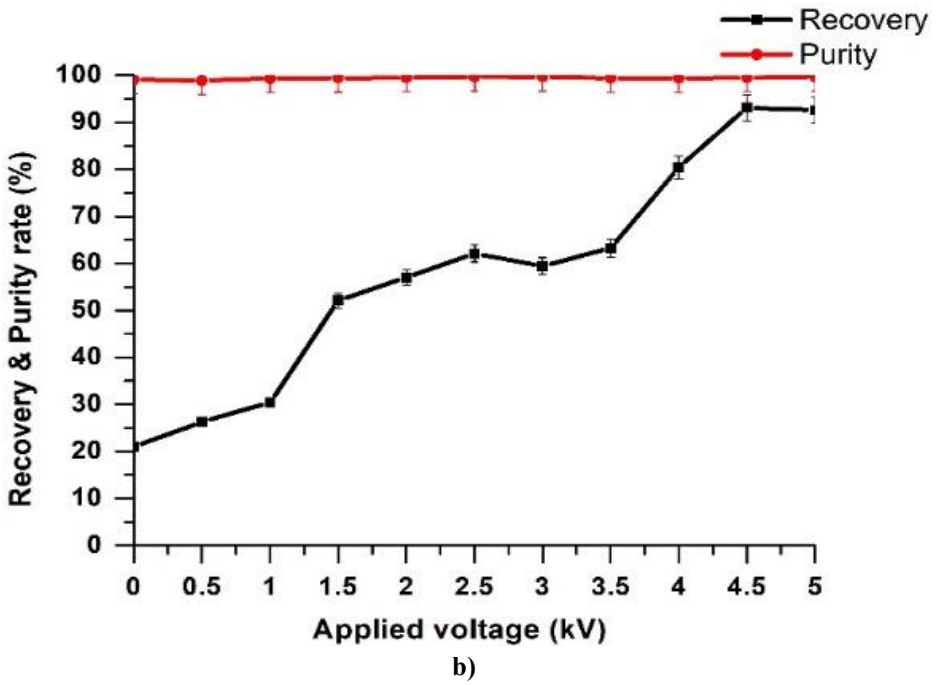

b)

Figure IV-12: Variation of the recovery and purity rates of copper particles as a function of the applied voltage delivered by a mid-point transformer supply.

Experimental conditions: D=0.08 g/s; Q=1.27m^3/min; n=40 rpm; RH=35–45%.
a) Range: 0-2kV; **b)** Range: 0-5kV.

(Figure IV.12) and (Figure IV.13) illustrate the variation of the recovery and purity rates of copper and plastic particles as a function of the applied voltage delivered by a mid-point transformer supply for two ranges [0-2 kV] and [0-5 kV], respectively.

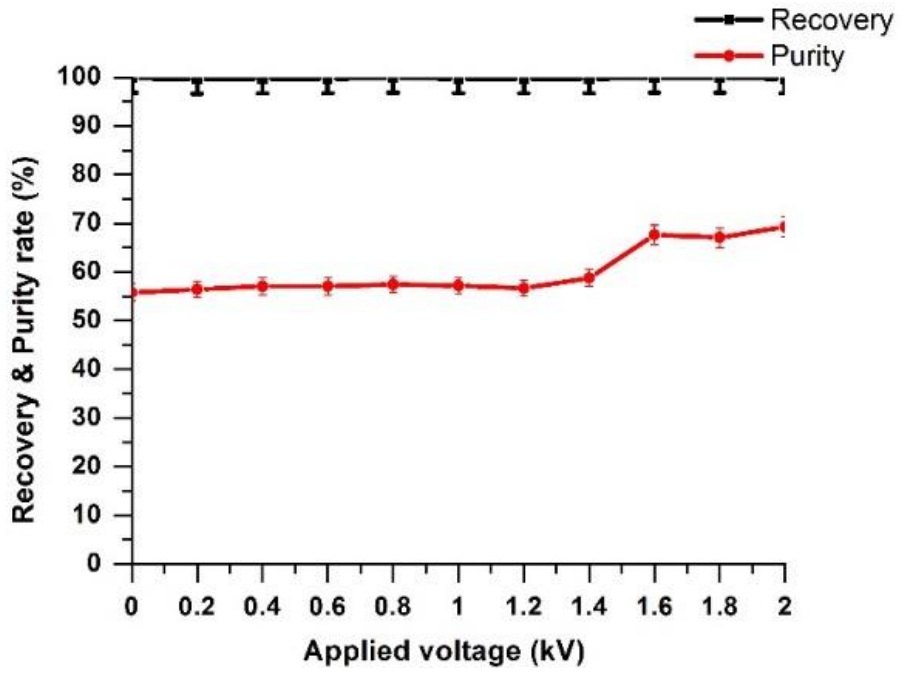

a)

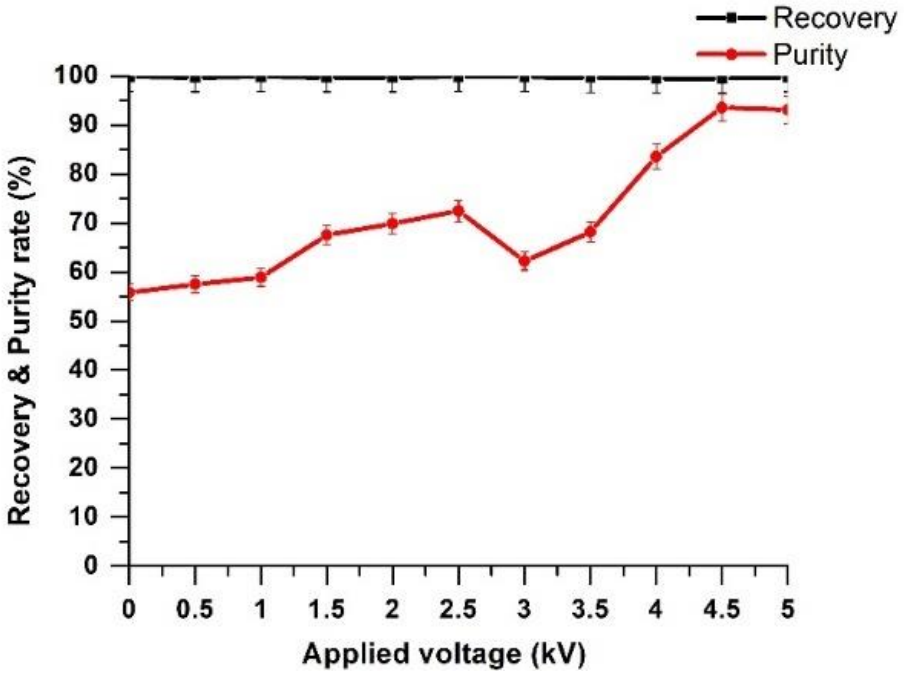

b)

Figure IV-13: Variation of the recovery and purity rates of plastic particles as a function of the applied voltage delivered by a mid-point transformer supply.

Experimental conditions: D=0.08 g/s; Q=1.27m^3/min; n=40 rpm; RH=35–45%.
a) Range: 0-2kV; **b)** Range: 0-5kV.

According to these results, the copper recovery rate was 50% at a maximum applied voltage of 2 kV, however, when the voltage was increased to 5 kV, 95% recovery was achieved. Because all of the plastic was recovered, the copper purity was always 100% regardless of the applied voltage value.

According to these results, the midpoint transformer can be used to supply the separator actuator in industry since it has the benefit of price and availability over the TREK supply.

b) Humidity Effect

The humidity effect was investigated by powering the DS-RDSA with a TREK supply while maintaining the following parameters: rotation speed n = 80 rpm; air suction flow rate Q = 1.27 m^3/min; and vibration feeding rate D = 0.08 g/s.

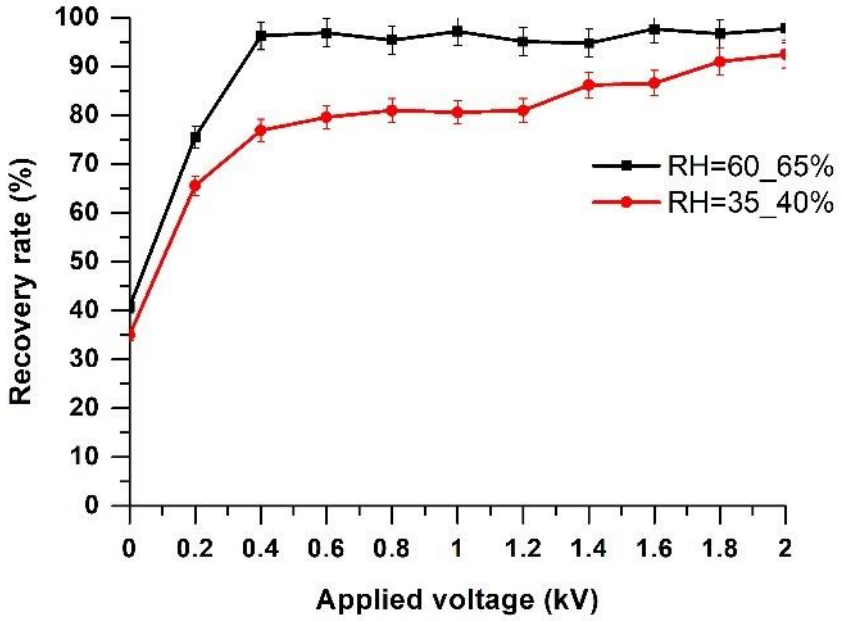

a)

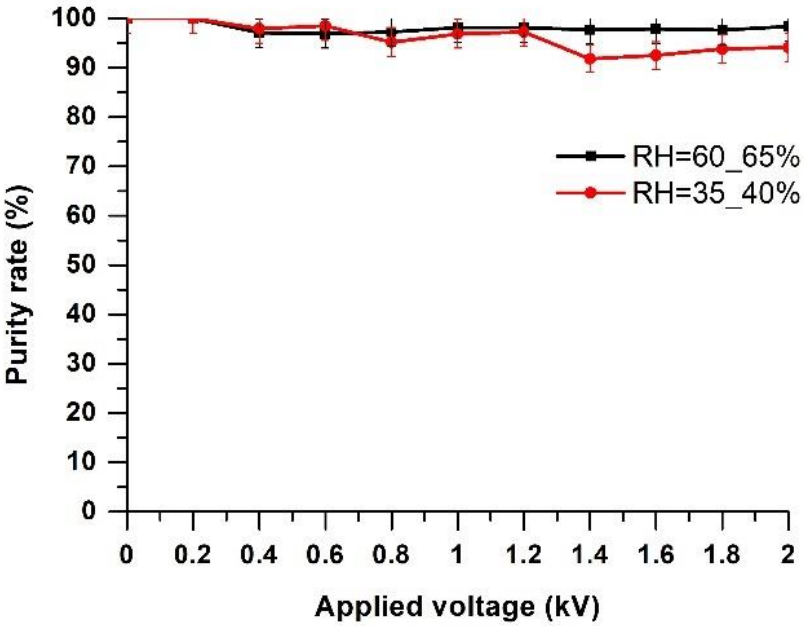

b)

Figure IV-14: Variation of the recovery and the purity rates of copper particles as a function of the applied voltage for two values of humidity.

Experimental conditions: D=0.08 g/s; Q=1.27m3/min and n=80 rpm.

a) Recovery; **b)** Purity.

In this section, the results related the plastic product have not been presented here because it has been observed that the vacuum blower recovers all of the plastic particles, regardless of the level of ambient humidity. The studies were conducted on two different days with different ambient conditions; the first day was humid (60–65%) and the second was dry (35–40%). This should be mentioned.

(Figure IV.15) illustrates the acquired results of variation of the recovery and the purity rates of copper particles as a function of the applied voltage for two humidity ambient levels.

These results confirm that humidity has a highly positive effect on this separating device when compared to electrostatic separators (tribo-electrostatic separator and corona separator). The water layer that restores the surface of copper particles actually gives them a higher "mechanical" adhesion due to the capillary force operating between the particle and the DS-RDSA surface.

c) Rotation speed Effect

In conditions of vibration feeding rate D=0.08 g/s, air suction flow rate Q=1.27 m^3/min, applied voltage V=2 kV and humidity ambient RH=35–45%, the rotation effect was analysed.

The variation of the recovery and the purity rates of copper and plastic particles as a function of the rotation speed is presented in (Figure IV.15).

The plotted results show that increasing the rotation speed reduces separation performance due to the rise in centrifugal force. This is because the copper particles are more easily detached and sucked away by air suction.

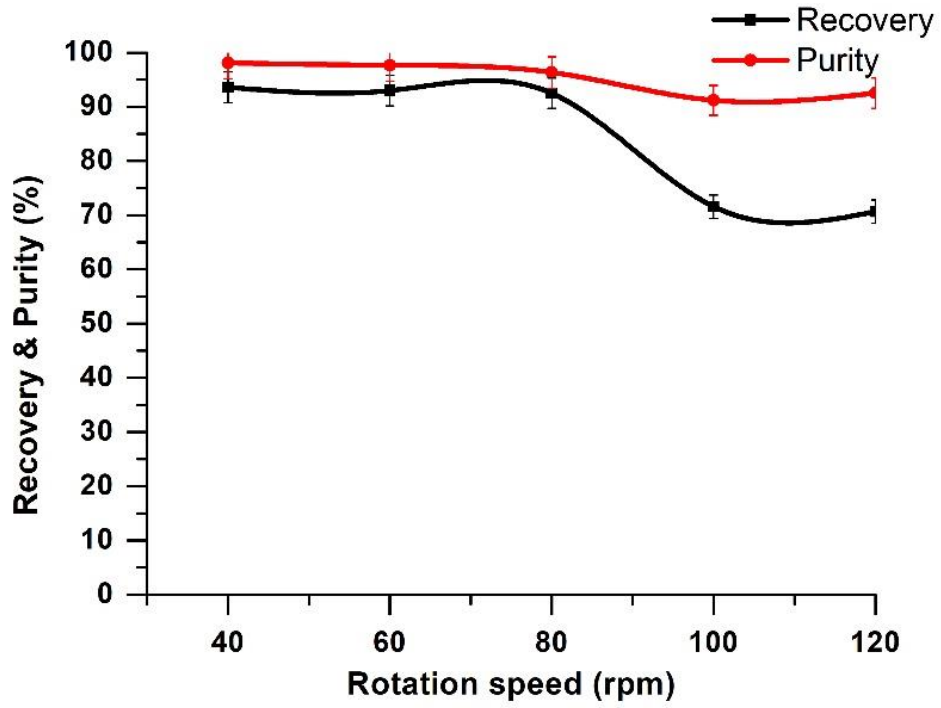

a)

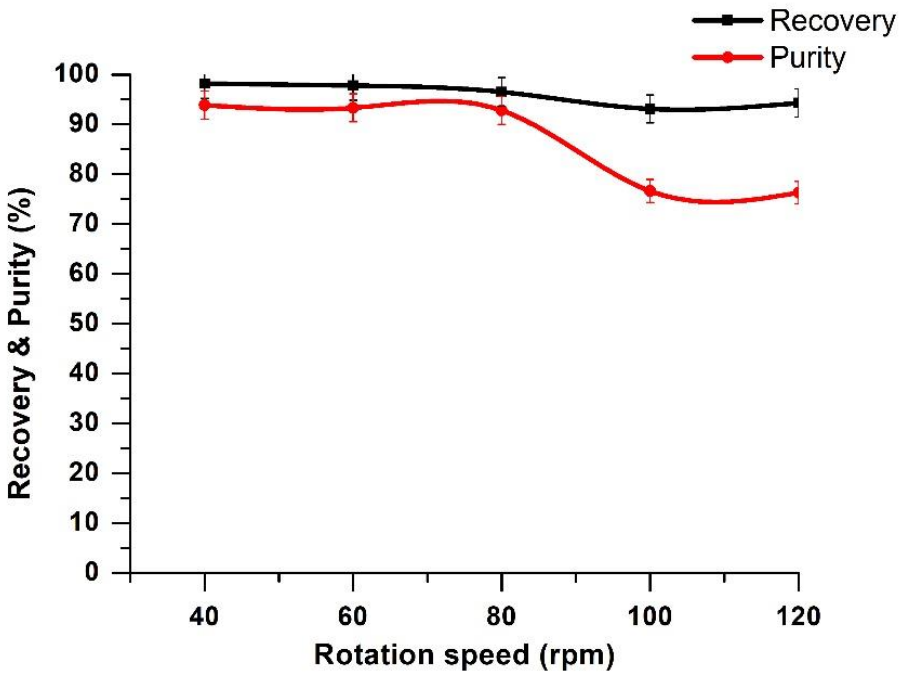

b)

Figure IV-15: Variation of the recovery and the purity rates of copper and plastic particles as a function of the rotation speed.

Experimental conditions: D=0.08 g/s; Q=1.27m3/min; V=2 kV and RH=35–45%.

a) Copper; **b)** Plastic.

d) Air suction flow rate Effect

In fixed settings of vibration feeding rate (D=0.08 g/s), applied voltage (V=2 kV), rotation speed (n=80 rpm) and humidity ambient (RH=35–45%), The air suction flow rate was examined in this section.

The results plotted in (Figure IV.16) demonstrate the impact of air suction flow rate on the purity and recovery rates of copper and plastic particles.

The copper recovery and plastic purity will both decrease as the air flow rate increases because some of the copper product will be sucked up by the vacuum blower. Copper purity and plastic recovery will both drop with a decreased flow rate, however, because some plastic products will remain on the actuator's surface.

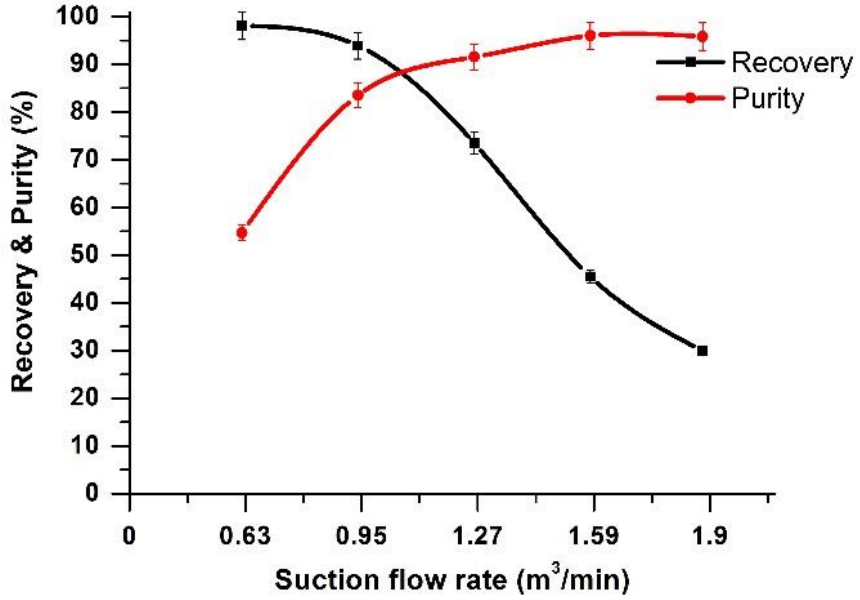

a)

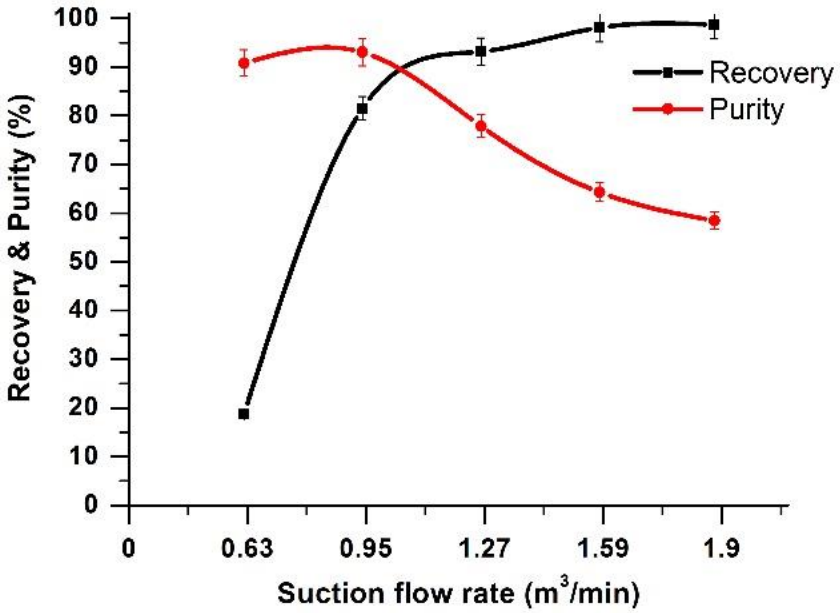

b)

Figure IV-16: Variation of the recovery and the purity rates of copper and plastic particles as a function of the air suction flow rate.

Experiment conditions: D=0.08g/s; V=2 kV; n=80 rpm and RH=35–45%.

a) Copper; **b)** Plastic.

e) Vibrator feeding rate effect

The vibrator feeding rate effect was studied in fixed parameter values of air suction flow rate (Q = 1.27 m^3/min), rotation speed (n = 80 rpm), applied voltage (V = 2 kV), and humidity ambient (RH = 35–45%).

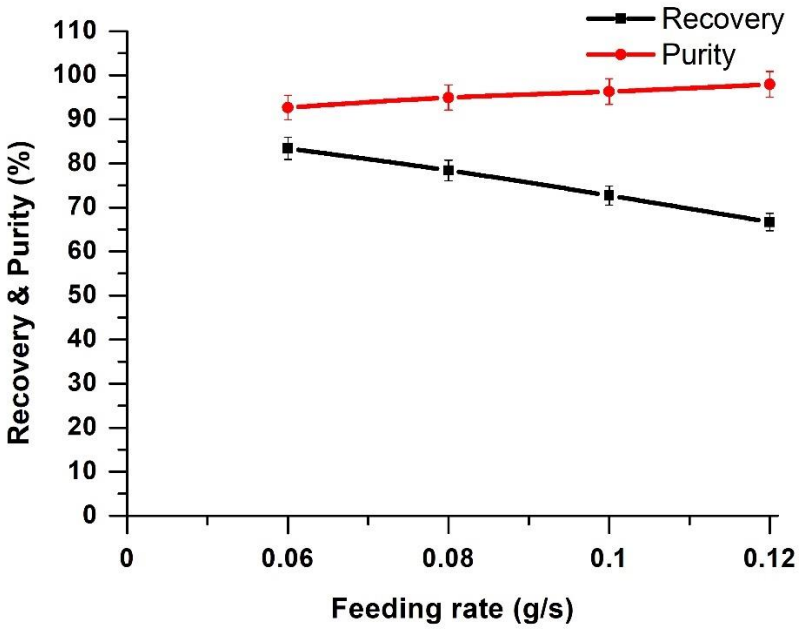

a)

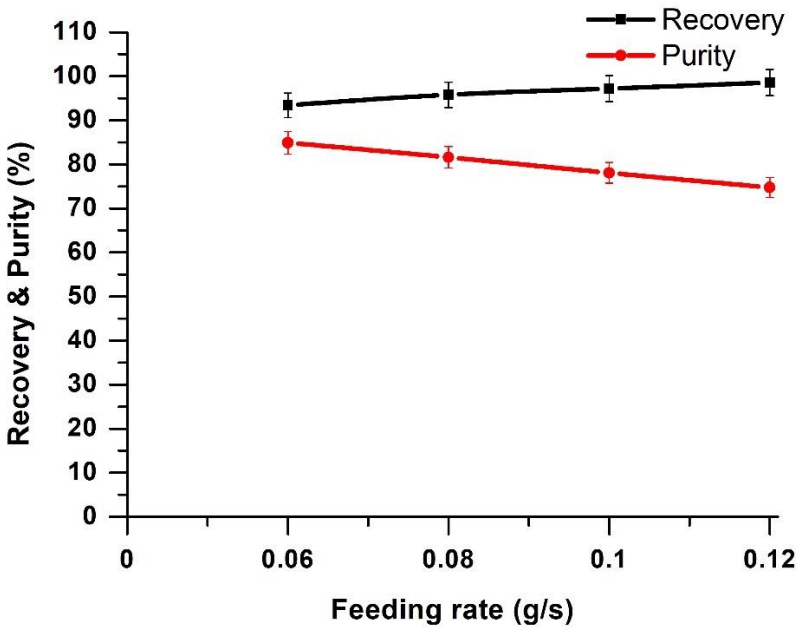

b)

Figure IV-17: Variation of the recovery and the purity rates of copper and plastic particles as a function of the vibration feeding rate.

Experimental conditions: Q=1.27m^3/min; RH=35–45%; n=80 rpm and V=2 kV.
a) Copper; **b)** Plastic.

(Figure IV.17) shows the obtained results of variation of the recovery and the purity rates of copper and plastic particles as a function of the vibration feeding rate. according to these results, the separation efficiency was increased with higher vibrating feeding rate because when the vibrator feeding rate rises, the product deposits in multiple layers, making the separation inefficient.

IV.4.2.2. Using a bigger-sized plastic particle

During the following studies, large plastic particles were utilised to ensure the effectiveness of the DS-RDSA in the separator device.

a) Applied high voltage Effect

By using a HV amplifier TREK to power the DS-RDSA and under conditions of vibration feeding rate D=0.08 g/s, air suction flow rate Q=1.43 m^3/min, rotation speed n=40 rpm, and humidity RH=50–60%, the concept of separating larger particles of plastic and metal was examined.

The experiments result of variation of the recovery and purity rates of copper and plastic particles bigger size as a function of the applied voltage is plotted in (Figure IV.18).

These findings demonstrate that as applied voltage is increased, the copper recovery rate and plastic purity rate also rise, reaching 95% at 2 kV. This separator device may therefore separate a larger size of mixture of plastic and metal.

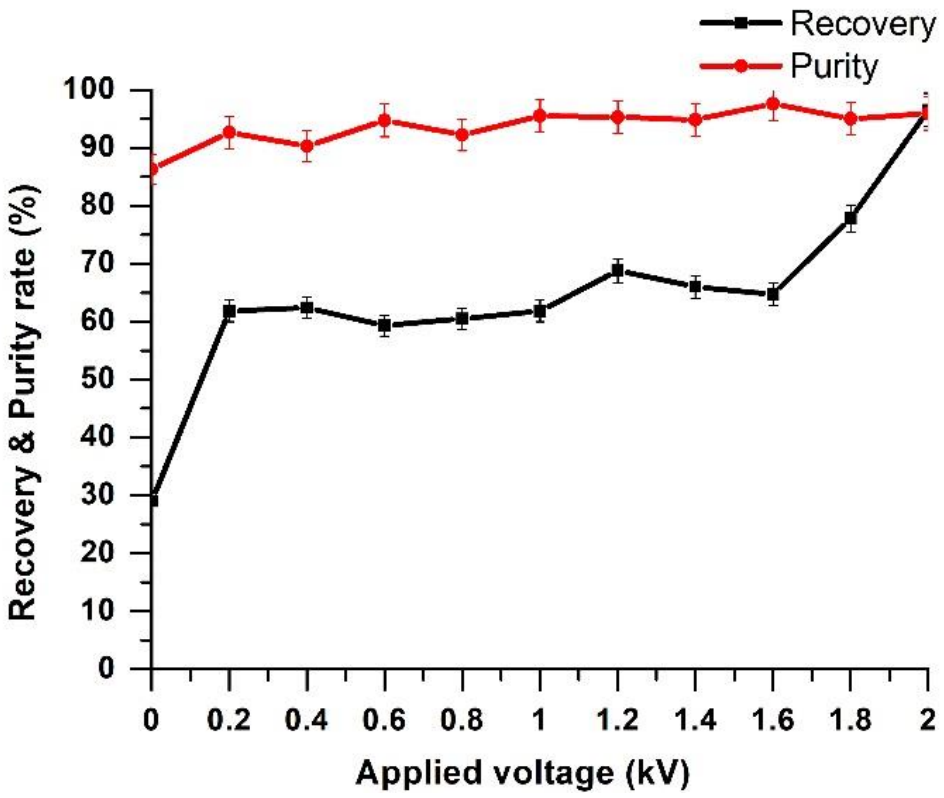

a)

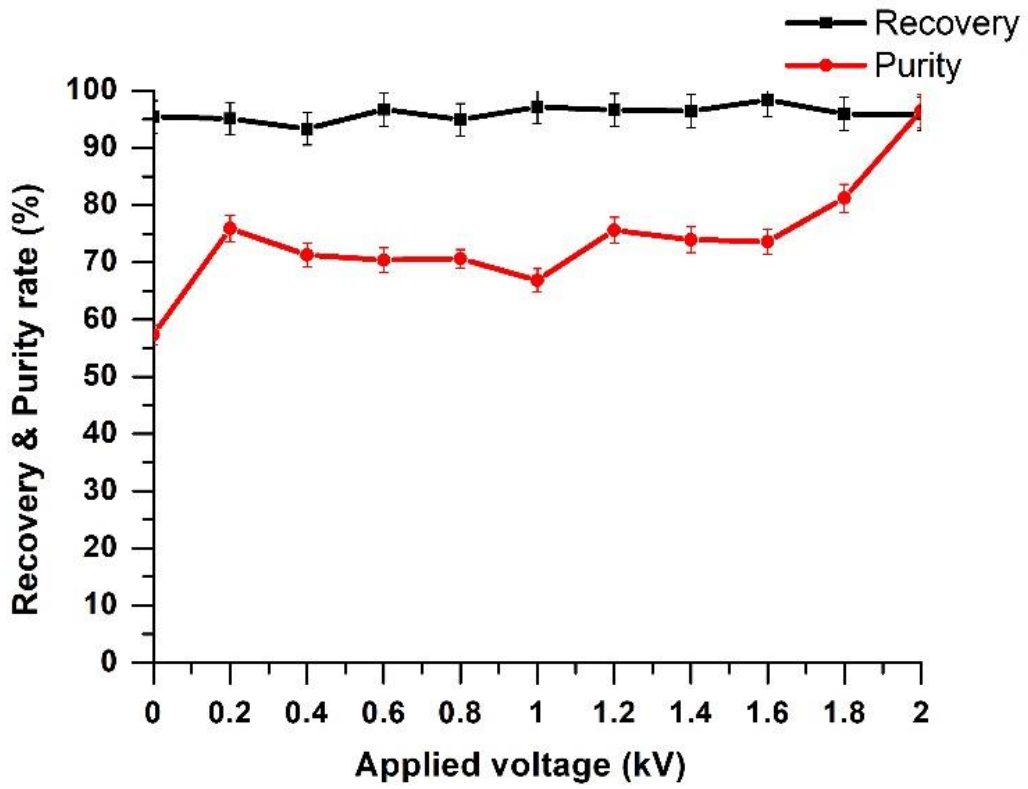

b)

Figure IV-18: Variation of the recovery and purity rates of copper and plastic particles as a function of the applied voltage.

Experimental conditions: D=0.08 g/s; Q=1.43m^3/min; n=40 rpm; RH=50–60%.

a) Copper; **b)** plastic (big size).

IV.5. Conclusion

In this chapter a Double-Sided Rotating Disk Actuator (DS-RDSA) was realized to study the electro adhesion force applied to conductor particles and the efficiency of the separation process for both smaller and larger plastic particles with metal particles.

The obtained findings highlighted the following points:

- ✓ For adhesion force, better results were achieved using DC and square wave forms of signals than sinusoidal form.
- ✓ The separation process is carried out by utilizing the mechanical force (air suction) applied to plastic particles and electrical force (electro adhesion) acting on the metal particle.
- ✓ According to the obtained results, the midpoint transformer can be used to supply the separator actuator in industry since it has the benefit of price and availability over the TREK supply.
- ✓ Also, the humidity has a positive effect to the separation performance.

GENERAL CONCLUSION

General conclusion

The growing amount of e-waste presents serious health and environmental risks, underscoring the need for sustainable waste management solutions and better recycling procedures.

This thesis examined the creation and assessment of a new electrostatic separator device that uses a rotating actuator to effectively separate metal/plastic combinations in e-waste. It also examined the electro-adhesion force applied to metal particles.

For this study, two different kinds of actuators were created: a Single Sided Rotating Disk Shape Actuator and a Double-Sided Rotating Disk Shape Actuator. The former was made from a single-sided printed circuit board (PCB), while the latter was made from a single-sided PCB.

There were two analyse sections for each kind of actuator used in this investigation. The first involved analysing the electro adhesion force exerted on the metal particle. A rotation actuator driven by a DC motor and powered by a high voltage supply was the experimental setup used in this portion. In the second section, the separation process of metal/plastic mixture was examined. The identical setup was employed, but the plastic particles were sucked using a vacuum blower and the metal/plastic mixture was deposited on the actuator surface employing a vibrating feeder.

The factors of applied high voltage, signal shape form, and rotation speed were investigated for the electro adhesion section. The separation process portion included an analysis of the applied high voltage, vibrating feeder rate, vacuum blower rate, and rotation speed. Furthermore, the impact of humidity was investigated. This study examined three types of high voltage sources for actuators: HV amplifier, continuous high voltage power supply, and midpoint transformer supply.

In the investigation of adhesion force, we noticed that the force acting on the metal particles is primarily influenced by the applied voltage level. Furthermore, a square-shaped, DC signal's electric field generates a stronger adhesion force than a sinusoidal signal. Further, due of the actuator's dielectric properties and the space between its electrodes, the single-sided rotating disk-shaped actuator produced a greater adhesion force than the double-sided one.

In the study on the separation process of metal/plastic mixtures, we observed that for both actuator types, the recovery rate of plastic particles and copper purity were 100%. This was because the lightweight plastic particles could be removed easily with a vacuum blower. The applied high voltage level had an effect on the purity of plastic and the recovery rate of copper particles, with a copper recovery rate greater than 95% at a voltage of 2 kV square was signalled. In addition, this separator device can be used to separate the bigger size mixture by raising the vacuum blower rate to suck larger plastic particles and applying a greater voltage value to stick metal particles on the actuator surface. Compared to previous electrostatic separators, this separator device is more adaptable to humidity.

As a perspective, we suggest:

- Thinner dielectric plates can be used to generate a stronger electric field on double-sided conveyors.
- Add a control system to this device to ensure optimal performance without the need for human involvement.

Bibliography

Bibliography

[1] Baldé, C.P., Forti V., Gray, V., Kuehr, R., Stegmann,P. : The Global E-waste Monitor – 2017, United Nations University (UNU), International Telecommunication Union (ITU) & International Solid Waste Association (ISWA), Bonn/Geneva/Vienna.

[2] Bin Lu, Jianxin Yang, Winifred Ijomah, Wenjie Wu, and Gabriel Zlamparet. Perspectives on reuse of weee in china: lessons from the eu. Resources, Conservation and Recycling, 135 :83–92, 2018.

[3] Akeeb Adepoju Fawole, Ochuko Felix Orikpete, Nwakamma Ninduwezuor Ehiobu, and Daniel Raphael Ejike Ewim. Climate change implications of electronic waste: strategies for sustainable management. Bulletin of the National Research Centre,47(1) :147, 2023.

[4] Seyi Rachel Dada, Agboola Suleiman, Esther Oluwaseun Adu, Adeniyi Adebayo, Akorede L Seriki, and Comfort Olajumoke Oluleke. The future of e-waste recycling: Emerging technologies and practices evaluating the social and economic benefits of advanced e-waste recycling technologies.

[5] Rajesh Ahirwar and Amit K Tripathi. E-waste management: A review of recycling process, environmental and occupational health hazards, and potential solutions. Environmental Nanotechnology, Monitoring & Management, 15 :100409, 2021.

[6] Jonovan Van Yken, Naomi J Boxall, Ka Yu Cheng, Aleksandar N Nikoloski, Navid R Moheimani, and Anna H Kaksonen. E-waste recycling and resource recovery:A review on technologies, barriers and enablers with a focus on oceania. Metals,11(8) :1313, 2021.

[7] Shubham Gupta, Gaurav Modi, Rahul Saini, Vijaya Agarwala, et al. A review on various electronic waste recycling techniques and hazards due to its improper handling. International Refereed Journal of Engineering and Science (IRJES), 3(5) :05–17,2014.

[8] Adrian Samuila, Lucian Dascalescu, Laur Calin, Mihai Bilici, and Andrei Catinean. Recent researches in electrostatic separation technologies for the recycling of waste 51electric and electronic equipment. In AIP Conference Proceedings, volume 2218. AIP Publishing, 2020.

[9] Hongzhou Lu, Jia Li, Jie Guo, and Zhenming Xu. Movement behavior in electrostatic separation: Recycling of metal materials from waste printed circuit board. Journalof materials processing technology, 197(1-3) :101–108, 2008.

[10] Mianqiang Xue, Guoqing Yan, Jia Li, and Zhenming Xu. Electrostatic separation for recycling conductors, semiconductors, and nonconductors from electronic waste. Environmental science & technology, 46(19) :10556–10563, 2012.

[11] Wu Jiang, Li Jia, and Xu Zhen-Ming. Optimization of key factors of the electrostatic separation for crushed pcb wastes using roll-type separator. Journal of hazardous materials, 154(1-3) :161–167, 2008.

[12] Jiang Wu, JIA Li, and Zhenming Xu. Electrostatic separation for recovering metals and nonmetals from waste printed circuit board: problems and improvements. Environmental science & technology, 42(14) :5272–5276, 2008.

[13] Felix Michael Moesner. Transportation and manipulation of particles by an AC Electric Field. PhD thesis, ETH Zurich, 1996.

[14] Yue Yu, Jan Cilliers, Kathryn Hadler, Stanley Starr, and Yanghua Wang. A review of particle transport and separation by electrostatic traveling wave methods. Journal of Electrostatics, 119 :103735, 2022.

[15] Pandey Rajagopalan, Manikandan Muthu, Yulu Liu, Jikui Luo, Xiaozhi Wang, and Chaoying Wan. Advancement of electro adhesion technology for intelligent and selfreliant robotic applications. Advanced Intelligent Systems, 4(7) :2200064, 2022.

[16] William C Hinds and Yifang Zhu. Aerosol technology: properties, behavior, and measurement of airborne particles. John Wiley & Sons, 2022.

[17] H Tarik Baytekin, Alexander Z Patashinski, M Branicki, Bilge Baytekin, S Soh, and Bartosz A Grzybowski. The mosaic of surface charge in contact electrification. Science, 333(6040) :308–312, 2011.

[18] Pierre Atten, Hai Long Pang, and Jean-Luc Reboud. Study of dust removal by standing-wave electric curtain for application to solar cells on mars. IEEE Transactions on Industry Applications, 45(1) :75–86, 2009.

[19] Harry J White. Electrostatic precipitation of fly ash. Journal of the Air Pollution Control Association, 27(1) :15–22, 1977.

[20] Ken R Parker. Why an electrostatic precipitator? In Applied electrostatic precipitation, pages 1–10. Springer, 1997.

[21] Guan-Yu Lin, Chuen-Jinn Tsai, Sheng-Chieh Chen, Tzu-Ming Chen, and Shou-Nan Li. An efficient single-stage wet electrostatic precipitator for fine and nanosized particle control. Aerosol Science and Technology, 44(1) :38–45, 2010.

[22] Jack R McDonald, Wallace B Smith, Herbert W Spencer III, and Leslie E Sparks. A mathematical model for calculating electrical conditions in wire-duct electrostatic precipitation devices. Journal of Applied Physics, 48(6) :2231–2243, 1977.

[23] Phil A Lawless and Ralph F Altman. Espm: an advanced electrostatic precipitator model. In Proceedings of 1994 IEEE industry applications society annual meeting, volume 2, pages 1519–1526. IEEE, 1994.

[24] G Divya Deepak. The modelling and characterization of dielectric barrier discharge based cold plasma jets. Cambridge Scholars Publishing, 2020.

[25] Branislav Pongrác, Hyun-Ha Kim, Nobuaki Negishi, and Zdenko Machala. Influence of water conductivity on particular electrospray modes with dc corona discharge optical visualization approach. The European Physical Journal D, 68 :1–7,2014.

[26] Romaric Landfried. Contribution à l'étude de la transition décharge luminescente/arc électrique dans l'air et dans l'argon au voisinage de la pression atmosphérique. PhD thesis, Supélec, 2011.

[27] Lipeng Liu and Marley Becerra. An efficient model to simulate stable glow corona discharges and their transition into streamers. Journal of Physics D: Applied Physics, 50(10) :105204, 2017.

[28] Ulrich Kogelschatz. Dielectric-barrier discharges: their history, discharge physics, and industrial applications. Plasma chemistry and plasma processing, 23(1) :1–46,2003.

[29] David J Griffiths. Introduction to electrodynamics. Cambridge University Press, 2023.

[30] Betty Isabelle Bleaney and Brebis Bleaney. Electricity and Magnetism, Volume 2, volume 2. Oxford University Press, USA, 2013.

[31] H Partridge, CW Bauschlicher Jr, R Ahlrichs, and SR Langhoff. Theoretical study of the dipole moments of selected alkaline-earth halides. 1986.

[32] Edwynn Wallace and Malav Shah. Introductory physics i & ii (mga). 2017.

[33] Gianfranco Spavieri, GT Gillies, andMRodriguez. Physical implications of coulomb's law. Metrologia, 41(5) :S159, 2004.

[34] Malay Mazumder, Mark N Horenstein, Jeremy W Stark, Peter Girouard, Robert Sumner, Brooks Henderson, Omar Sadder, Ishihara Hidetaka, Alexandru Sorin Biris, and Rajesh Sharma. Characterization of electrodynamic screen performance for dust removal from solar panels and solar hydrogen generators. IEEE Transactions on industry applications, 49(4) :1793–1800, 2013.

[35] Hiroyuki Kawamoto. Some techniques on electrostatic separation of particle size utilizing electrostatic traveling-wave field. Journal of Electrostatics, 66(3-4) :220–228, 2008.

[36] Senichi Masuda, MasaoWashizu, and Masahiro Iwadare. Separation of small particles suspended in liquid by non-uniform travelling field produced by three phase electric curtain device. In 1985 Annual Meeting Industry Applications Society, pages 1418– 1423. IEEE, 1985.

[37] Masato Adachi, Hirofumi Moroka, Hiroyuki Kawamoto, Sachiko Wakabayashi, and Takeshi Hoshino. Particle-size sorting system of lunar regolith using electrostatic traveling wave. Journal of Electrostatics, 89 :69–76, 2017.
[38] Hiroyuki Kawamoto, M Uchiyama, BL Cooper, and DS McKay. Mitigation of lunar dust on solar panels and optical elements utilizing electrostatic traveling-wave. Journal of Electrostatics, 69(4) :370–379, 2011.

[39] Hiroyuki Kawamoto and Kyogo Seki. Mechanism on traveling wave transport of particles. Nihon Kikai Gakkai Ronbunshu, C Hen/Transactions of the Japan Society of Mechanical Engineers, Part C, 71(4) :1161–1168, 2005.

[40] Jonas Schmöle, Mathias Dragosits, Hans Hepach, and Markus Aspelmeyer. A micromechanical proof-of-principle experiment for measuring the gravitational force of milligram masses. Classical and Quantum Gravity, 33(12) :125031, 2016.

[41] Philipp G Grützmacher, Andreas Rosenkranz, Sebastian Rammacher, Carsten Gachot, and Frank Mücklich. The influence of centrifugal forces on friction and wear in rotational sliding. Tribology International, 116 :256–263, 2017.

[42] Peter J Blau. The significance and use of the friction coefficient. Tribology International, 34(9) :585–591, 2001.

[43] Fritz London. The general theory of molecular forces. Transactions of the Faraday Society, 33 :8b–26, 1937.

[44] S Sh Rekhviashvili, Boris Aleksandrovich Rozenberg, and Vyacheslav Vsevolodovich Dremov. Influence of the size-dependent surface tension of a liquid film on a capillary force in an atomic force microscope. JETP letters, 88 :772–776, 2008.

[45] Peter A Kralchevsky and Nikolai D Denkov. Capillary forces and structuring in layers of colloid particles. Current opinion in colloid & interface science, 6(4) :383– 401, 2001.

[46] Soumia LOUHADJ. Contribution à l'étude de la séparation de particules micronisées en utilisant des convoyeurs à ondes mobiles. PhD thesis, Université de Sidi Bel Abbès- Djillali Liabes, 2021.

[47] Ayyoub Zouaghi. Manipulation de particules diélectriques micrométriques par ondes électrostatiques progressives et stationnaires-Études théorique, expérimentale et numérique. PhD thesis, Université de Poitiers, 2019.

[48] Y Higashiyama and K Asano. Recent progress in electrostatic separation technology. Particulate science and technology, 16(1) :77–90, 1998.

[49] Hugo Marcelo Veit, Taina Rose Diehl, Anderson Paulo Salami, Joel da Silva Rodrigues, Andrea Moura Bernardes, and Jorge Alberto Soares Tenório. Utilization of magnetic and electrostatic separation in the recycling of printed circuit boards scrap. Waste management, 25(1) :67–74, 2005.

[50] Amar Tilmatine, Karim Medles, Salah-Eddine Bendimerad, Fodil Boukholda, and Lucien Dascalescu. Electrostatic separators of particles: Application to plastic/metal, metal/metal and plastic/plastic mixtures. Waste management, 29(1) :228–232, 2009.

[51] Alexandru Iuga, Laur Calin, Vasile Neamtu, Adrian Mihalcioiu, and Lucian Dascalescu. Tribocharging of plastics granulates in a fluidized bed device. Journal of Electrostatics, 63(6-10) :937–942, 2005.

[52] Lucian Dascalescu, Amar Tilmatine, Florian Aman, and Michaela Mihailescu. Optimization of electrostatic separation processes using response surface modeling. IEEE Transactions on Industry Applications, 40(1) :53–59, 2004.

[53] M Miloudi, K Medles, A Tilmatine, M Brahami, and L Dascalescu. Optimisation of belt-type electrostatic separation of granular plastic mixtures tribocharged in a propeller-type device. In Journal of Physics: Conference Series, volume 301, page 012067. IOP Publishing, 2011.

[54] DK Yanar and BA Kwetkus. Electrostatic separation of polymer powders. Journal of Electrostatics, 35(2-3) :257–266, 1995.

[55] Ho-Seok Jeon, Chul-Hyun Park, Bong-Gyoo Cho, and Jai-Koo Park. Separation of pvc and rubber from covering plastics in communication cable scrap by tribocharging. Separation Science and Technology, 44(1) :190–202, 2009.

[56] Jen-Shih Chang, Arnold J Kelly, and Joseph M Crowley. Handbook of electrostatic processes. CRC Press, 1995.

[57] Alexandru Iuga, Adrian Samuila, Roman Morar, Mihai Bilici, and Lucian Dascalescu. Tribocharging techniques for the electrostatic separation of granular plastics from waste electric and electronic equipment. Particulate Science and Technology, 34(1) :45–54, 2016.

[58] Yong-Wha Oh, Ki-Joon Jeon, An-Ick Jung, and Yong-Won Jung. A simulation study on the collection of submicron particles in a unipolar charged fiber. Aerosol Science & Technology, 36(5) :573–582, 2002.

[59] Hui Zhao and Haim H Bau. Effect of double-layer polarization on the forces that act on a nanosized cylindrical particle in an ac electrical field. Langmuir, 24(12) :6050– 6059, 2008.

[60] TS Simonova, VN Shilov, and OA Shramko. Low-frequency dielectrophoresis and the polarization interaction of uncharged spherical particles with an induced debye atmosphere of arbitrary thickness. Colloid Journal, 63 :108–115, 2001.

[61] Arun TJ Kadaksham, Pushpendra Singh, and Nadine Aubry. Dielectrophoresis of nanoparticles. Electrophoresis, 25(21-22) :3625–3632, 2004.

[62] Abdelkader BELGACEM et al. Etude du déplacement et de la séparation des particules micronisées avec la technique des ondes mobiles. PhD thesis, 2020.

[63] A Belgacem, A Tilmatine, Y Bellebna, F Miloua, N Zouzou, and L Dascalescu. Experimental analysis of the transport and the separation of plastic and metal micronized particles using travelling waves conveyor. IEEE Transactions on Dielectrics and Electrical Insulation, 25(2) :435–440, 2018.

[64] Sven Salomon. Manipulation de microparticules exploitant la force de diélectrophorèse: applications dédiées au tri d'espèces biologiques et à l'assemblage de nano objets. PhD thesis, Université Paul Sabatier-Toulouse III, 2011.

[65] Gaofa He, Chuande Zhou, and Zelun Li. Review of self-cleaning method for solar cell array. Procedia Engineering, 16 :640–645, 2011.

[66] Hiroyuki Kawamoto and Takuya Shibata. Electrostatic cleaning system for removal of sand from solar panels. Journal of Electrostatics, 73 :65–70, 2015.

[67] Louis C Weiss and Devron P Thibodeaux. Electrodynamic method for separating components, August 13 1985. US Patent 4,534,856.

[68] Louis C Weiss and Devron P Thibodeaux. Separation of seed by-products by an ac electric field. Journal of the American Oil Chemists' Society, 61(5) :886–890, 1984.

[69] Hiroko Imasato, Takeshi Yamakawa, and Masanori Eguchi. Separation of leukemia cells from blood by employing dielectrophoresis. Intelligent Automation & Soft Computing, 18(2) :139–152, 2012.

[70] Pablo García-Sánchez, Antonio Ramos, Nicolas G Green, and Hywel Morgan. Experiments on ac electrokinetic pumping of liquids using arrays of microelectrodes. IEEE Transactions on Dielectrics and Electrical Insulation, 13(3) :670–677, 2006.

[71] AP Washabauch, M Zahn, and JR Melcher. Electrohydrodynamic traveling-wave pumping of homogeneous semi-insulating liquids. IEEE transactions on electrical insulation, 24(5) :807–834, 2002.

[72] Peter RC Gascoyne and Jody Vykoukal. Particle separation by dielectrophoresis. Electrophoresis, 23(13) :1973, 2002.

[73] Meng H Lean, AR Volkel, H Ben Hsieh, J-P Lu, JH Daniel, BT Preas, and SJ Limb. Traveling wave bio-agent concentrator. In 2005 3rd IEEE/EMBS Special Topic Conference on Microtechnology in Medicine and Biology, pages 80–83. IEEE, 2005.

[74] Luke A MacQueen, Michael D Buschmann, and Michael RWertheimer. Gene delivery by electroporation after dielectrophoretic positioning of cells in a non-uniform electric field. Bioelectrochemistry, 72(2) :141–148, 2008.

[75] LA MacQueen, M Thibault, Michael D Buschmann, and Michael R Wertheimer. Electro-manipulation of biological cells in microdevices. IEEE Transactions on Dielectrics and Electrical Insulation, 19(4) :1261–1268, 2012.

[76] Hywel Morgan, Nicolas G Green, MP Hughes, W Monaghan, and TC Tan. Largearea travelling-wave dielectrophoresis particle separator. Journal of micromechanics and Microengineering, 7(2) :65, 1997.

[77] Sander Van den Driesche, Vivek Rao, Dietmar Puchberger-Enengl, Wojciech Witarski, and Michael J Vellekoop. Continuous cell from cell separation by traveling wave dielectrophoresis. Sensors and Actuators B : Chemical, 170 :207–214, 2012.

[78] Sander van den Driesche, Vivek Rao, Dietmar Puchberger-Enengl, Wojciech Witarski, and Michael J Vellekoop. Continuous separation of viable cells by travelling wave dielectrophoresis. Procedia Engineering, 5 :41–44, 2010.

[79] Imene Mahi, Radjaa Messafeur, Abdelkader Belgacem, Yassine Bellebna, Hamza Louati, and Amar Tilmatine. New separation method of metal/plastic micronized particles using travelling wave conveyors. International Journal of Environmental Studies, 75(5) :788–799, 2018.

[80] H Louati, A Tilmatine, R Ouiddir, A Alibida, and N Zouzou. New separation technique of metal/polymer granular materials using an electrostatic sorting device. Journal of Electrostatics, 103 :103410, 2020.

[81] Amar Tilmatine, Ahmed Alibida, Samir Zelmat, Hamza Louati, Yassine Bellebna, and Farid Miloua. On the attraction force applied on metal pieces in a traveling wave conveyor. Journal of Electrostatics, 96 :64–68, 2018.

[82] Ahmed Alibida, Samir Zelmat, Mohamed Elmouloud Zelmat, Marian Bogdan Neagoe, Farid Miloua, Lucien Dascalescu, and Amar Tilmatine. Experimental analysis of a new attraction force applied on metal particles. Particulate Science and Technology, 38(4) :505–510, 2020.

[83] Hamza Louati, Noureddine Zouzou, Amar Tilmatine, Ayyoub Zouaghi, and Rabah Ouiddir. Experimental investigation of an electrostatic adhesion device used for metal/polymer granular mixture sorting. Powder Technology, 391 :301–310, 2021.

[84] Soumia Louhadj, Nacera Hammadi, Seddik Touhami, Hamza Louati, Aicha Hadjali, Imad-Eddine Kimi, and Amar Tilmatine. Experimental analysis of the attraction force applied on metal particles using a double-side electrical curtain. Journal of Electrostatics, 105 :103448, 2020.

[85] Aicha Hadj Ali, Mohamed Elmouloud Zelmat, Seddik Touhami, Soumia Louhadj, Youcef Benmimoun, Hamza Louati, and Amar Tilmatine. Using a vibrating electrical curtain conveyor for separation of plastic/metal particles. Powder Technology, 373 :267–273, 2020.

[86] Rafik Sayah, Abdelkader Semmak, Mohamed Bouhmama, Farid Miloua, and Amar Tilmatine. Experimental analysis of a new separation technique of metal/plastic particles using a double-side electrostatic actuator. Journal of Electrostatics, 118 :103734, 2022.

[87] Imane Zennani, Samir Zelmat, and Amar Tilmatine. Procédé de séparation électrostatique de mélange de particules métal/plastique avec un disque rotatif. Inovation patent from INAPI. Nº11892,23 novembre 2021.

[88] Imane Zennani, Samir Zelmat, Amar Tilmatine, "Experimental Investigation of a New Electrostatic Separation Process of Metal/Plastic Particles using a Horizontal Rotating Disk", national conference, International Journal of Electronics and Electrical Engineering Systems (ISSN: 2602-7437) Volume 6, Issue 3 (September 2023)

[89] Imane Zennani, Samir Zelmat, Amar Tilmatine, (2023): Electrostatic separation process of metal/plastic granular mixtures using a horizontal rotating disk, Particulate Science and Technology, DOI: 10.1080/02726351.2023.2201920

[90] Hamza Louati. Utilisation de la technique des ondes voyageuses pour la séparation des mélanges de particules métal/plastique. PhD thesis, Université de Poitiers ; Université des Sciences et de la Technologie d'Oran, 2022.

[91] Imane Zennani, Samir Zelmat, Amar Tilmatine, "Experimental analysis of a new separation tech- nique using an electrostatic device based on an electro-adhesion force applied on metal particles," International Conference on Applied Science and Engineering ICASE 2022.

[92] Imane Zennani, Samir Zelmat, and Amar Tilmatine. A new electrostatic separator device using a double-side rotating actuator. In 2024 3rd International Conference on Advanced Electrical Engineering (ICAEE), pages 1–6. IEEE, 2024.